2005

Myosin-Like Proteins in S. cerevisiae: Multifunctional, Structural Components of the Nuclear Envelope

Mario Niepel

The Myosin-like Proteins in *S. cerevisiae*: Multifunctional, Structural Components of the Nuclear Envelope

A Dissertation
Presented to the Faculty of The Rockefeller University
in Partial Fulfillment of the Requirements for
the Degree of Doctor of Philosophy

by
Mario Niepel
June 2005

Acknowledgements

I am in deep gratitude to my advisor Dr. Michael P. Rout for his continuous guidance and support throughout my Ph.D. studies and to Dr. Caterina Strambio de Castillia for our close scientific collaboration. Working together with you on the Mlp project has not only been scientifically rewarding, but it has made my time in the laboratory an enjoyable exeperience.

I am grateful for all the dedication and helpful advice of Drs Titia de Lange, Frederick Cross and Mark Winey. Thank you very much for serving as members of my faculty advisory committee.

I am indebted to Helen Shio for performing all electron microscopy imaging; to Dr. Alison J. North and Dan Elreda for their help with fluorescence microscopy; and to Drs Andrew Krutchinsky and Brian T. Chait for teaching me how to perform mass spectrometry.

I would also like to thank all members of the Rout laboratory for all the helpful discussion and the continuous collaborative effort in the development and optimization of novel methods. In particular I would like to thank Joseph Fasolo for his contributions to this project.

My work was supported in part by the Boehringer Ingelheim Fonds.

Table of Contents

List of Tables

List of Figures

List of Abbreviations

FG Nup	phenylalanine-glycine repeat Nucleoporin
IEM	immuno-electron microscopy
Kap	Karyopherin
NA	nuclear accumulation
NBD	nuclear binding domain
NE	nuclear envelope
NEBD	nuclear envelope breakdown
NES	nuclear export signal
NLS	nuclear localization signal
NPC	nuclear pore complex
Nup	Nucleoporin
PrA	Protein A
rER	rough endoplasmatic reticulum
RNAi	RNA interference
SPB	spindle pole body
TEM	transmission electron microscopy

Abstract

The nuclear envelope (NE) separates the genetic material from the rest of the cell, delimits and defines the nucleus, organizes the intranuclear architecture and serves as a regulator for multiple nuclear processes. In all eukaryotes, filamentous coiled-coil proteins are associated with the intranuclear surface of the NE and are integral to proper nuclear function. One such protein, called Tpr in vertebrates, attaches to the NPC and appears to form the nuclear basket structure, is conserved throughout all eukaryotes. The two yeast homologs of Tpr are termed Mlp1p and Mlp2p. The Mlp proteins also attach to the nuclear face of the NPC and form a layer underneath the NE.

For my thesis work I examined the structure and function of the Mlp proteins. A proteomic study of Mlp associated complexes revealed that the Mlp proteins interact predominantly with components of the NPC, the mRNA transport and processing machinery, and the spindle pole body (SPB; the yeast microtubule organizing center). Structural and microscopic analyses show that the Mlp proteins may form the nuclear basket in yeast, as well as interconnect NPCs into a network. Finally, a detailed functional study demonstrated that Mlp2p binds directly to the SPB and promotes the incorporation of components into the core structure of the SPB.

The data presented in this thesis supports a model in which the Mlp proteins integrate the NPCs and the SPBs into a continuous structure at the nuclear periphery. This network supports the stability of the NE and, by its interaction with soluble factors, directly influences nuclear functions like SPB maintenance and mRNP metabolism.

Chapter 1: Introduction.

The Nuclear Envelope in Higher Eukaryotes.

Intracellular compartmentalization is the defining feature of eukaryotic cells, allowing them to achieve novel levels of regulation in many cellular processes. The most obvious example of such compartmentalization is the segregation of the genetic material away from the cytoplasm into the nucleus by the nuclear envelope (NE; reviewed in Nigg 1989). Besides forming a passive barrier surrounding the nucleus, the NE is a complex organelle and plays a regulatory role in cellular processes, such as DNA replication, and aides in the organization of nuclear content and in the maintenance of nuclear shape.

The NE is a double membraned coat, consisting of the cytoplasmic outer membrane and the nuclear inner membrane, which surrounds the luminal space. The two membranes are connected at the nuclear pore complexes (NPCs), the sole mediator of transport across the NE. While the outer nuclear membrane is contiguous with the rough endoplasmatic reticulum (rER) and is lined with functional ribosomes, the inner nuclear membrane contains a separate set of proteins and performs distinct functions. The NE lumen is a physical extension of the rER lumen. In metazoans, underlying the inner nuclear membrane is a network of nuclear-specific intermediate filaments, called the nuclear lamina. In vertebrates it is comprised of a polymer of two types of lamins (lamin B and lamin A/C) anchored at the NE by a number of integral membrane proteins, including lamin B receptor, emerin and lamin-associated proteins.

During mitosis in higher eukaryotes the NE disassembles to allow spindles access to the kinetochores. This process is called NE breakdown (NEBD) and defines the transition from prophase to prometaphase. It is believed that the driving forces of NEBD are microtubules emanating from the centrosomes, which may literally tear the NE apart and subsequently move the NE fragments away from the chromosomes (Beaudouin et al., 2002; Salina et al., 2002). It was previously thought that the NE remains separated from the ER during this process by forming compositionally distinct vesicles, but now it appears that the NE and its integral membrane proteins are reabsorbed by the ER (Ellenberg et al., 1997; Zaal et al., 1999). After the physical breakdown of the NE has been initiated, the NPC and the lamina disassemble and their components disperse in the mitotic cell, triggered through phosphorylation by the maturation-promoting factor (Collas, 1999; Gerace and Blobel, 1980; Macaulay et al., 1995; Yang et al., 1997). The early disassembly of the NPC might indeed play a role in the further breakdown of the NE (Terasaki et al., 2001). As early as anaphase, the nucleus starts to reassemble around ER-like cisternae, coating the newly segregated chromatids (Ellenberg et al., 2002). Sequentially, the dispersed NE proteins are recruited back to the NE: first nucleoporins (Nups; Bodoor et al., 1999) and integral membrane proteins (Ellenberg et al., 1997) and then the lamins (Moir et al., 2000).

The nuclear lamina forms an extensive protein network at the nuclear periphery with multiple functions, many of which have not been well characterized. The lamin network is thought to maintain nuclear structure by interlinking neighboring NPCs. This theory is supported by the concerted movement of NPCs and the lamina observed in photobleaching experiments (Daigle et al., 2001). Lamins influence transcription by

binding to transcription factors (Mancini et al., 1994) and the disruption of the lamina significantly inhibits RNA polymerase II activity (Spann et al., 2002). DNA replication factors have been reported to co-localize with lamins in late S phase (Moir et al., 1994) and the disruption of the lamina can cause inhibition of DNA synthesis (Spann et al., 1997).

A number of genetic disease have been linked to mutations in Lamin A, suggesting for example a role in early onset aging (reviewed in Mounkes and Stewart, 2004). Nuclei carrying mutations in A-type lamins show blebbing of nuclei, including large alterations in nuclear shape, increased membrane separation, and clustering of pores (Muchir et al., 2003; Sullivan et al., 1999). Affected cells are mechanically weakened, leaving them prone to damage and eventual apoptosis when exposed to mechanical stress. (Lammerding et al., 2004). The weakened state of the nuclei may account for the premature wasting of muscle tissue in affected patients.

Even though lamins appear to play a role in multiple functions central to the nucleus, they are not universally conserved among eukaryotes. However, it does appear that all eukaryotes have some architectural proteins associated with the NE. Examples include Nup-1 in *Trypanosoma* and the FPP family of proteins in *Arabidopsis* (Gindullis et al., 2002; Ogbadoyi et al., 2000; Rout and Field, 2001). Among these perinuclear proteins, only one family appears to be well conserved in all eukaryotes: the Tpr/Mlp family (Kuznetsov et al., 2002).

Tpr, a coiled-coil protein of the nuclear periphery.

The Tpr (translocated promoter region) gene encodes a filamentous protein that localizes to the nuclear periphery in metazoans. Unlike lamins, Tpr is well conserved amongst species and appears to have homologs in all eukaryotes studied to date (Figure 1). The 5' segment of mammalian Tpr was originally discovered as an activator of the protooncogene *met* in human gastric carcinoma cells (Park et al., 1986; Soman et al., 1991) and *trk* in human papillary thyroid carcinoma (Greco et al., 1992). Full-length Tpr has a molecular weight of 267kD and a bipartite secondary structure (Byrd et al., 1994). Structure prediction based on the sequence of Tpr suggests that its C-terminus may form an acidic globular domain, consisting mainly of beta barrels and random coils (Byrd et al., 1994). The N-terminal 70% of the protein are predicted to be predominantly alpha helical and contain heptad repeats typical of coiled-coil domains (Byrd et al., 1994). Experiments with recombinant fragments show that the N-terminus of Tpr forms a rod-like structure, capable of homodimerization in parallel and in register with the heptad repeats (Hase et al., 2001). Genomic analysis suggests that there are no paralogs of Tpr in higher eukaryotes and that the murine Tpr gene gives rise to only one major protein product (Kuznetsov et al., 2002).

The exact localization of Tpr is subject to debate, possibly due to species and cell type specific differences. In mammalian cells Tpr is localized predominantly to the nuclear periphery, extending from NPCs into the nuclear interior (Cordes et al., 1997). In *Xenopus laevis* oocytes Tpr filaments have been shown to extend up to 300nm into the nuclear interior, exceeding the predicted length of a single Tpr dimer (Cordes et al., 1997). One report indicated that in human cells these filaments can form an intranuclear

network that stretches from the NPC to the periphery of the nucleolus (Fontoura et al., 2001). However, a later study in human cells showed that endogenous Tpr localizes exclusively to the NE and even overexpression of Tpr does not induce the assembly of defined, filamentous, intranuclear structures (Hase et al., 2001). In fact, all studies suggesting that Tpr forms intranuclear filaments rely on fixation techniques that are prone to form artifacts, while fluorescence microscopy in live cells finds no evidence of an intranuclear network (Frosst et al., 2002). Yet, in *Drosophila melanogaster* the Tpr homologue Megator also has been shown to localize to the intrachromosomal channels of the nuclear interior (Qi et al., 2004; Zimowska et al., 1997), to the spindle during mitosis (Qi et al., 2004) and to a single transcriptionally active locus after heat shock (Zimowska and Paddy, 2002).

Tpr forms the basket of the NPC.

Irrespective of its contentious localization within the nuclear interior, the bulk of Tpr localizes to the NPC at the nuclear periphery (Bangs et al., 1998; Byrd et al., 1994; Cordes et al., 1997). Deletion analysis coupled with immunofluorescence shows that Tpr is tethered to the NPC by a short NPC binding domain (NBD) located about halfway along the N-terminal coiled-coil region (Figure 2; Hase et al., 2001).

Nup153 is considered to be the most peripheral nucleoporins of the nuclear face of the NPC and was suggested to be part of the nuclear basket (Frosst et al., 2002; Krull et al., 2004). Depletion of Nup153 by RNA interference (RNAi) disrupts the localization of Tpr to the NPC with other peripheral NPC components being unaffected, while removal

of Tpr by RNAi leaves the NPC unchanged (Hase and Cordes, 2003). In addition, yeast two-hybrid experiments and *in vitro* binding assays confirm that Tpr interacts specifically with Nup153 fragments (Hase and Cordes, 2003). Taken together, the data suggests that Tpr is only peripherally associated with the NPC and does not act as a scaffold for the binding of other Nups. This is confirmed by immuno-electron microscopy (IEM) using gold-labeled antibodies against specific regions of Tpr (Frosst et al., 2002; Krull et al., 2004). While the region around the NPC binding domain localizes closest to the NPC, both the N- and the C-terminus localize roughly 70nm away from the mid-plane of the pore. This localization is distinct and more peripheral than any other studied nucleoporin, yet it overlaps well with the apparent dimensions of the basket (Krull et al., 2004), suggesting that Tpr is the major component of the nuclear basket of the NPC.

Tpr function is ill-defined.

The localization of Tpr at the NPC suggests that it might be involved in the transport of proteins and RNA between the nucleus and the cytoplasm. This is supported by the fact that both the overexpression of full length Tpr (Bangs et al., 1998) and the depletion of Tpr by injection of Tpr specific antibodies (Shibata et al., 2002) lead to the accumulation of high levels of poly(A)+ RNA within the nucleus, which co-localizes with SC35 positive speckles (Shibata et al., 2002). Furthermore, the *Drosophila* homolog localizes to a transcriptionally active heat shock puff, suggesting a possible role in mRNA metabolism (Zimowska and Paddy, 2002). However, even though in *Xenopus* oocytes Tpr associates with karyopherins (Shah et al., 1998), protein import does not

seem to be dependent on Tpr (Frosst et al., 2002; Shibata et al., 2002), while the effect on protein export by Tpr depletion is inconclusive. The study Megator (Bx34) has revealed intriguing additional functions of Tpr. Megator was first identified as an antigen in fractions of chromosomal proteins and linked to functions in mitotic cell division (Frasch et al., 1988). During spindle formation in prometaphase, Megator and the putative spindle matrix protein Skeletor co-localize with the tubulin to the spindle (Qi et al., 2004). Interestingly, Qi et al. (2004) found that the formation of the spindle-like structure by Skeletor and Megator is independent of tubulin. During telophase, Megator disperses away from the spindle to assume its normal distribution at the rim and the intrachromosomal channels in interphase (Zimowska and Paddy, 2002). Unlike Skeletor, the depletion of Megator by RNAi does not lead to abnormal spindles, but it greatly reduces the number of cells undergoing mitosis (Qi et al., 2004). Thus, in addition to its function at the spindle, Megator might very well have other essential functions in the cell, consistent with its dynamic localization.

Mlp proteins are the S. cerevisiae Tpr homolog.

The Myosin-like proteins (Mlp1p and Mlp2p), the Tpr homologs in the budding yeast *Saccharomyces cerevisiae*, were identified in a screen for proteins associated with the NE which are not bona-fide nucleoporins (Strambio-de-Castillia et al., 1999). Mlp1p had been previously been described as a protein crossreacting with a human anti-myosin antibody (Kolling et al., 1993). Mlp1p shares 28% identity and 52% similarity with its paralog Mlp2p and 18% identity and 28% similarity with its ortholog Tpr (as determined

by BLAST). Like Tpr, the Mlps are large proteins predicted to form an N-terminal coiled-coil domain (Strambio-de-Castillia et al., 1999), however their C-terminal globular domain is significantly smaller and not as acidic (Kuznetsov et al., 2002). Localization by fluorescence microscopy and IEM shows that the Mlp proteins localize to the nuclear periphery and are excluded from the region around the nucleolus (Galy et al., 2000; Kosova et al., 2000; Strambio-de-Castillia et al., 1999). While there appears to be some Mlp protein that is not associated with the NPC, both at the nuclear periphery and the nuclear interior (Strambio-de-Castillia et al., 1999), the bulk of it seems to be tethered as filaments to the pore (Kosova et al., 2000; Strambio-de-Castillia et al., 1999). Indeed, analysis of Nup deletion mutants confirms that the intact NPC is required for the localization of Mlp1p and Mlp2p to the nuclear periphery (Feuerbach et al., 2002; Galy et al., 2004).

Mlp proteins are involved in mRNA processing/export.

Although the deletion of either one of the MLP genes does not confer a lethal phenotype, the viability of strains lacking both genes is significantly compromised, suggesting that Mlp1p and Mlp2p have largely redundant functions (Strambio-de-Castillia et al., 1999). Colonies of the *mlp1*Δ *mlp2*Δ strains are small, slow growing and 'nibbled' (Strambio-de-Castillia, 1998; Zhao and Blobel, 2005) and individual *mlp1*Δ *mlp2*Δ cells are often enlarged, multi-budded and have enlarged nuclei with aberrant morphology (Strambio-de-Castillia, 1998). Consistent with its localization to the NPC, some data indicate a role for the Mlps in nucleocytoplasmic transport, since cells lacking

both Mlps show reduced nuclear import and passive diffusion rates of SV40- GFP reporters (Strambio-de-Castillia et al., 1999).

To date, the most thoroughly studied function of Mlp proteins is their role in mRNA processing and export. Early results showed that the steady-state distribution of poly(A)+ RNA is not grossly altered in *mlp1*Δ *mlp2*Δ cells (Strambio-de-Castillia et al., 1999). However, cells over-expressing Mlp1p accumulate poly(A)+ RNA inside the nucleus (Green et al., 2003; Kosova et al., 2000) and deletion analysis shows that the globular C-terminus of Mlp1p is necessary for this accumulation (Green et al., 2003). The Mlp proteins also physically interact with components of the mRNA maturation and export machinery. The C-termini of both Mlp1p and Mlp2p directly bind to Nab2p, a protein involved in the polyadenylation and export of mRNAs, *in vitro* (Green et al., 2003) and *in vivo* (Vinciguerra et al., 2005). Mlp proteins also interact with Mex67p, Yra1p and Msl5p in an RNA dependent manner (Galy et al., 2004; Vinciguerra et al., 2005), with Yra1p and Msl5p complexed preferentially with Mlp2p compared to Mlp1p. In addition, Mlp1p has been found to interact with Sac3p, an NPC associated protein involved in mRNA export which interacts with Mex67p (Lei et al., 2003) as well as with Sub2p, an essential pre-mRNA splicing factor required for nuclear export of mRNA (Strasser et al., 2002).

In genetic screens, the Mlp proteins have been shown to be involved in mRNA metabolism. Deletion of *MLP1* was found to be synthetically lethal with *prp18*Δ, a U5 snRNP-associated factor involved in the second step of mRNA splicing (Galy et al., 2004). The overexpression of an N-terminal fragment of Mlp1p, or the deletion of either of the MLP genes acts as a suppressor for temperature sensitive mutations of yra1 (Vinciguerra et al., 2005), a gene required for proper packaging and export of poly(A)+

mRNAs. The deletion of either *MLP1* or *MLP2* also rescues the temperature dependent growth defect of an N-terminal deletion of *nab2* (Vinciguerra et al., 2005). The genetic interaction between MLP genes and genes involved in RNA metabolism does seem to be specific, since a number of other mutants involved in mRNA metabolism, for example *pap1-8*, *rna14-1*, *rna15-1*, *mex67-5* or *rat7-1*, do not show synthetic lethality or rescue in conjunction with deletion of the MLP genes (Vinciguerra et al., 2005).

The biochemical and genetic evidence for a role of the Mlp proteins in mRNA metabolism notwithstanding, the direct function of the Mlp proteins in this process remains undefined. This is partially due to the fact that the deletions of either one of the MLP genes causes only minor phenotypes in a *wild type* background. The overall distribution of poly(A)+ RNA does not seem to be perturbed (Strambio-de-Castillia et al., 1999), the transcription and expression of a LacZ reporter is only subtly affected (Vinciguerra et al., 2005) and only minor amounts of unspliced RNA leak into the cytoplasm (Galy et al., 2004). Only in the background of specific RNA metabolic mutations does the role of the Mlp proteins become more pronounced. Deletion of *RRP6*, a component of the nuclear exosome, causes an increase in the amount of improperly spliced or packaged pre-mRNAs within the nucleus (Hilleren et al., 2001). In this background, the leakage of unspliced RNA into the cytoplasm due to the deletion of MLP1 becomes more pronounced. In the background of the yra1-8, which causes increased degradation of poly(A)+ RNA via the nuclear exosome, (Zenklusen et al., 2002), the removal of MLP can partially restore normal mRNA levels (Vinciguerra and Stutz, 2004).

Taken together, the data suggests that the Mlp proteins do play a role in the late steps of mRNA processing and export. Packaged and mature mRNAs may dock to the Mlp proteins, possibly via Nab2p, where they are checked for the suitability for export. This might be achieved by the requirement for a suitable licensing complex, possibly consisting of Yra1p, Mex67p and Nab2p. Specifically, Nab2p has been proposed to participate in the proper formation of the poly(A) tail; thus it could mediate a signal for proper 3' end formation (Hector et al., 2002). Transcripts suitable for export are transported through the NPC, possibly involving a mechanism involving Mex67p and Sac3p, while the remaining RNAs are retained in the nucleus and degraded. In healthy cells this quality control step might only be of minor importance, since the majority of RNAs docking to the Mlps should be suitable for export. However, if the rate of faulty transcripts is elevated, or if rate of mRNA export is reduced, the role of the Mlp proteins becomes critical for cell survival.

Mlp proteins and global transcription.

A surprising finding from the study of the involvement of Mlp proteins in mRNA export leads to the suggestion that the Mlp proteins might also play a role in the regulation of global transcription (Vinciguerra et al., 2005). Vinciguerra et al. (Vinciguerra et al., 2005) found that in the GFP-*yra1-8* mutant, transcription of a LacZ reporter is upregulated by the deletion of MLP2; in fact, a genome-wide screen shows that about sixty different transcripts are affected by Mlp2p in this manner. It has been suggested that the Mlp proteins are part of a feedback mechanism that downregulates

transcription in response to defects in the mRNA export pathway (Vinciguerra et al., 2005) Further evidence for an influence of the transcriptional state by the nuclear periphery has been discovered: transcriptional activation of the GAL genes results in their association with the NPC (Casolari et al., 2004) and the transcriptional activity of genomic loci can be influenced by tethering to the NPC (Ishii 2002). Furthermore, a proteomic study indicated that Mlp1p is associated with the transcription machinery (Gavin et al., 2002). Thus, Mlp proteins could affect global regulation of transcription, either through an interaction with the mRNA processing machinery, by participating in the tethering of the genome to the periphery, or by a direct influence on the transcription machinery.

Mlp proteins have additional functions.

The Mlp proteins have been implicated in other nuclear functions. Since Mlp deletion strains exhibit a low level sensitivity to DNA damaging agents like bleomycin (Galy et al., 2000) and UV light (Kolling et al., 1993; Kosova et al., 2000), it has been suggested that Mlp proteins play a role in DNA repair (Galy et al., 2000). The Mlps have been proposed to be telomeric anchoring sites and involved in the establishment of silent chromatin (Feuerbach et al., 2002; Galy et al., 2000). Subsequent studies have called these roles into question, although they did indicate that that the Mlps might be implicated in telomere maintenance (Hediger et al., 2002a; Hediger et al., 2002b). Recently, it was found that the levels of 2-micron circles are increased in *mlp1*Δ*mlp2*Δ cells, possibly mediated by the Mlp proteins binding and stabilizing Ulp1p, a

desumoylating enzyme (Zhao and Blobel, 2005). Interestingly, since the reduction of the 2-micron circle levels in *mlp1*Δ*mlp2*Δ strains restores normal growth, it is possible that the accumulation of 2-micron circles contribute significantly to the clonal lethality and poor growth of the *mlp1*Δ*mlp2*Δ strain.

A new approach to investigate the function of the Mlp proteins.

The study of the Mlp proteins has been proven challenging to date. Genetic screens have brought to light a number of potential functions for the Mlp proteins, and recent biochemical evidence has shed some light on the proteins with which Mlp1p and Mlp2p might form a complex. The main rationale for my thesis work is that the function of a protein is influenced by two major factors: the localization of the protein within the cell and the components the protein interacts with. So, a thorough characterization of the Mlp localization and the proteins in complex with the Mlps would be a valuable starting point for future research. The information thus obtained could guide me and others to focus our research on specific Mlp functions, made plausible by its localization and interaction data. In addition, the ability to isolate Mlps in complex with other proteins can be a valuable starting point for the further biochemical analysis of Mlp interactions.

The results of my research presented in this thesis are divided into five chapters. First, using cell biological and biochemical methods, I further characterized the structure, localization, and function of the Mlp proteins. Next, I studied in more detail the phenotype of the *mlp1*Δ*mlp2*Δ strain. I then characterized the role Mlp proteins play in nucleo-cytoplasmic transport. Adapting proteomic techniques developed in our

laboratory, I isolated and identified a large number of proteins with which Mlp1p and Mlp2p are in complex. Finally, I focused on the very prominent interaction discovered between Mlp2p and spindle pole body (SPB) components to determine its functional significance for the cell.

This scope of this project required that a major part of this research project was undertaken in collaboration. The data presented here was obtained by Dr. Caterina Strambio-de-Castillia (CS) and myself (MN) in our laboratory, with the aid of our technician Joseph Fasolo (JF). The close division of labor makes it difficult to separate the work done. This is highlighted by the fact that the data presented in Chapter 6 has been submitted for publication with both Dr. Strambio-de-Castillia and me as joint first authors. However, all of the data presented in this thesis were obtained either entirely by me or contained a substantial contribution on my part as judged by my advisor. In each figure legend the investigator who performed the majority of the work in acquiring and analyzing the data is indicated. However, additional work in designing and preparing the experiments and experimental trials or repetitions may have been performed by either Dr. Caterina Strambio-de-Castillia or myself.

Figure 1: **Tpr homologs in eukaryotes.**

Graphical display of the phylogenetic relationship between multiple Tpr/Mlp family members. Sequences of the Tpr/Mlp family from multiple organisms were aligned by ClustalX. As reference MyosinII was included. Highlighted in red are the Mlp proteins in *S. cerevisiae*, in blue Megator in *D. melanogaster* and in green Tpr in vertebrates. It is interesting to note that while the two Mlp paralogs in *S. bayanus* and *S. cerevisiae* have arisen from the same genome duplication, *S. pombe* evolutionary diverged from this group before the genome duplication and evolved its second copy of Mlp independently.

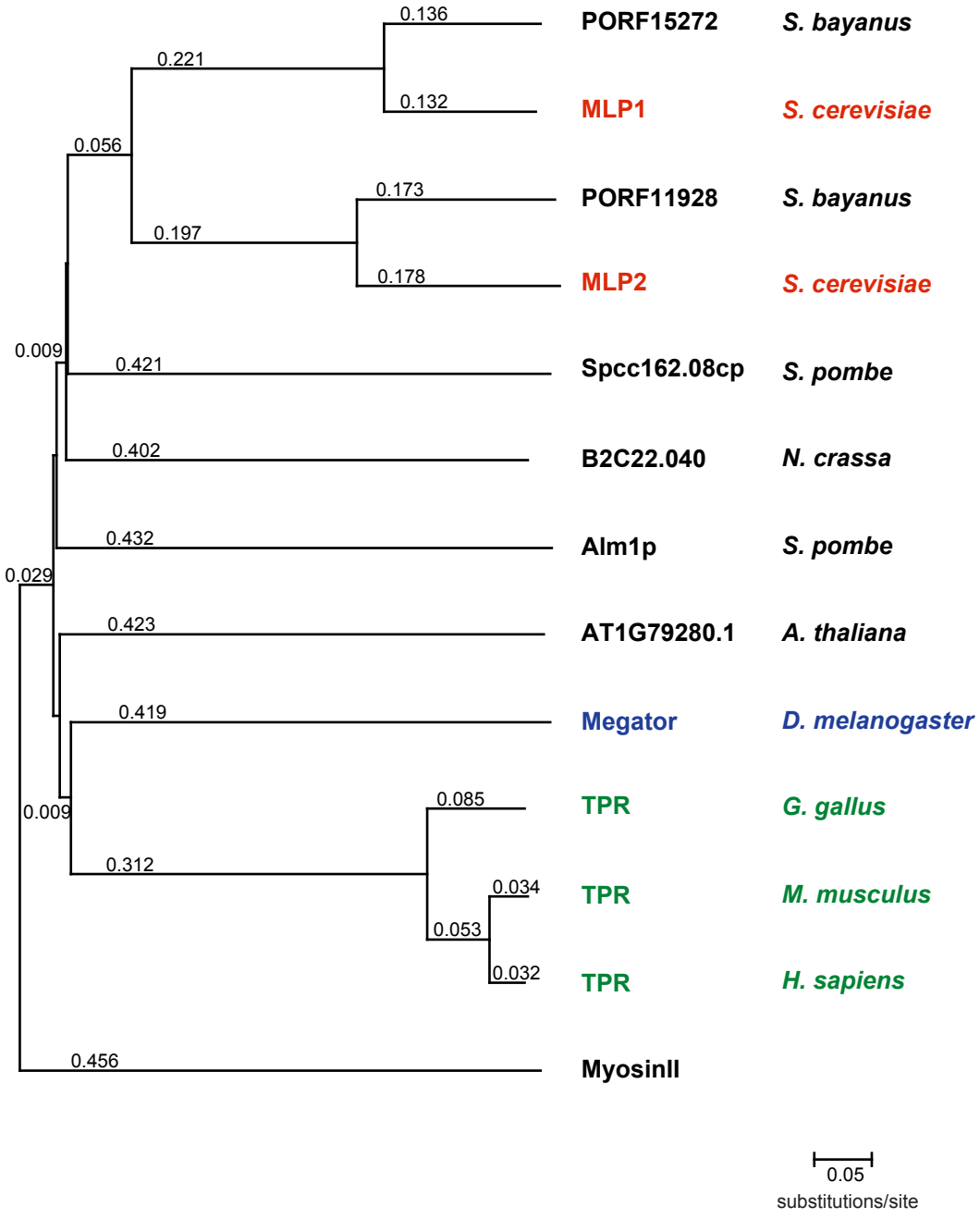
0.136
PORF15272
S. bayanus
0.221
0.132
MLP1
S. cerevisiae
0.056
0.173
PORF11928
S. bayanus
0.197
0.178
MLP2
S. cerevisiae
0.009
0.421
Spcc162.08cp
S. pombe
0.402
B2C22.040
N. crassa
0.432
Alm1p
S. pombe
0.029
0.423
AT1G79280.1
A. thaliana
0.419
Megator
D. melanogaster
0.085
TPR
G. gallus
0.009
0.312
0.034
TPR
M. musculus
0.053
0.032
TPR
H. sapiens
0.456
MyosinII
0.05
substitutions/site

Figure 2: **Localization of Tpr at the NPC.**

Schematic view of the organization of Tpr at the NPC in relation to the nuclear basket (adapted from Krull et al., 2004). Tpr is attached to the NPC at its nuclear binding domain (NBD) via Nup153. Tpr takes on a hair-pin conformation, with both the N- and the C-terminus facing away from the NPC. The globular domain at the C-terminus of Tpr may be responsible for forming the distal ring of the nuclear basket

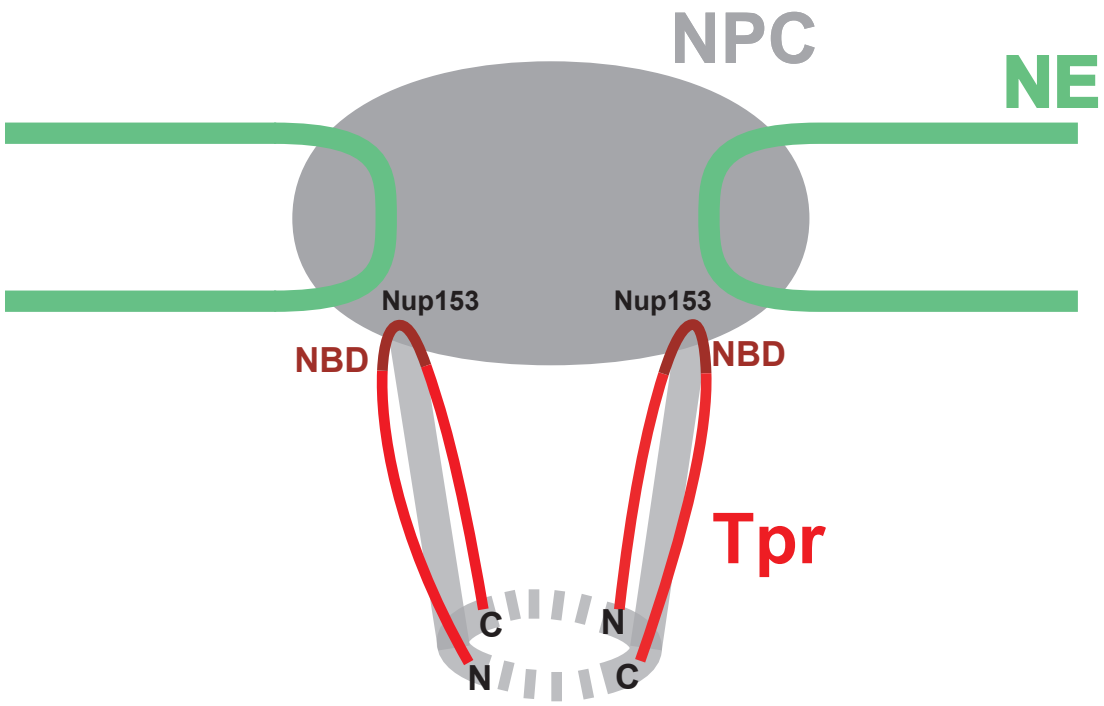
NPC
NE
Nup153
Nup153
NBD
NBD
Tpr
C
N
N
C

Chapter 2: Studies of Mlp localization.

Mlp1p and Mlp2p have different localization patterns.

The Mlp proteins have been identified as proteins of the NE, peripherally associated with NPCs (Strambio-de-Castillia et al., 1999). To directly compare the localization of the Mlp proteins with respect to each other, we used CFP-Mlp1p and YFP-Mlp2p to visualize their localization within the same cell (Figure 3a). The fluorescence signals of both Mlp1p and Mlp2p localized to the NE, resulting in asymmetrical and patchy rim staining of the nuclear periphery (Galy et al., 2004; Strambio-de-Castillia, 1998; Strambio-de-Castillia et al., 1999). Even though the Mlp proteins occupied the same general area of the nuclear periphery, there were differences in their localization patterns. While CFP-Mlp1p was distributed fairly evenly along a C-shaped portion of the nuclear periphery, YFP-Mlp2p showed a different pattern. It was concentrated into fewer foci and did not spread as far along the NE. This difference became even more obvious when the signals of CFP-Mlp1p and YFP-Mlp2p from the same cell were digitally overlaid, as their patterns only partially overlap (Figure 3a, *Merge*).

Mlp proteins are excluded from the nucleolus and localize to the SPB.

Localization studies showed that the Mlp proteins do not completely overlap with NPC markers both in *wild type* and in NPC clustering strains (Strambio-de-Castillia et al.,

1999). To extend these findings *in vivo* and to compare the localization of Mlp proteins to other nuclear markers, we expressed Mlp1p-YFP or YFP-Mlp2p in conjunction with the Nucleoporin Nup49p-CFP, the nucleolar marker Nop1p-CFP and the SPB component Spc42p-CFP (Figure 3b-d).

Mlp proteins covered only a C-shaped portion of the nuclear periphery, while NPCs were distributed evenly throughout the whole NE (Figure 3a). Since our data (see below) and previous studies (Kosova et al., 2000; Strambio-de-Castillia et al., 1999) suggest that the Mlp proteins are anchored at the NPC, this finding shows that not all NPCs in yeast are equal. A number of pores must be virtually free of Mlps, suggesting that the presence of Mlp proteins is not essential for NPC function. When comparing the localization of the Mlp proteins to a nucleolar protein, Nop1p, the polar organization of the nucleus became apparent (Figure 3b). The nucleolus formed a sickle shaped structure, covering approximately 30% of the NE, while both Mlp1p and Mlp2p appeared to be excluded from this region.

Since the SPB is localized to the nuclear hemisphere opposite the nucleolus (Yang et al., 1989), and the Mlp proteins are also excluded from the nucleolus, it is to be expected that the SPB is found in the region of the Mlp layer. Indeed, when we expressed Spc42p-CFP in combination with Mlp1p-YFP or YFP-Mlp2p, we found that the SPB occupies the Mlps' hemisphere (Figure 3c). We analyzed 500 nuclei in which the Mlp proteins are localized in a C shape, indicating that the nucleolus is present in the midplane of the nucleus. In this configuration, the nucleolus covers approximately 20% of the NE. We find that the SPB localizes within the Mlp layer in over 90% of nuclei. Analysis under the

test hypothesis that the Mlp proteins are excluded from 20% of the NE surface area showed that this overlapping localization was significant (chi-squared value = 2.27×10^{-08}).

Mlp1p and Mlp2p show a similar localization as the vertebrate basket protein.

To examine the localization of the Mlp proteins in more detail, we mapped their position in respect to the NPC by IEM. We genomically tagged the Mlps both at the N- and the C-terminus using the Protein A (PrA) affinity tag. Figure 4a shows a digital overlay of multiple gold-labeled NPCs from C-terminally tagged Mlp strains and a PrA tagged peripheral Nup is shown as control. The gold-particles labeling the Mlp proteins were spread out much further from the center of the NPC horizontally along the NE in comparison to Nup1p. In addition, the bulk of the gold label was located further away from the midplane of the NE.

Using a modeling technique developed in our laboratory (Rout et al., 2000; Suprapto, 2002) to extract the position of the affinity tag from the distribution of the gold particles in the digitally overlaid images, we were able to map the localization of both the N- and the C-terminus of Mlp1p and Mlp2p (Figure 4b). When fitted into a model of the NPC obtained by the same method (Rout et al., 2000), we found that the Mlp proteins localized more than twice as far away from the midplane of the NPC as the most peripheral nucleoporin (Nup1p), underscoring the fact that the Mlp proteins do not behave like any nucleoporin. Interestingly, both the N- and the C-terminus of the Mlp proteins localized to approximately the same area. This suggests that both ends of the Mlp proteins are extended away from the NPC, while a region roughly halfway along the C-terminal

coiled-coil domain interacts with the NPC. These results are strikingly similar to the detailed localization results for human Tpr (Frosst et al., 2002; Krull et al., 2004), suggesting that the overall structure and localization of Mlp and Tpr is conserved (see also Figure 2). The localization of the N- and C-termini at about 40nm away from the nuclear face of the NPC suggests that the length of a single Mlp dimer is approximately 80nm, which is consistent with the estimated length of purified Tpr and Mlp1p [Kosova, 2000; Hase 2001]. We note that the termini of Mlp2p localized about 10nm closer to the periphery of the NPC than Mlp1p, consistent with the roughly 10% difference in molecular mass between the two proteins.

Mlp1p is a highly elongated protein.

To determine if the Mlp proteins indeed form filamentous structures as predicted from their primary structure (Strambio-de-Castillia et al., 1999), we extracted PrA tagged Mlp proteins under mild conditions, purified them using IgG conjugated Sepharose and eluted them using a peptide that competes with the PrA binding site (Figure 5a). This technique enables us to isolate proteins in a native state (see below, Strambio-de-Castillia et al., manuscript in preparation).

To determine their sedimentation coefficient (S-value), we subjected the eluted proteins to analytical sucrose gradient centrifugation and compared their sedimentation to control proteins with known S-values. Although a portion of Mlp1p showed a discrete detectable peak in the range of the control proteins, the bulk of Mlp1p sediments to the bottom of the centrifuge tube (Figure 5b). The experimentally determined S-value for this

soluble portion of Mlp1p-PrA is S_{exp}=7.1. This is very similar to the experimentally determined S-value of a Tpr homodimer (S_{exp}=7.5; Hase et al., 2001; Krull et al., 2004). Since the primary sequence of Mlp1p suggests that it can homodimerize and the S-values for Tpr and Mlp1p-PrA were comparable, we assume for the further calculations that Mlp1p was also purified as a homodimer. The calculated maximum S-value for a protein of the same molecular weight as an Mlp1p-PrA dimer is S_{max}=22.4. The ratio between S_{max}/S_{exp} gives a measure of how elongated a tested protein is. For a typical globular protein the ration will be smaller than 1.5, while highly elongated proteins (e.g. tropomyosin) will have a ratio of 2.0 or higher (Rickwood, 1984). Since the S_{max}/S_{exp} of Mlp1p-PrA is 3.1 we can conclude that the soluble Mlp1p-PrA is not globular, but highly elongated. If Mlp1p-PrA were present as a monomer instead of a dimer, the S_{max}/S_{exp} would be 2.0, still in the range of a highly elongated protein. The molecular weight of the PrA affinity tag has roughly 10% of the molecular weight of the Mlp proteins and should not greatly affect the overall sedimentation coefficient of the tagged proteins.

In all sedimentation trials the entire amount of Mlp2p, as well as the bulk of Mlp1p, remained far out of the range of the molecular markers, sedimenting to the bottom of the centrifuge tube. This suggests that isolated Mlp proteins are assembled into a larger protein structure.

Mlp1p and Mlp2p form a molecular assembly.

To investigate the hypothesis that the Mlp proteins form an interconnected network at the nuclear periphery, we performed co-immunoprecipitation experiments followed by

Western blotting using PrA tagged Mlps as bait and Myc tagged Mlps as targets (Figure 6). PrA-containing complexes were isolated from strains expressing Mlp1p-PrA together with either Mlp1p-Myc or Mlp2p-Myc. Mlp1p-PrA co-immunoprecipitates both of the Myc-tagged Mlps (Figure 6a, *co-expressed*). This interaction did not occur when cells expressing the two proteins separately were mixed after cell lysis, demonstrating that the interaction required a physiologically relevant assembly process and does not occur post-lysis (Figure 6a, *mixed*). We obtained similar results when either Mlp1p-Myc or Mlp2p-Myc were tested in conjunction with Mlp2p-PrA (Figure 6b). In both experiments we found smaller amounts of Mlp2p-Myc purifying with the PrA tagged bait than Mlp1p-Myc. This is consistent with Mlp1p forming a more extensive structure at the nuclear periphery (Figure 3a) than Mlp2p.

Our data suggests that the Mlp proteins form a large molecular assembly at the nuclear periphery. We found only a small amount of purified Mlp1p is present as an elongated homodimer, while the bulk of purified Mlp1p and Mlp2p are assembled into a complex with a sedimentation coefficient greater than 20S. It is unlikely that this assembly process occurs post-lysis, since in our co-immunoprecipitation experiments neither Mlp1p nor Mlp2p associated with each other in solution. We consistently isolate more Mlp1p-Myc than Mlp2p-Myc with the PrA tagged baits. This may mean that Mlp1p forms a more extensive interlinked molecular assembly than Mlp2p, which is indeed consistent with the localization patterns observed in Figure 3a.

The structure of mlp1Δmlp2Δ nuclei is compromised.

Since the Mlp proteins are arranged in a layer underneath the NE, possibly forming a interlinking network, it is possible that they might have a structural role in supporting the NE, analogous to the lamina in vertebrates. It has been reported that certain lamin mutants have structurally compromised nuclei (Lammerding et al., 2004), which are deformed easily (Sullivan et al., 1999). To investigate the structure of the NE, we visualized the NE of *wild type* and *mlp1Δmlp2Δ* by expressing GFP labeled Nup49p and determined their shape factor from projections of 3D z-stacks. The shape factor (r_o/r_i) is defined as the ratio of the smallest distance and the largest distance from the centroid of an object to its edge (Figure 7a). While nuclei from *wild type* cells appeared to be close to circular, with a shape factor peaking at about 1.5, the nuclei of the mlp deletion strain had a more irregular shape (Figure 7b). The majority of *mlp1Δmlp2Δ* had a shape factor of around 2, while a substantial percentage of nuclei deviated even further from a circle. This difference is significant with a p value<0.001 in a Student's t-test.

While the shape factor analysis gives a static view of the distortion of the nucleus, we also visualized nuclei in real time (Figure 7c). To appreciate the deformation of the NE over time, we overlaid the shape of the nucleus at time zero over the pictures of each of the following time points. The shape of the *wild type* nucleus remained fairly constant over time, in agreement with its regular shape factor. The NE of the *mlp1Δmlp2Δ* strain on the other hand deformed rapidly over a period of seconds. It should be noted that such rapid deformation is not seen at all times in the *mlp1Δmlp2Δ*, and at this point the force driving the movement is not known.

mlp1Δmlp2Δ cells are sensitive to weakening of the NE.

Since the absence of Mlp proteins at the nuclear periphery appears to destabilize the shape of the nucleus, we set out to further weaken the NE in the *mlp1*Δ*mlp2*Δ background, hypothesizing that this might cause significant growth defects, possibly due to loss of nuclear integrity (Figure 8a).

In yeast, the size of the nucleus is dependent on the ploidy of the cell (Galitski et al., 1999). We created *wild type* and *mlp1*Δ*mlp2*Δ strains with a ploidy of 3n and 4n and tested their viability at 30ºC and 37ºC. While the polyploid strains in the *wild type* background did not show any growth deficiency, the tetraploid *mlp1*Δ*mlp2*Δ strain showed a marked decrease in viability at 37ºC (Figure 8b). Clustering of the NPCs might likewise weaken the stability of the nuclear periphery, since the pores are an integral part of the NE. We crossed the *mlp1*Δ*mlp2*Δ strain with a *nup133ΔN* strain which causes NPC clustering. A caveat to this result is that *nup133*Δ has defects in mRNA export which might also be responsible for a loss of viability in conjunction with the MLP deletion, however, the N terminal deletion does only exhibit mild mRNA export phenotypes (Doye et al., 1994). While we would expect to recover 25% of *mlp1*Δ*mlp2*Δ, we found only 1% of the spores carrying this genotype, showing that the viability of the *mlp1*Δ*mlp2*Δ is markedly reduced in the *nup133*Δ*N* clustering background (Figure 8c). The fact that we recover less *mlp1*Δ *nup133*Δ*N* and the *mlp2*Δ *nup133*Δ*N* suggests that indeed functions other than the structure of the NE might play a role in the lethality observed. Taken together our results suggest that in the absence of the Mlp proteins, the NE is weakened and becomes more sensitive to further perturbations.

Figure 3: **The Mlp proteins are excluded from the nucleolus and localize to the nuclear hemisphere occupied by the SPB.**

Images represent two-dimensional projections of 3D image stacks containing 10-15 0.3µm sections. **(a)** Mlp1p and Mlp2p have different localization patterns. Live fluorescence images of homozygous diploid cells expressing both CFP-Mlp1p (red) and YFP-Mlp2p (green). Diploid cells were used to obtain a higher intensity fluorescent signal. To visualize the fluorescent signals in the context of the whole cell, a DIC image was merged with both of the CFP and YFP pictures from the same field (*Merge*). **(b)** Live fluorescence images of haploid cells expressing either Mlp1p-YFP or YFP-Mlp2p (green) and Nup49-CFP (red). **(c)** Live fluorescence images of haploid cells expressing either Mlp1p-YFP or YFP-Mlp2p (green) and Nop1p-CFP (red). **(d)** Live fluorescence images of haploid cells expressing either Mlp1p-YFP or YFP-Mlp2p (green) and Spc42-CFP (red). Bars, 2µm. (a) MN (b) CS and MN.

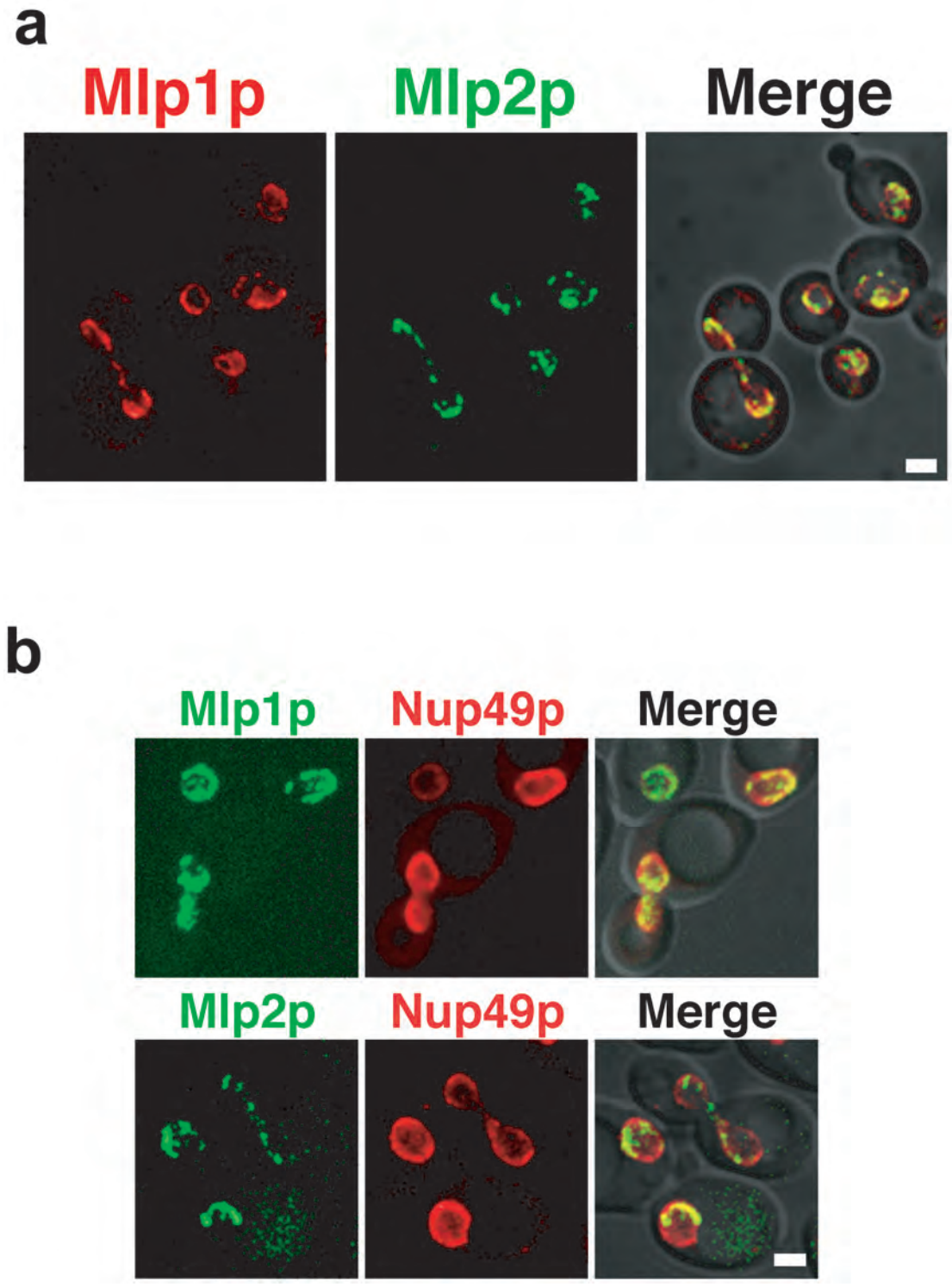
a
Mlp1p
Mlp2p
Merge
b
Mlp1p
Nup49p
Merge
Mlp2p
Nup49p
Merge

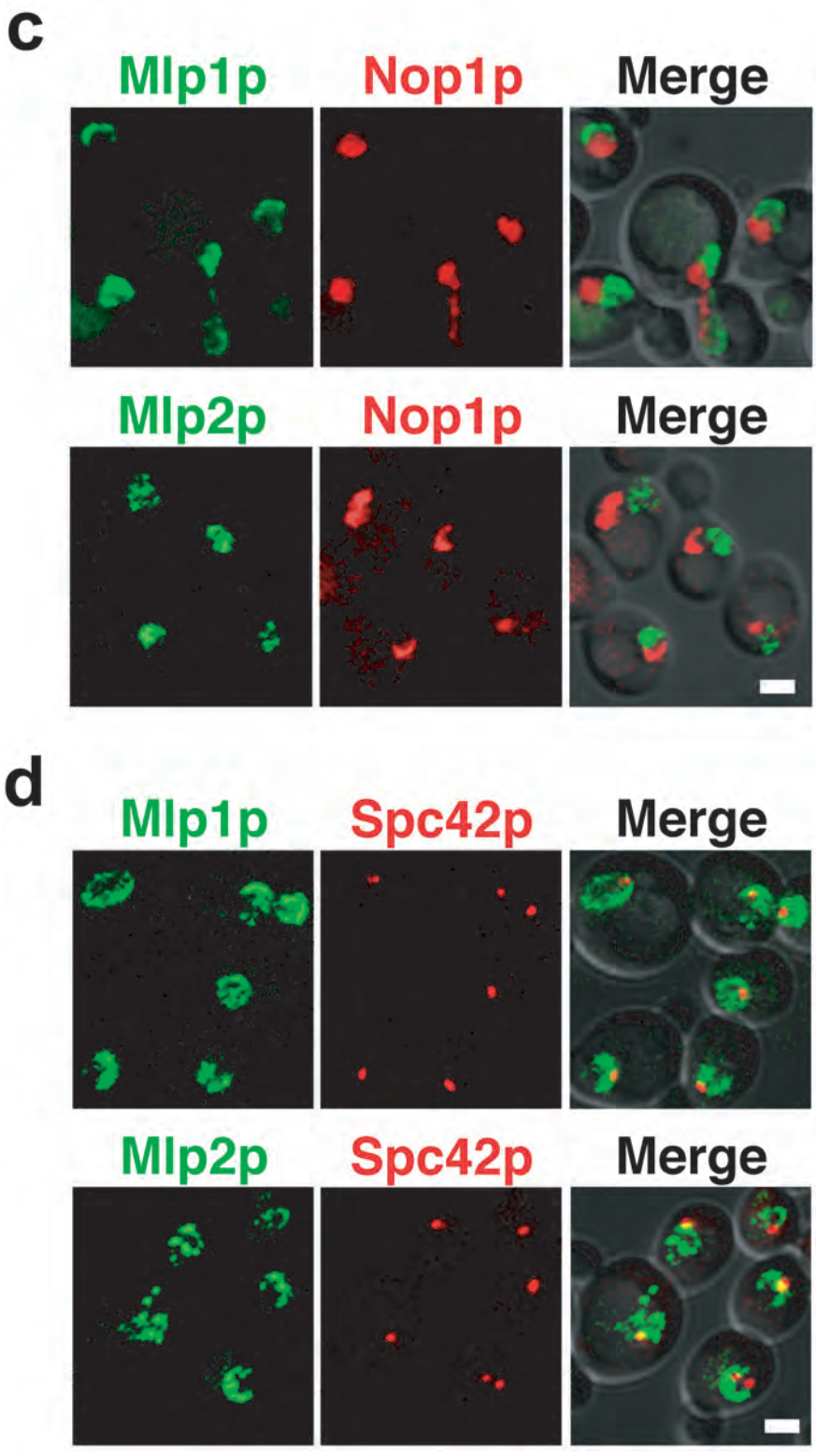
c
Mlp1p
Nop1p
Merge
Mlp2p
Nop1p
Merge
d
Mlp1p
Spc42p
Merge
Mlp2p
Spc42p
Merge

Figure 4: **The N- and C-termini of the Mlp proteins localize away from the NPC.**

(a) Montages of multiple electron microscopy images of immunolabeled Mlp1p-PrA, Mlp2p-PrA or Nup1p-PrA at NPCs. **(b)** Modeled position of the N- and C-termini of the Mlp proteins in respect to the central axis (R) and the central plane (Z) of the NPC (n>200). The position of the Mlp proteins is superimposed on the modeled position of all Nups in the NPC (modified from Rout et al., 2000). CS and MN.

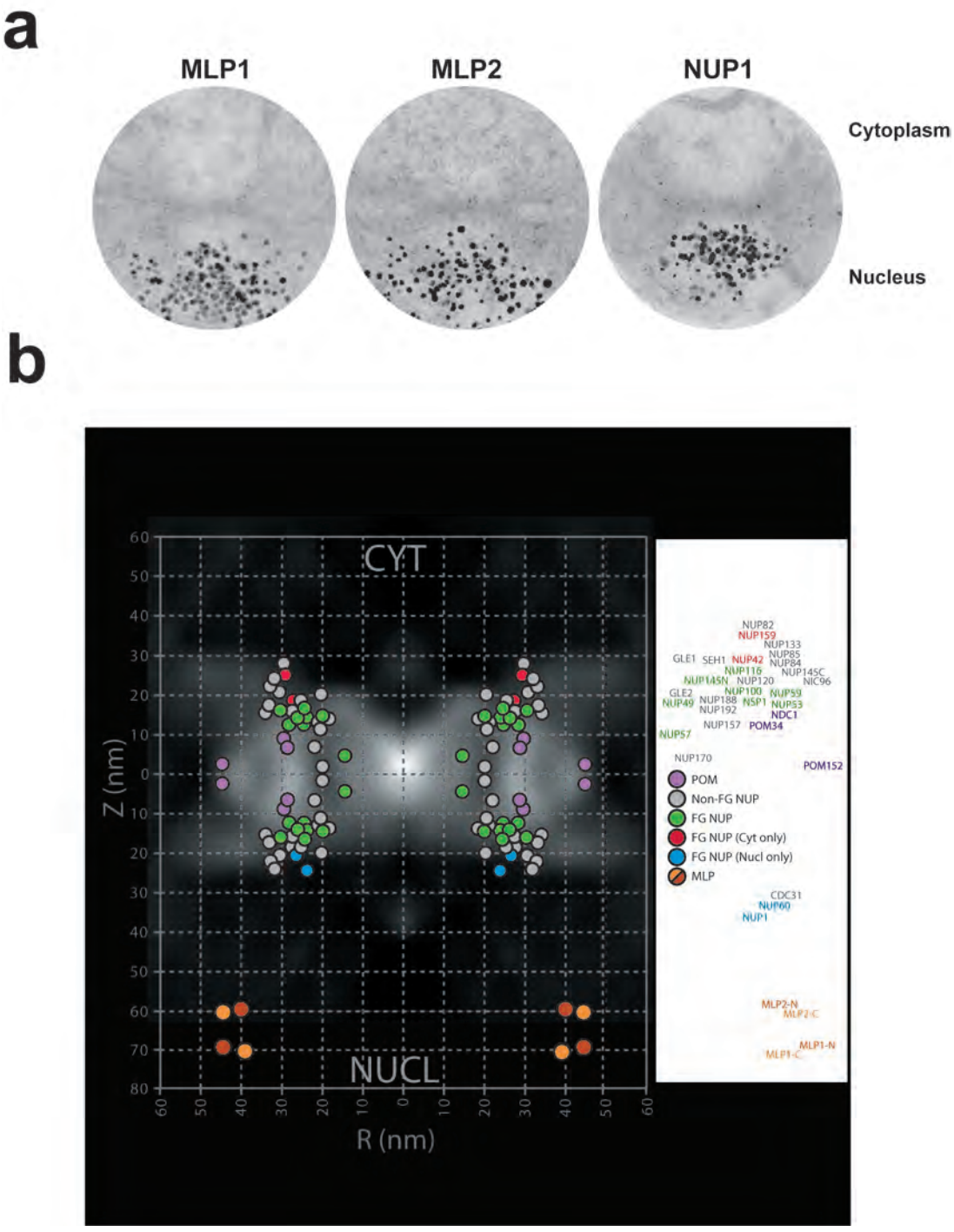
a
MLP1
MLP2
NUP1
Cytoplasm
Nucleus
b
CYT
NUCL
Z (nm)
R (nm)
NUP82
NUP159
NUP133
GLE1
SEH1
NUP42
NUP85
NUP84
NUP116
NUP145C
NUP145N
NUP120
NIC96
GLE2
NUP100
NUP59
NUP49
NUP188
NSP1
NUP53
NUP192
NDC1
NUP157
POM34
NUP57
NUP170
POM152
POM
Non-FG NUP
FG NUP
FG NUP (Cyt only)
FG NUP (Nucl only)
MLP
CDC31
NUP60
NUP1
MLP2-N
MLP2-C
MLP1-N
MLP1-C

Figure 5: **Mlp1p is a highly elongated protein.**

(a) Mlp1p-PrA and Mlp2p-PrA were purified from genomically tagged strains under native conditions using IgG Sepharose and eluted using a peptide competing for the PrA-IgG interaction. The peptide was removed by gel filtration on G25 Quickspin columns. **(b)** Proteins from (a) were separated by centrifugation through a continuous sucrose gradient and fractions were collected for analysis. Western blot of the tagged protein in each collected fraction (top). Plotted intensity and fitted peak curve of the signal detected (bottom). Three marker proteins of known sedimentation coefficients were used to determine the S-value corresponding to each collected fraction. The observed sedimentation coefficient for the soluble Mlp1p-PrA peak is 7.1S. CS.

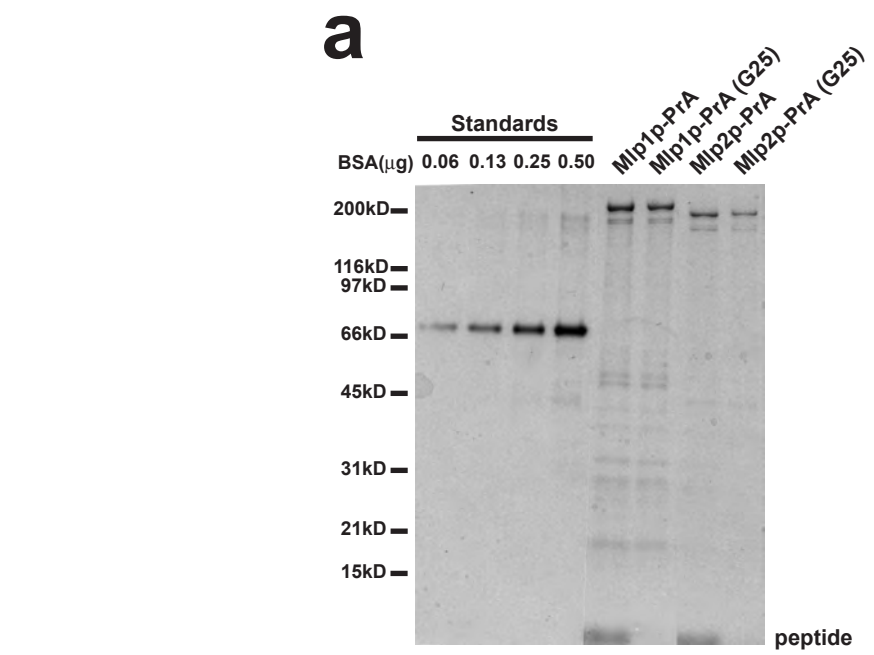
a
Standards
BSA(μg) 0.06 0.13 0.25 0.50
Mlp1p-PrA
Mlp1p-PrA (G25)
Mlp2p-PrA
Mlp2p-PrA (G25)
200kD
116kD
97kD
66kD
45kD
31kD
21kD
15kD
peptide

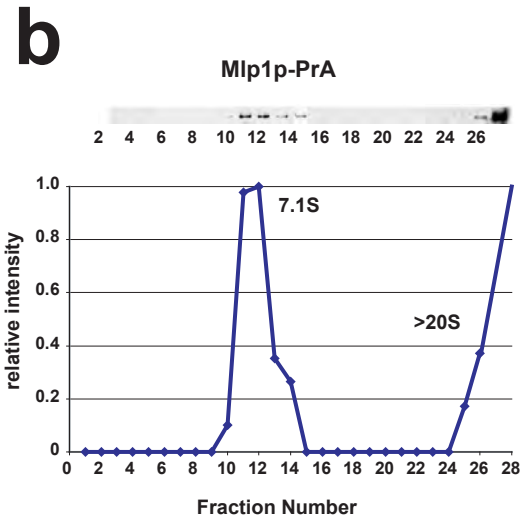
b
Mlp1p-PrA
2 4 6 8 10 12 14 16 18 20 22 24 26
1.0
0.8
0.6
0.4
0.2
0
7.1S
>20S
relative intensity
0 2 4 6 8 10 12 14 16 18 20 22 24 26 28
Fraction Number

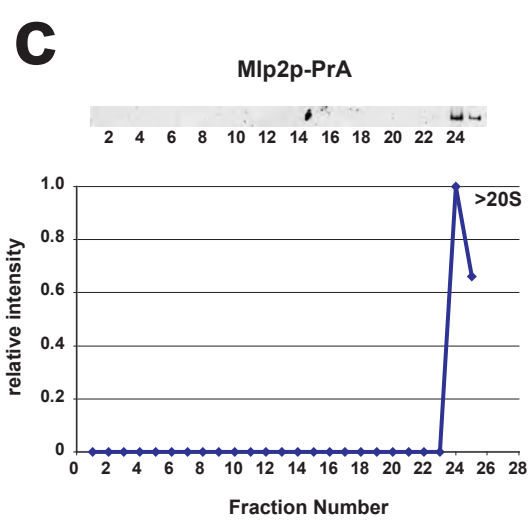
c
Mlp2p-PrA
2 4 6 8 10 12 14 16 18 20 22 24
1.0
0.8
0.6
0.4
0.2
0
>20S
relative intensity
0 2 4 6 8 10 12 14 16 18 20 22 24 26 28
Fraction Number

Figure 6: **Mlp1p and Mlp2p are in complex with each other.**

PrA containing affinity purified complexes (*IP*) and whole cell lysates (*lysate*) of strains co-expressing combinations of **(a)** Mlp1p-PrA or **(b)** Mlp2p-PrA as baits and Myc-tagged Mlp1p or Mlp2p as targets, were probed by immunoblotting for Myc and PrA (*co-expressed*). To control for interactions occurring post-lysis, strains expressing either one PrA-tagged bait or one Myc-tagged target were mixed after cell lysis and analyzed as above (*mixed*). MN.

a

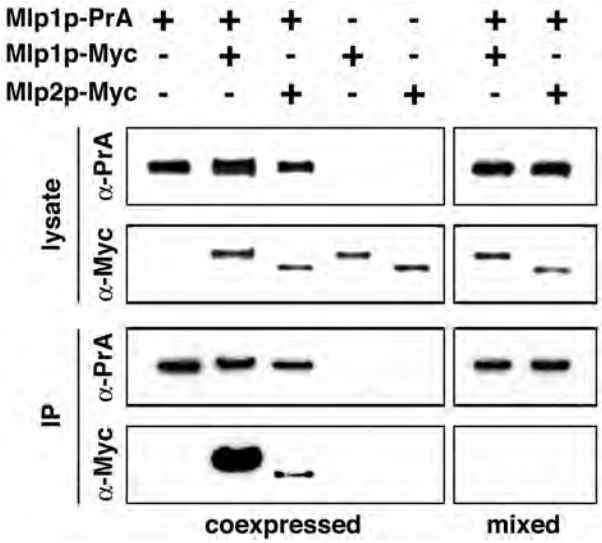
Mlp1p-PrA + + + - - + +
Mlp1p-Myc - + - + - + -
Mlp2p-Myc - - + - + - +
lysate
α-PrA
α-Myc
IP
α-PrA
α-Myc
coexpressed
mixed

b

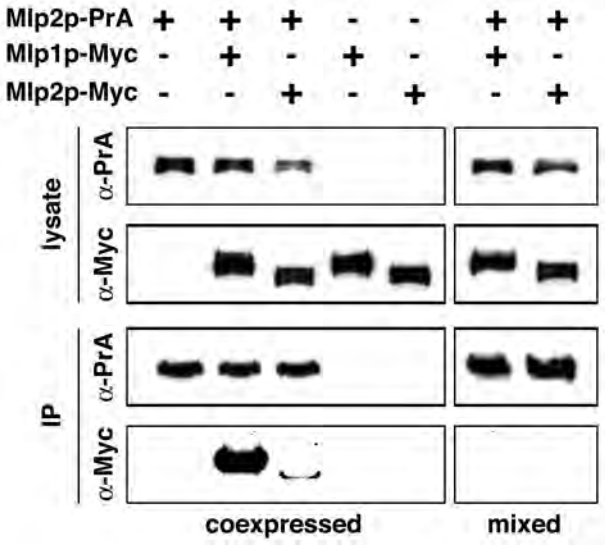
Mlp2p-PrA + + + - - + +
Mlp1p-Myc - + - + - + -
Mlp2p-Myc - - + - + - +
lysate
α-PrA
α-Myc
IP
α-PrA
α-Myc
coexpressed
mixed

Figure 7: ***mlp1*Δ*mlp2*Δ strains have deformed nuclei.**

(a) Schematic view of the determination of the shape factor (r_o/r_i). The shape factor is the ratio of the shortest and the longest distance from the centroid of an object to its edge. Close to circular have a shape factor of approximately 1, while more irregular objects will have a shape factor greater than 1. **(b)** Histogram plot of shape factors. Nup49p-GFP expressing *wild type* and *mlp1*Δ*mlp2*Δ cells were imaged as in Figure 3. The shape factor measurements were collected using the Morphometric Analysis module of MetaMorph. **(c)** Images of individual nuclei from Nup49p-GFP expressing *wild type* and *mlp1*Δ*mlp2*Δ cells. Images were taken every four seconds. To show the deformation the outline of the nucleus at t=0 is superimposed at each timepoint. (b) CS (c) MN.

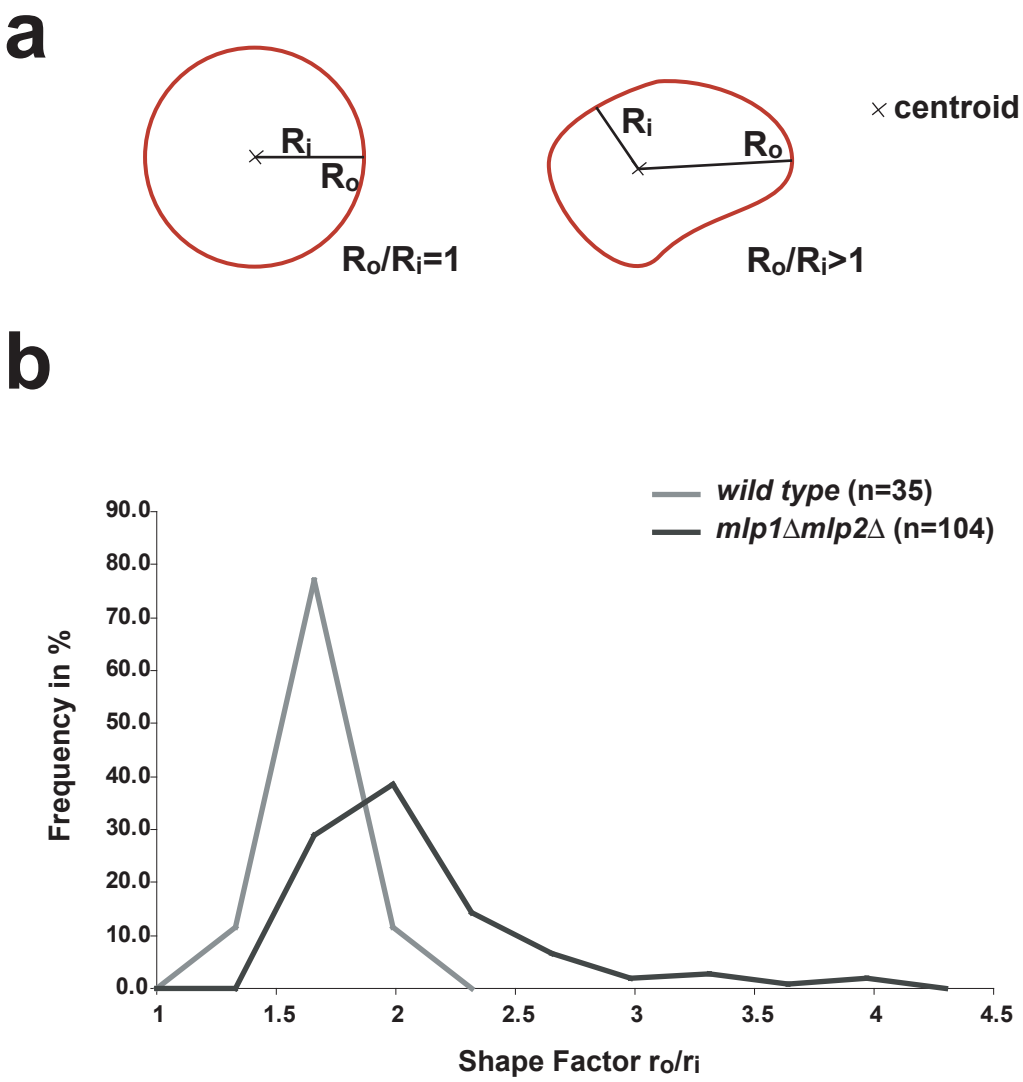
a
Ri
Ro
Ro/Ri=1
Ri
Ro
centroid
Ro/Ri>1
b
wild type (n=35)
mlp1Δmlp2Δ (n=104)
Frequency in %
90.0
80.0
70.0
60.0
50.0
40.0
30.0
20.0
10.0
0.0
1
1.5
2
2.5
3
3.5
4
4.5
Shape Factor ro/ri
c
wild type
0
4
8
12
16
20
24
28
time(sec)
mlp1Δmlp2Δ
0
4
8
12
16
20
24
28
time(sec)

Figure 8: **Mlp proteins stabilize the NE.**

(a) Model on how the presence of Mlp proteins and other factors may influence the stability of the NE. **(b)** Tetraploid *mlp1*Δ*mlp2*Δ cells with an enlarged nuclei show a growth defect at 37ºC. Cells were spotted in 10-fold dilutions on YPD plates and grown for two days at the indicated temperatures. **(c)** Deletion of MLP in a clustering background causes synthetic lethality. A *nup133*Δ*N* clustering strain was mated with a *mlp1*Δ*mlp2*Δ strain. Shown are the genotypes of the recovered spores. MN.

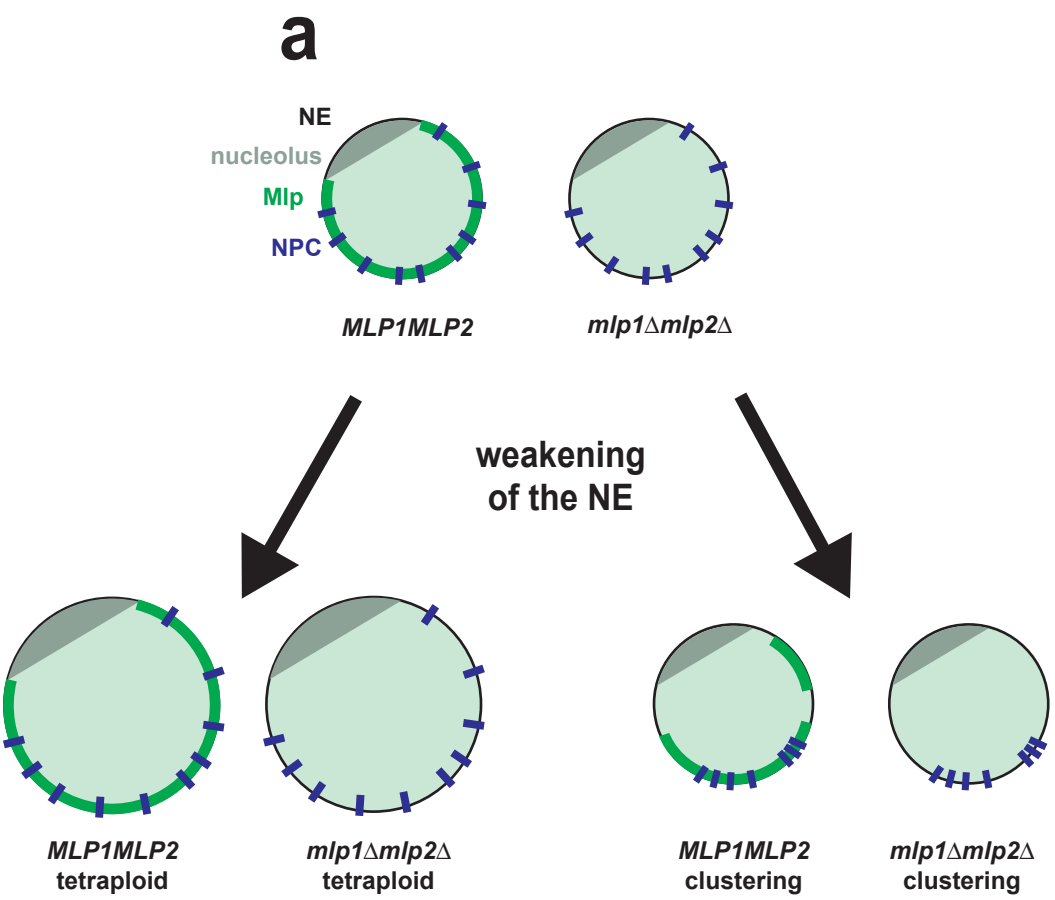

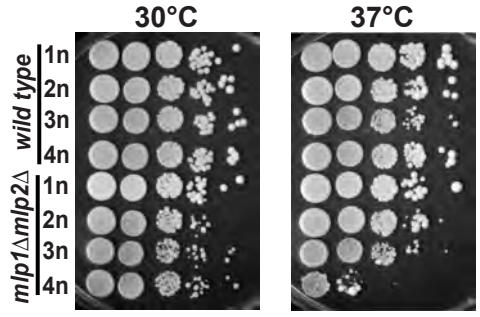

c

nup133ΔN
X
mlp1Δmlp2Δ

	expected	observed
wild type	25%	69%
mlp1Δ	25%	5%
mlp2Δ	25%	25%
mlp1Δmlp2Δ	25%	1%

Chapter 3: Mitotic Defects in *mlp1*Δ*mlp2*Δ.

Previous studies have shown that cells lacking both Mlp proteins exhibit gross morphological alterations: cells are bigger, frequently large budded and often occur as multibudded cells (Strambio-de-Castillia, 1998). Their competitive fitness is reduced in comparison to *wild type* cells (Strambio-de-Castillia et al., 1999) and colonies exhibit signs of clonal lethality (Strambio-de-Castillia, 1998; Zhao et al., 2004). To further investigate the basis for this growth defect, we examined in more detail the role Mlp proteins play in the progression through the cell cycle.

*mlp1*Δ*mlp2*Δ *cells have an abnormal DNA content.*

We first measured the DNA content of asynchronous populations of *wild type* and *mlp1*Δ*mlp2*Δ cells by FACS analysis (Figure 9a). The *wild type* cells showed the normal two peaked distribution typical of an asynchronously growing cell culture, containing roughly 50% of cells with an 1C DNA content. In contrast, in the *mlp1*Δ*mlp2*Δ only 15% of the cells exhibited an 1C DNA content and a significant fraction of cells appeared to have re-replicated their genome. As judged by the side scatter, we also confirmed that the average cell size was increased in the *mlp1*Δ*mlp2*Δ strain (Strambio-de-Castillia, 1998). Analysis of the budding index was in good agreement with the defects observed by FACS analysis (Figure 9b). Approximately 50% of *wild type* cells were unbudded, corresponding to the cells with 1C DNA content, while in the *mlp1*Δ*mlp2*Δ strain we

found only 20% of cells without a bud. In addition, a disproportionally large number of cells in the *mlp1*Δ*mlp2*Δ culture had abnormally large buds or was multibudded, probably corresponding to the cells with a DNA content larger than 2C. The data shows that *mlp1*Δ*mlp2*Δ do not progress normally through mitosis. They sometimes re-replicate their genome and form a new bud before cytokinesis has occurred.

*mlp1*Δ*mlp2*Δ *cells are impaired in the transition from metaphase to anaphase.*

To examine the defect in cell cycle progression in more detail, we expressed Spc42p-GFP or GFP-Tub1p in *wild type* and cells lacking the *MLP* genes, visualizing the spindle and the SPB in asynchronous cultures.

While the SPBs in *wild type* and *mlp1*Δ appeared normal, cells lacking Mlp2p showed an excess number of cells with two SPBs per nucleus as compared to *wild type* and *mlp1*Δ cells, indicating a difficulty in proceeding past the initial stages of SPB maturation and separation (Figure 10a). Consistent with this observation, we found that the number of cells between S-phase and metaphase with an abnormally short distance between SPBs (i.e. 1μm or less) was significantly increased in mutants lacking Mlp2p with respect to *wild type* (Figure 10c and d). This points to a role for Mlp2p in facilitating SPB separation and in promoting the formation of a complete metaphase spindle (Byers and Goetsch, 1975a). The SPBs in the *mlp1*Δ*mlp2*Δ cells showed an even more pronounced phenotype. Cells often exhibited three or more Spc42p-GFP containing foci, making up nearly 20% of the total *mlp1*Δ*mlp2*Δ population. We did not observe a high incidence of SPB doublets as in the *mlp2*Δ strain and the distance between SPBs appeared to be

normal. It should be noted that cells with more than two MTOC were not used for the SPB distance measurements.

We also found striking morphological changes in the spindles of *mlp1*Δ*mlp2*Δ cells (Figure 10b). Some spindles were very large and hyperpolymerized, often forming a multipolar structure, which completely filled the budneck. The spindles also were often short and thick, and were localized closer to the budneck, in comparison to the *wild type* spindles. Although some of these altered spindles did manage to invade the budneck, they did not show the typical thin and elongated morphology of anaphase spindles. The high incidence of these aberrant spindles was reflected in the spindle morphology index, which illustrated that significantly more *mlp1*Δ*mlp2*Δ cells were in transition from S to early M than in the *wild type* control (Figure 10c). In cells lacking Mlp2p we observed an increased incidence of short spindles with respect to *wild type* and *mlp1Δ* cells, characteristic of cells transitioning between S-phase and early mitosis (Figure 10b and c).

We further measured the spindle migration index, the minimal distance between the spindle and the bud neck in cells with an early spindle configuration normalized for cell size (Figure 10e). While we observed no significant difference between *wild type*, *mlp1*Δ and *mlp2*Δ cells in this assay, we found that spindles in cells lacking Mlps migrated much closer to the budneck than the *wild type* control, also indicative of a delayed progression past metaphase. These results exclude a defect in nuclear migration to the bud neck, suggesting that the Mlp proteins are not involved in the regulation of the activity of cytoplasmic microtubules.

mlp1Δmlp2Δ require a functional DNA checkpoint for normal growth.

Since the *mlp1Δmlp2Δ* strain exhibits altered DNA content, increased intranuclear microtubule organizers and aberrant spindles, we tested this strains' dependence on specific cell cycle checkpoints. We performed plating assays of *mlp1Δmlp2Δ* and control cells deficient for either the DNA damage checkpoint or the two spindle check points (Figure 11a). We found that *mlp1Δmlp2Δ* cells had a slightly lower plating efficiency than their *wild type* control strain, consistent with an overall growth defect. When both spindle checkpoints were removed, the plating efficiency of neither the *wild type* nor the mutant was substantially altered. However, *mlp1Δmlp2Δ* cells deficient in the DNA damage checkpoint showed a strong reduction in plating efficiency in comparison to their control strain, suggesting that DNA damage might occur in the Mlp deletion strain at elevated levels or that DNA repair is impaired. One consequence of an elevated rate of DNA damage might be a reduced fidelity of chromosome segregation. Indeed, we found the rate of chromosome loss in the *mlp1Δmlp2Δ* strain to be more than one order of magnitude higher than in the *wild type* control, while the single MLP deletions do not exhibit a similar defect (Figure 11b). These observations suggest that the appropriate response to DNA damage, namely the arrest of the cell cycle and repair of the DNA, is impaired in strains lacking both Mlp proteins.

Even though the *mlp1Δmlp2Δ* strain did not exhibit an obvious genetic interaction with the spindle checkpoint genes, we tested whether Mlp deletion alone, or in conjunction with deletion of these checkpoints causes sensitivity to the spindle depolymerization agent benomyl. While there appeared to be no increased sensitivity to

benomyl in the *mlp1*Δ*mlp2*Δ strain by itself or in the context of *mad1*Δ, the deletion of *BUB2* significantly decreased the viability in the *mlp1*Δ*mlp2*Δ strain (Figure 11c). A similar effect was observed in the *mad1*Δ*bub2*Δ double deletion. This suggests that under conditions where the spindle structure is weakened, the cell lacking Mlps show an increased dependence on the presence of the Bub2p spindle checkpoint. This is in agreement with the increased frequency of multibudded cells with greater than 2C DNA content, since Bub2p has been implicated in preventing the occurrence of multibudded cells (Daum et al., 2000). It is interesting to note that the *mlp1*Δ*mlp2*Δ strain does not have a dependency for the presence of Mad1p, which is part of the checkpoint monitoring the transition from metaphase to anaphase. This suggests that the metaphase delay observed in the *mlp1*Δ*mlp2*Δ cells is not caused by a defect in capturing the kinetochores.

Deletion of the single MLP genes does not show an increased sensitivity to benomyl over the *wild type* control strain. Only in conjunction with the inactivation of both spindle checkpoints by deletion of *BUB2* and *MAD1* did we find an approximately tenfold higher sensitivity to benomyl in both the *mlp1*Δ and the *mlp2*Δ strain as compared with *wild type*. These results suggest that if unperturbed, the strains lacking either Mlp1p or Mlp2p do not develop spindle failures that lead to the activation of cell cycle checkpoints. Only in the presence of a spindle depolymerization agent do the *MLP1* and *MLP2* deletion strains show an elevated dependence on the spindle checkpoint, possibly due to cumulative damage to the spindle.

Ageing

Loss of genomic stability has been linked to premature ageing in humans and yeast (reviewed in Bitterman et al., 2003). In addition, mutations of the lamina causing a weakening of the NE in higher eukaryotes have been implied to cause certain types of progeria (De Sandre-Giovannoli et al., 2003; Eriksson et al., 2003). In yeast cells, the phenotypes of premature ageing include an increase in cell size, lengthening of the generation time, morphological changes to the nucleolus, loss of silencing and loss of genomic stability (Bitterman et al., 2003). Since the *mlp1*Δ*mlp2*Δ strain does exhibit a number these phenotypes (this study; Strambio-de-Castillia, 1998; Strambio-de-Castillia et al., 1999), we tested if loss of Mlp proteins causes premature ageing.

To this end we separated newly budded daughter cells from their mothers and spotted them onto a dissection plate. We followed individual cells through their complete lifespan, by moving away each newly formed daughter cell, until all the original daughter cells had ceased dividing. We found that while the maximum lifespan in *mlp1*Δ*mlp2*Δ was similar to *wild type* strains, the mean lifespan for the *mlp1*Δ*mlp2*Δ was reduced by about 25% in comparison to their *wild type* counterparts (Figure 12). However, this difference was not as drastic as seen in other yeast mutants (Sinclair and Guarente, 1997). Therefore we did not confirm whether other criteria for premature ageing are met in the *mlp1*Δ*mlp2*Δ strain. It is likely that the reduced mean survival rate in the Mlp mutant strain is caused by cells terminally arresting because of the frequent occurrence of intranuclear microtubule organizers, which cause irresolvable problems during mitosis.

Figure 9: ***mlp1*Δ*mlp2*Δ display increased re-budding and increased DNA content.**

(a) FACS analysis of asynchronous *wild type* and *mlp1*Δ*mlp2*Δ cultures, showing cell size and DNA content by propidium iodide signal. **(b)** Budding index of asynchronous *wild type* and *mlp1*Δ*mlp2*Δ cultures. MN.

a

FACS Analysis

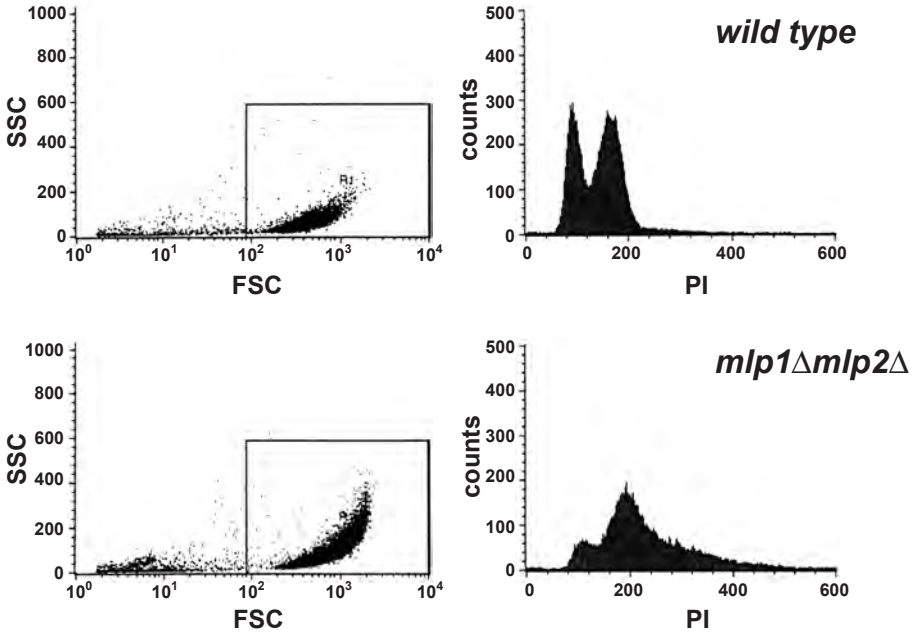

b

Budding Index

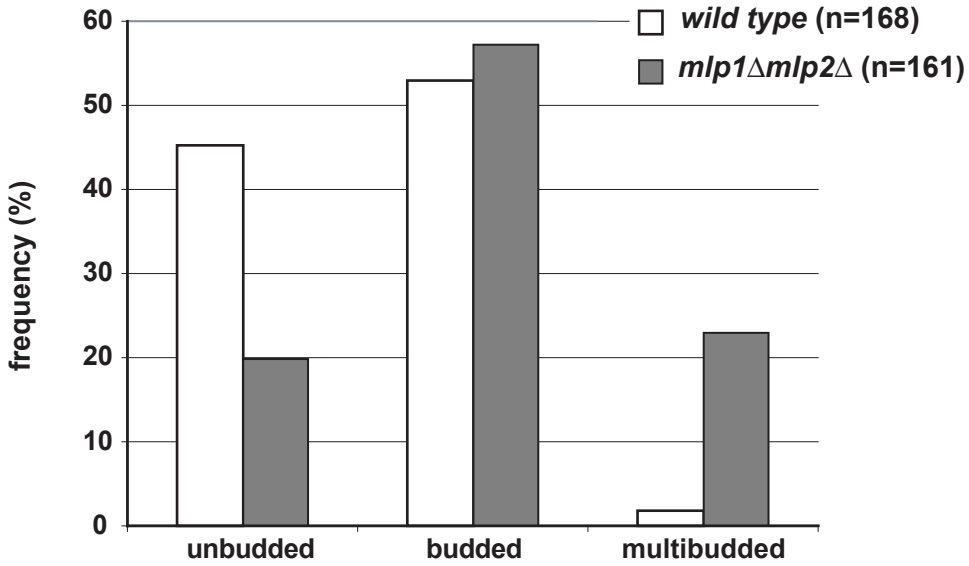

Figure 10: ***mlp1Δmlp2Δ* cells have aberrant SPBs and spindles.**

Images of *wild type* and *mlp1Δmlp2Δ* cells expressing GFP-Tub1p **(a)** or Spc42p-GFP **(b)**. Images were obtained as described for Figure 3. **(c)** Cells with monopolar spindles (*G1*), short spindles (*S to early M*), or elongated spindles spanning the bud neck (*anaphase*) were scored for each cell samples (n>300; two repeats; error bars, +/- standard deviation). **(d)** Tukey plots displaying the SPB-to-SPB distance distribution in *wild type* and mutant cells lacking either Mlp1p or Mlp2p. Only cells between S and early M were used for this analysis. The top and bottom of each rectangle represent the 75th and 25th percentiles, respectively; the center bar of the rectangle marks the median SPB-to-SPB distance. The top and bottom horizontal marks show the 90th and 10th percentiles, respectively. Black dots represent outlying data points. The median SPB-to-SPB distance was 1.58µm (n=60) in *wild type*, 1.35µm (n=54) in *mlp1Δ*, 1.10µm (n=120) in *mlp2Δ* and 1.82µm (n=53) in *mlp1Δmlp2Δ* cells. Comparisons by the Sudent's t test showed a high degree of significance in all cases: *wild type* versus *mlp1Δ*, $P < 0.0003$; *wild type* versus *mlp2Δ*, $P < 0.0001$; *wild type* versus *mlp1Δmlp2Δ*, $P < 0.0003$. **(e)** The spindle migration index was scored for *wild type* and mutant cells presenting a short spindle. The mean spindle migration index was 0262µm (n=59) in *wild type* cells and 0157µm (n=122) in *mlp1Δmlp2Δ* cells. Comparison by Sudent's t test shows a high degree of significance between *wild type* versus *mlp1Δmlp2Δ*, $P < 0.00001$. Bar, 2µm. CS.

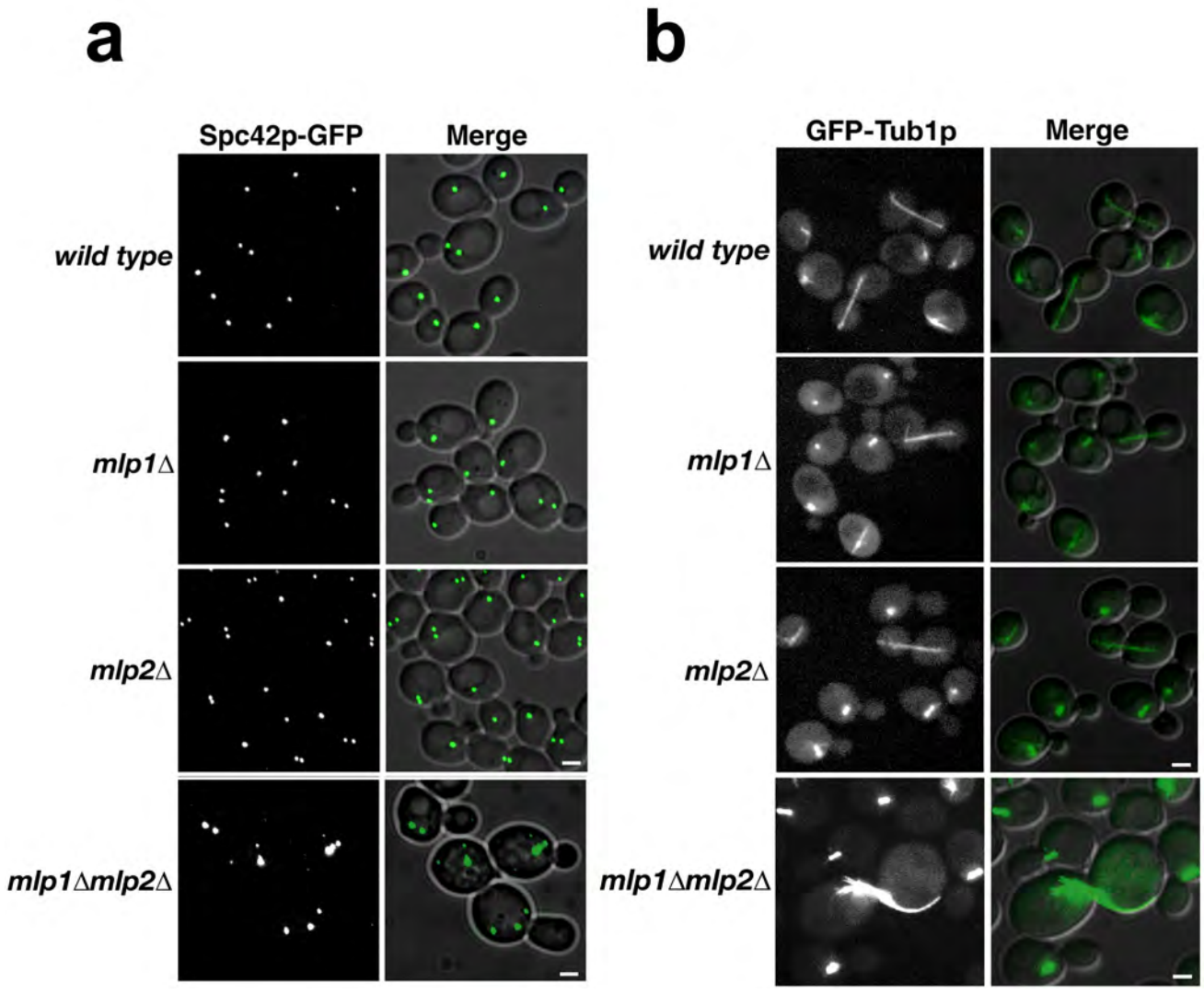
a
Spc42p-GFP
Merge
wild type
mlp1Δ
mlp2Δ
mlp1Δmlp2Δ
b
GFP-Tub1p
Merge
wild type
mlp1Δ
mlp2Δ
mlp1Δmlp2Δ

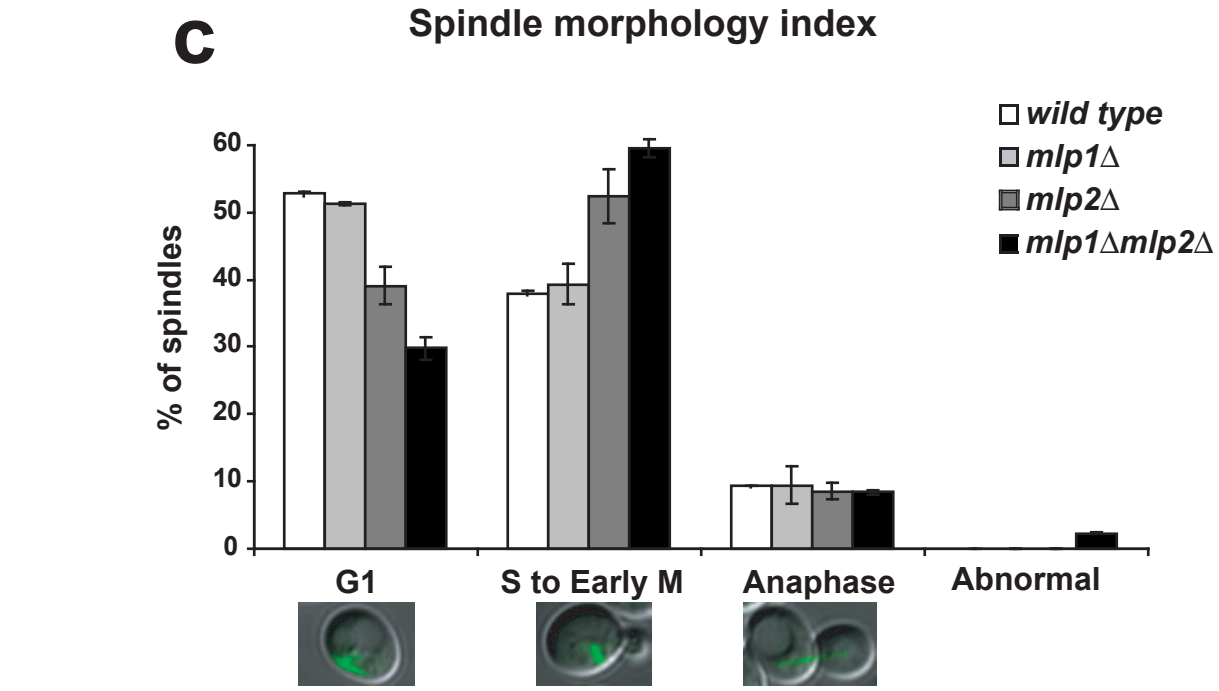
c
Spindle morphology index
wild type
mlp1Δ
mlp2Δ
mlp1Δmlp2Δ
% of spindles
60
50
40
30
20
10
0
G1
S to Early M
Anaphase
Abnormal

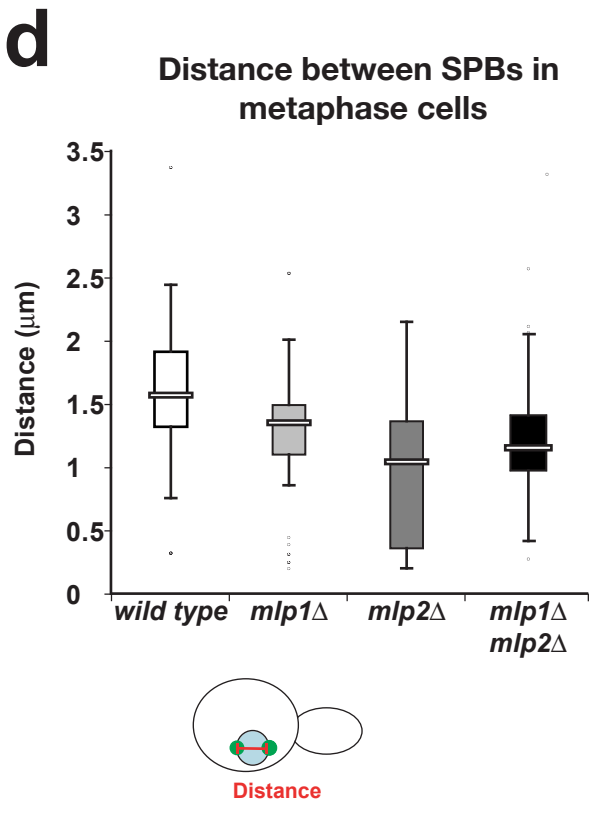
d
Distance between SPBs in metaphase cells
Distance (μm)
3.5
3
2.5
2
1.5
1
0.5
0
wild type
mlp1Δ
mlp2Δ
mlp1Δ mlp2Δ
Distance

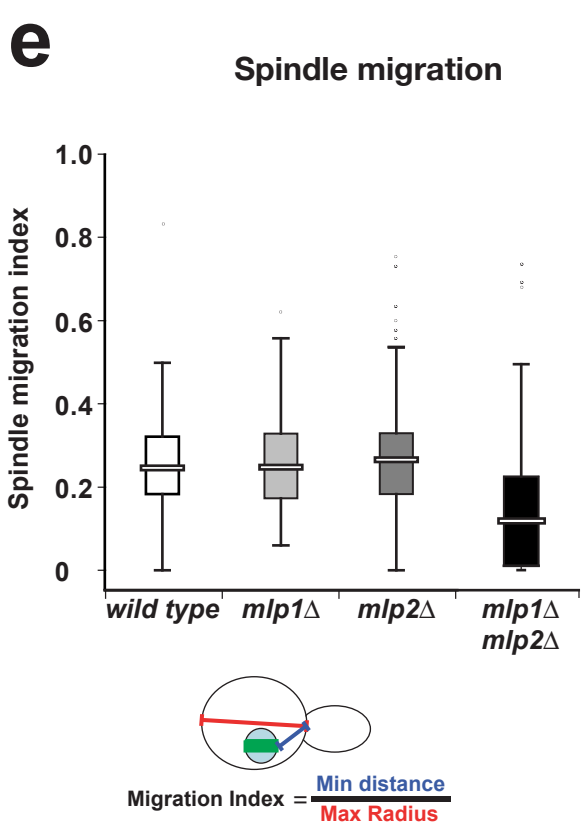
e
Spindle migration
Spindle migration index
1.0
0.8
0.6
0.4
0.2
0
wild type
mlp1Δ
mlp2Δ
mlp1Δ mlp2Δ
Migration Index = Min distance / Max Radius

Figure 11: ***mlp1*Δ*mlp2*Δ have increased DNA damage and are sensitive to the loss of *BUB2* in the presence of benomyl.**

(a) Equal numbers of cells of the indicated strains were grown on YPD plates for two days to test for the effects of loss of the spindle checkpoints (*mad1*Δ*bub2*Δ) or the DNA damage checkpoint (*mec1*Δ*sml1*Δ). Colony numbers were normalized against growth of *wild type* cells. **(b)** The frequency of chromosome loss in *wild type* and *mlp1*Δ*mlp2*Δ cells was determined by a chromosome III stability assay. **(c)** The sensitivity to benomyl was determined by spotting 5-fold dilutions of the indicated strains onto benomyl containing YPD plates or benomyl free control plates. Mlp deletion strains and a control strain were tested for the effects of the presence (+) or absence (-) of the *MAD1* or *BUB2* spindle checkpoint pathways. (a and b) Averages of three experiments are shown with the standard deviation as error bars. MN.

a

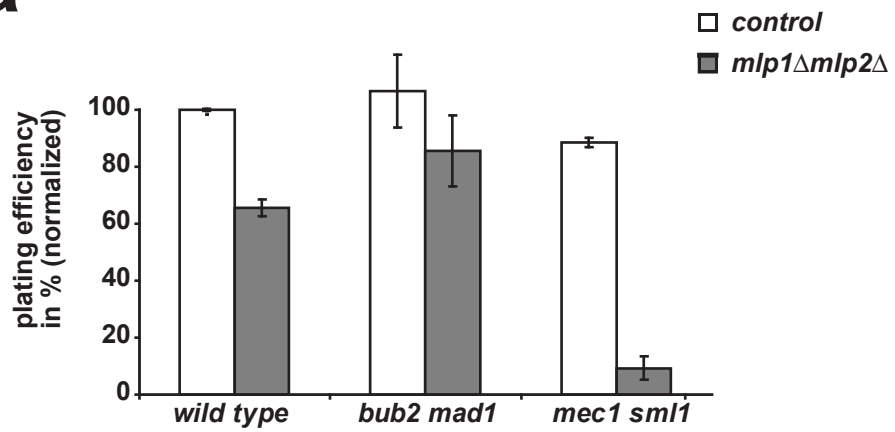
control
mlp1Δmlp2Δ
plating efficiency in % (normalized)
100
80
60
40
20
0
wild type
bub2 mad1
mec1 sml1

b

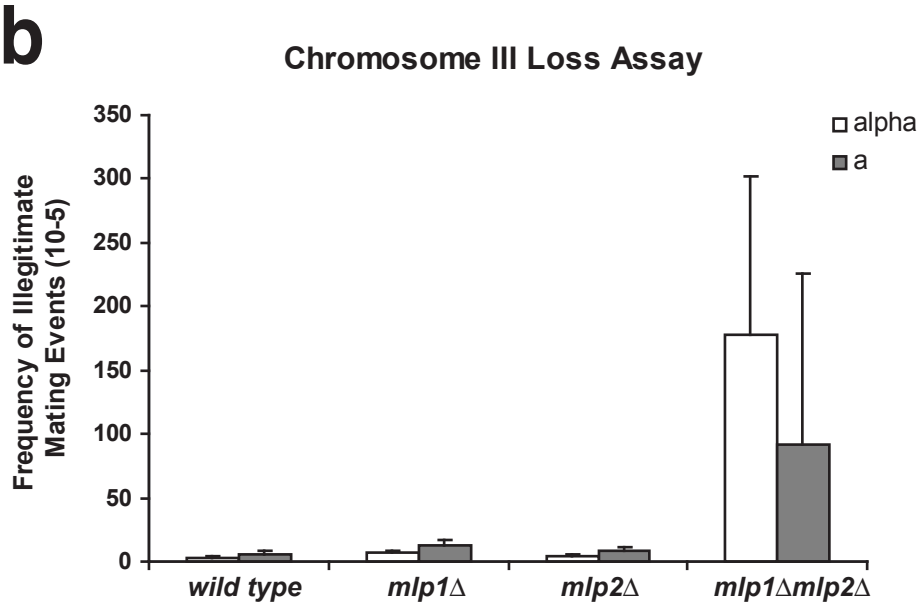
Chromosome III Loss Assay
alpha
a
Frequency of Illegitimate Mating Events (10-5)
350
300
250
200
150
100
50
0
wild type
mlp1Δ
mlp2Δ
mlp1Δmlp2Δ

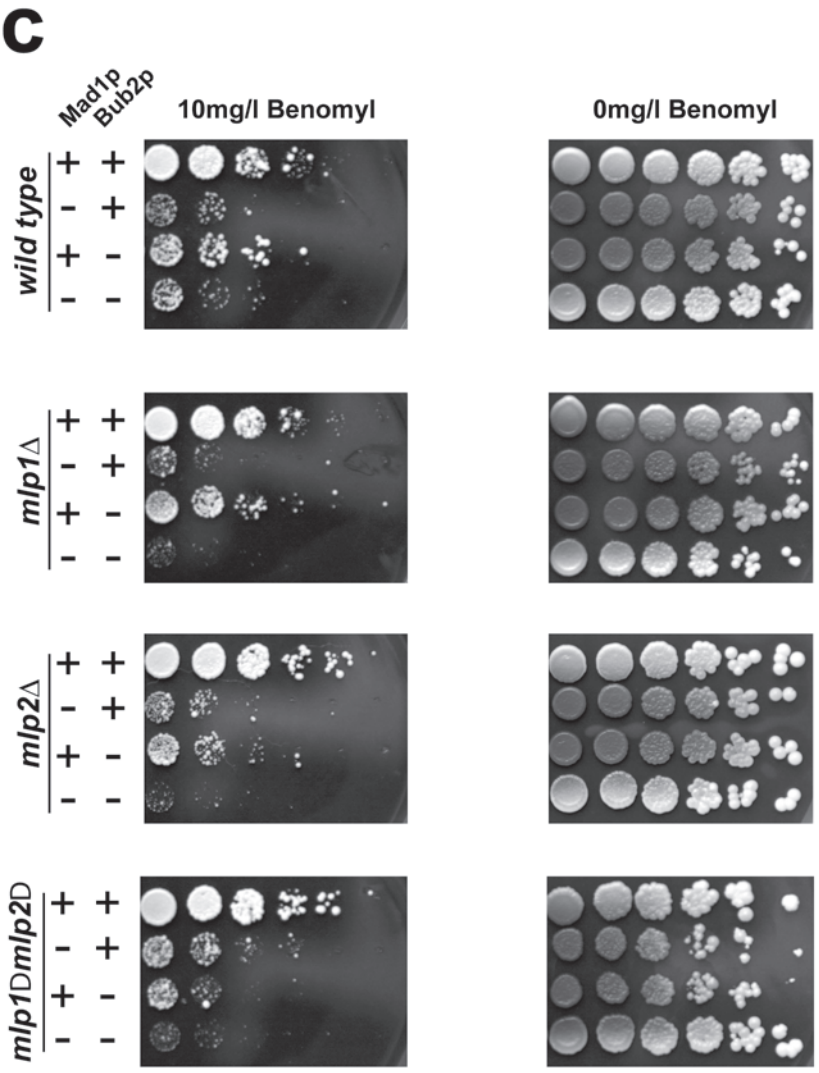
c
Mad1p
Bub2p
10mg/l Benomyl
0mg/l Benomyl
wild type
mlp1Δ
mlp2Δ
mlp1Δmlp2Δ
+ +
- +
+ -
- -

Figure 12: **The *mlp1*Δ*mlp2*Δ strain enters senescence prematurely.**

Wild type and *mlp1*Δ*mlp2*Δ cells were tested in an ageing assay. Newly budded daughter cells are separated from their mothers and spotted onto a dissection plate. Individual cells are followed through their complete lifespan by moving away each newly formed daughter cell, until all the original cells cease dividing. The percent survival is plotted against the generation number. The mean survival rate, the generation at which 50% of the tested cells cease dividing, is 17.8 for *wild type* and 13.8 for *mlp1*Δ*mlp2*Δ cells. The experiment was repeated once with similar results. CS and MN.

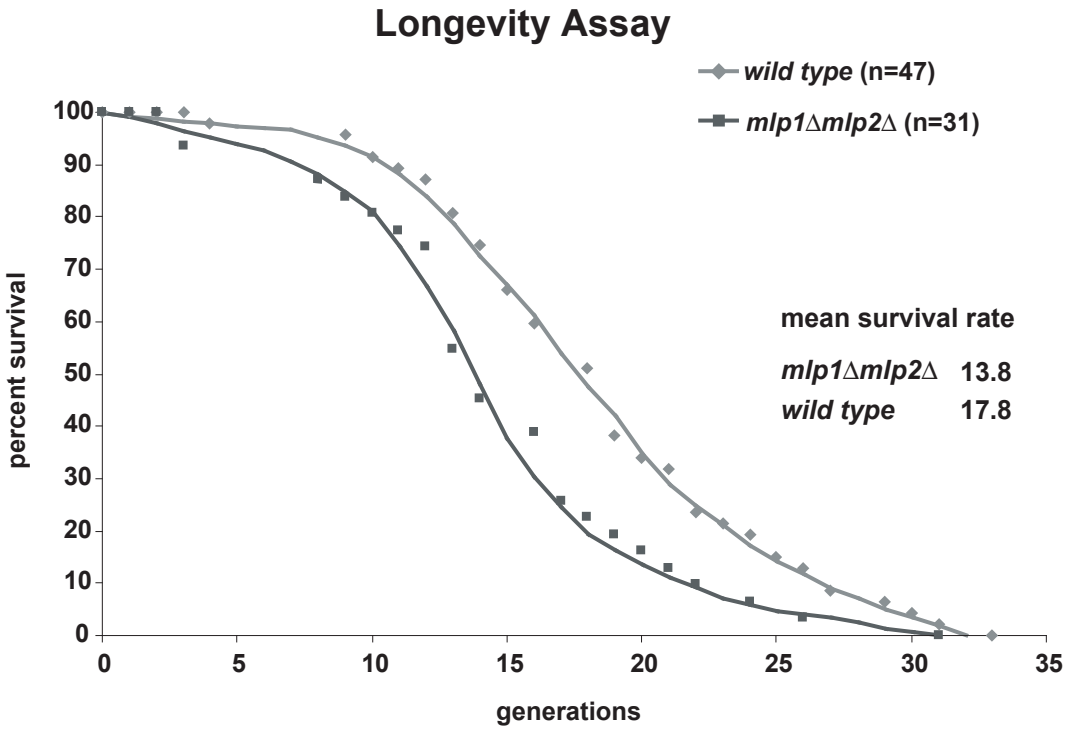
Longevity Assay
wild type (n=47)
mlp1Δmlp2Δ (n=31)
mean survival rate
mlp1Δmlp2Δ 13.8
wild type 17.8
percent survival
generations
0
10
20
30
40
50
60
70
80
90
100
0
5
10
15
20
25
30
35

Chapter 4: Mlp Proteins and Nuclear Transport.

Background.

The compartmentalization of the genetic material into the nucleus in eukaryotic cells necessitates the regulated exchange of material across the double-membraned NE. This nucleocytoplasmic transport is mediated exclusively by the NPC. mRNPs and ribosomal subunits are synthesized and processed within the nucleus, but must be exported to the cytoplasm, while a number of the proteins synthesized in the cytoplasm must be imported into the nucleus, for example ribosomal proteins. The components required for transport can be divided into two classes: the stationary phase, consisting of the NPC embedded into pores within the NE and the mobile phase, consisting of the transport substrates, transport factors and RAN and its regulators (reviewed in Rout and Aitchison, 2000).

The yeast NPC is a large organelle of about 50MDa (Rout and Blobel, 1993), consisting of an eightfold symmetrical, cylindrical assembly (~100nm diameter) with a central tube (~30nm diameter) connecting the nucleoplasm and the cytoplasm. Notwithstanding its mass, the NPC is comprised only of about 30 different proteins, termed nucleoporins (Nups), most of which are present as two copies per one of the eight spokes, each copy localized symmetrically on either side of the NE. The Nups can be separated into the membrane proteins, which anchor the NPC to the NE, structural Nups, which give the NPC its overall shape and anchor the third class, termed FG Nups,

because they contain multiple copies of a phenylalanine-glycine motif. The FG Nups provide the main binding sites for transport factors and are present in ~200 copies per NPC or half the mass of the NPC. Interestingly, they appear to be the major component of the filament-like extensions at either face of the pore. It appears that this arrangement of FG Nups is the key to the function of the NPC. By their presence alone, the FG Nups form an energy barrier to large molecules, blocking them from freely entering the central tube of the NPC from either side. Molecules that need to be transported through the pore can overcome this barrier by specifically increasing their affinity to the FG Nups during transport and lowering their affinity to the FG Nups once transport has concluded. This process is facilitated by the mobile phase of nuclear transport (reviewed in Rout et al., 2003).

Macromolecules larger than ~40kD, the diffusion limit of the NPC (Adam, 2001), require the mediation of soluble transport factors in order to cross the NE. These factors are called karyopherins (Kaps) and are recruited to the cargo by small regions protein sequences called nuclear localization signals (NLS) for importing cargo into the nucleus and nuclear export signals (NES) for exporting cargo into the cytoplasm. A classical NLS, like the bipartite nucleoplasmin NLS (Dingwall et al., 1982) or the monopartite SV40 large T-antigen NLS (Kalderon et al., 1984), consist of a short stretch of basic amino acids. Other NLS have been identified, for example the RL25-NLS of the ribosomal protein Rpl25p (Schaap et al., 1991) or the RGG-NLS of the nuclear protein Nab2p (Truant et al., 1998). The most commonly found NES is rich in leucine or other hydrophobic amino acids, but other efficient NESs can have different sequences (Klemm et al., 1997). Upon binding to their cargo, the Kaps undergo a conformational change

which allows them to dock to the NPC via the FG-repeats of the peripheral nucleoporins (Iovine et al., 1995; Iovine and Wente, 1997; Radu et al., 1995) and translocate through the central tube of the NPC. The cargo/karyopherin complex then dissociates, releasing the cargo at its destination and freeing the karyopherin to facilitate another round of transport.

Transport is driven by a concentration gradient of the small GTPase Ran. Ran-GDP is predominantly found in the cytoplasm while the majority of nuclear Ran is bound to GTP (Izaurralde et al., 1997). This gradient is maintained by sequestering the Ran GTPase-activating protein in the cytoplasm (Hopper et al., 1990) and the Ran guanine nucleotide exchange factor in the nucleus, where it is tightly bound to chromatin (Ohtsubo et al., 1989). Ran mediates correct transport by stabilizing or destabilizing the interaction between the karyopherin and its cargo, by causing conformational changes in the karyopherin that displaces the cargo (Chook and Blobel, 1999; Vetter et al., 1999). Ran-GTP in the nucleus promotes the dissociation of karyopherin bound to an NLS (Floer et al., 1997; Moroianu et al., 1996), while Ran-GDP promotes the dissociation of transport factors bound to an NES (Askjaer et al., 1999; Floer and Blobel, 1999). Thus, the cargos are released and retained in their appropriate target compartments.

Recent observations have suggested that the NPC is far more versatile in its functions, than was suggested by the initial model for transport. For example, there appears to be a soluble pool of the FG repeat containing Nup2p, which shuttles between the nucleoplasm and the cytoplasm, possibly aiding in the distribution of karyopherins (Dilworth et al., 2001). The transport machinery has been implicated in regulating transcription by binding preferentially to transcriptionally active regions of the genome (Casolari et al.,

2004). Components of the cell cycle checkpoints reside at the NPC until activated (Iouk et al., 2002). This suggests that the transport machinery is not just dedicated to facilitate the macromolecular exchange across the NE, but rather is a multifunctional complex, involved in a number of diverse cellular processes, signifying a further level of regulation afforded by the interaction of nuclear components with the nuclear periphery.

Early studies on the *mlp1*Δ*mlp2*Δ strain showed that the import rate and diffusion rate of a reporter protein fused to the NLS of the SV40 T antigen is impaired (Strambio-de-Castillia et al., 1999) and the depletion of Tpr can lead to defects in protein export (Frosst et al., 2002). We therefore set out to extend the study on the role of Mlp proteins in the transport of proteins across the NE.

Transport assay.

To test in detail the effects of the removal of Mlp proteins on nucleocytoplasmic transport, we devised a novel modification of the published yeast nucleocytoplasmic import assay (Shulga et al., 1996) that has made data collection automatic and quantitative (Figure 13). Yeast transformed with an NLS-GFP expression plasmid, were grown to mid-log phase and the two strains to be compared were labeled covalently with different fluorescent dyes on their cell walls. The cells were then mixed together in equal cell numbers and treated together for the remainder of the experiment. Thus, all subsequent procedures are internally controlled for experimental variations. The cells were resuspended in a metabolic poison, causing ATP production to stop and thereby halting active transport. Thus, allowing the NLS-GFP cargoes to diffuse through the NPC

and become fully equilibrated between nucleus and cytoplasm. For each import assay a small sample of the poisoned cells was washed and resuspended in glucose containing media on a microscopy slide. With ATP production recovering within seconds, images of the NLS-GFP cargo were taken at interval of thirty seconds for seven minutes. After collection of the timecourse reference images of the fluorescent cell wall dyes were taken to discriminate between the two cell types used. For analysis, 2D projections of z-stacks are created and the integrated fluorescence intensity of the nucleus and cytoplasm were measured for each cell. Transport curves were plotted as percent change of nuclear accumulation (NA; nuclear versus cytoplasmic signal) over time and NA rates were determined as the maximum change of NA over time.

Nuclear accumulation rates are decreased in mlp1Δmlp2Δ cells.

Using GFP fused to the RL25-NLS as a transport substrate, we found that NA was slowed down in the *mlp1Δmlp2Δ* strain (Figure 14a). When plotting the average progression of NA for all cells measured, we saw that the highest rate of NA was reached at roughly sixty seconds after release from the poison for both strains. However, the maximum rate of NA in the *wild type* (R_{wt}=0.34) strain was markedly higher than in the mutant (R_{mut}=0.23). Under the conditions tested, transport had not reached equilibrium at seven minutes, precluding us from determining whether the steady state distribution in both strains is equal. To statistically analyze the difference in NA rates, we plotted the individual import rates of each measured cell as a histogram (Figure 14b). While nearly fifty percent of all *mlp1Δmlp2Δ* cells measured fell into the two categories with the

lowest NA rate, the *wild type* cells showed predominantly a higher rate of NA. Comparison by a z-test determined that the difference between the two strains was significant ($p<0.0001$).

When testing the RGG-NLS substrate we obtained results similar to the RL25-NLS. Looking at the average NA curve, we found that NA proceeded slower in the *mlp1*Δ*mlp2*Δ strain ($R_{mut}=1.0$) than in the *wild type* control ($R_{wt}=1.8$; Figure 15a). Also the distribution of NA rates of the *mlp1*Δ*mlp2*Δ was skewed towards the lower end of the plot (Figure 15b). In a z-test analysis, the difference observed was significant ($p<0.0175$).

These results are in close agreement with data published previously on the import of SV40-NLS substrates in *mlp1*Δ*mlp2*Δ cells (Strambio-de-Castillia et al., 1999). It is interesting to note that in our assay the RL25 substrate accumulates in the nucleus at a much higher rate than the RGG substrate, in good agreement with experimentally determined import rates for these substrates in *wild type* strains (Timney et al., manuscript in preparation), suggesting that the NA rates of different cargoes plotted in Figures 14a and 15a are proportional to the absolute import rates for these substrates.

*Aberrant mlp1*Δ*mlp2*Δ *cells are not the predominant cause of slow nuclear accumulation.*

Since the *mlp1*Δ*mlp2*Δ strain exhibits clonal defects, and a number of cells are part of large cell chains with altered morphology, it is possible that the reduced rate of NA is due to a drastically reduced rate in the subset of these morphologically abnormal cells. To determine if this is indeed the case, we divided the *mlp1*Δ*mlp2*Δ cells into groups with either normal or aberrant appearance and plotted their NA rates separately (Figure 16a).

As comparison, the *wild type* curve from Figure 14a was included in the graph. Overall, the NA appeared to be identical for both groups of cells, suggesting that there is no specific correlation with the morphological appearance of the cells and the NA rates. When looking at the distribution of NA rates, again we found no significant difference between the two groups (Figure 16b).

This result is in agreement with the distribution of NA rates we observed in Figures 14b and 15b. If the reduced rate of import in the *mlp1*Δ*mlp2*Δ were due to a drastically reduced rate of import in a subset of cells, while the remaining fraction of the population behaved like *wild type* cells, we should have seen a distribution with two peaks. Instead we found the overall distribution of RA rates was merely shifted towards the lower end.

Steady State Distribution.

To draw meaningful conclusions from the reduced NA rates observed for the RGG-NLS and RL25-NLS reporter in the mutant strain, we had to determine how the steady state distribution of the cargoes was affected by the same mutation. Since the transport assays were not carried out long enough for transport to reach equilibrium, we determined the steady state distribution in a separate experiment by measuring the ratio of nuclear versus cytoplasmic distribution of the reporter in untreated cells. In addition to the RGG-NLS and RL25-NLS substrates used for the previous experiments, we also tested the SV40-NLS used in an earlier study (Strambio-de-Castillia et al., 1999). Furthermore, we also determined the steady state distribution in cells lacking either only Mlp1p or only Mlp2p.

For neither of the substrates measured we found a significant change in the steady state distribution in cells lacking Mlp proteins (Figure 17). In particular, we found that the steady state distributions of the RGG and the RL25 reporter did not significantly differ between the *wild type* and the *mlp1*Δ*mlp2*Δ strains. This means that even though the NA of these two reporters is significantly slower in the *mlp1*Δ*mlp2*Δ cells, over time the concentration of the reporter in the nucleus will reach *wild type* levels, indicating that the deficiency in protein translocation is most likely not a major contributing factor to the defects observed in the Mlp deletion strain.

*Model for the transport defect in the mlp1*Δ*mlp2*Δ *strain.*

It is surprising to find that *mlp1*Δ*mlp2*Δ cells have significantly impaired rates of NA, while the steady state distribution for the same substrates remains the same as in *wild type* cells. The overall rate of NA (plotted in Figures 14a and 15a) is dependent on two separate factors: the active rate of import into the nucleus and the opposing rate of diffusion out of the nucleus (Figure 18a). Since in the early stages of our transport assay diffusion of substrates out of the nucleus is negligible due to the small concentration gradient across the NE, our data indicates that the *mlp1*Δ*mlp2*Δ strains do indeed have a reduced active rate of import. However, if this is the case, then the steady state distribution for the cargo should also be reduced, unless an equal and opposite change in the diffusion rate would cancel out this difference (Figure 18b). A reduced diffusion rate is, in fact, consistent with previous observations which illustrated that both the import

rate and the diffusion rate of an SV40-NLS substrate are impaired in the *mlp1*Δ*mlp2*Δ strain (Strambio-de-Castillia et al., 1999).

Multiple models could explain how both the active rate of import and the rate of diffusion can be altered in equal but opposite ways. For example, a reduction of the numbers of NPCs per nucleus in the *mlp1*Δ*mlp2*Δ strain would lead to a slower accumulation of nuclear signal, while the steady state distribution would remain unchanged. If there are fewer NPCs active in transporting a substrate, the rate at which the cargo accumulates within the nucleus will be reduced proportionally. Likewise, the diffusion of the substrate out of the nucleus would be affected in proportion to the change in NPC numbers (Figure 18b). It should be noted that this model does not require the *mlp1*Δ*mlp2*Δ nuclei to physically contain fewer NPCs than the *wild type* strain. The number of NPCs available for transport and diffusion might be influenced by other factors, like temporarily blocking the transport channel of individual pores. Another factor that could explain our observation is an increase in the size of the nucleus, with the number of NPCs involved in transport remaining unchanged (Figure 18c). In this case, in the larger nucleus the accumulating substrate would be more dilute, leading to a slower rate of NA. Since the *mlp1*Δ*mlp2*Δ cells have been reported to be enlarged and have bigger nuclei, this might very well account for the results we observe. However, if this were the case we would expect to see this effect to be exaggerated in the *mlp1*Δ*mlp2*Δ cells displaying an abnormal morphology. Yet, we observe that their NA rates are indistinguishable from *mlp1*Δ*mlp2*Δ cells with normal morphology. The role of Mlp proteins in protein import and diffusion is discussed further in Chapter 7 in context with other Mlp functions.

Figure 13: **Model of the modified nuclear import assay.**

Two strains transformed with an NLS-GFP expression plasmid are covalently labeled with different fluorescent dyes on their cell wall, mixed and resuspended in a metabolic poison, halting active transport. The NLS-GFP cargoes diffuse through the NPC and equilibrate between nucleus and cytoplasm. For each assay the poisoned cells are washed and resuspended in glucose containing media causing transport to start within seconds. The accumulation of nuclear GFP signal is imaged and compared to the cytoplasmic signal over time (see also text).

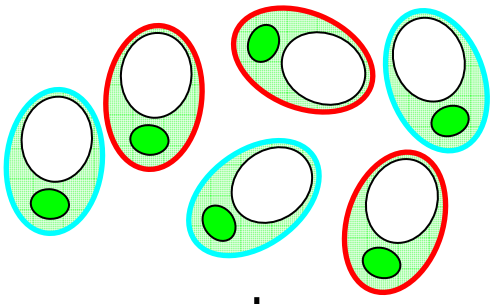

The NLS-GFP import-cargo, shown in green, is largely accumulated in the nucleus.

Poison stops transport

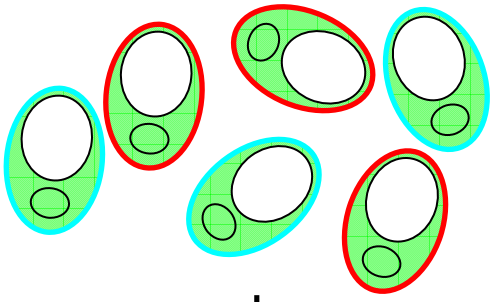

After transport is stopped the cargoes diffuse through the NPCs and equilibrate between nucleus and cytoplasm.

Glucose restarts transport

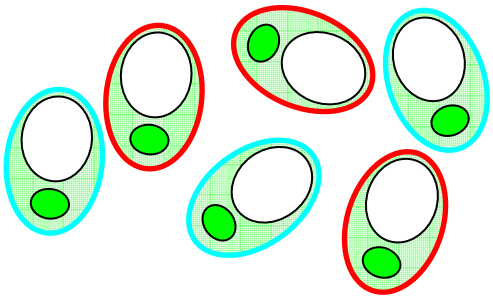

Removal of poison and addition of glucose restarts of the cargo in seconds.

Figure 14: ***mlp1*Δ*mlp2*Δ cells have a reduced nuclear accumulation rate of a RL25-NLS reporter.**

(a) Import assays as described in Figure 13 were carried out using an RL25-NLS-GFP reporter and the average change of nuclear/cytoplasmic signal is plotted over time (thick lines). For each cell measured the nuclear/cytoplasmic ratio was normalized to 1 at t=0sec. In addition, the 1st and 3rd quartile for each strain is plotted (thin lines). **(b)** Histogram of the nuclear accumulation rates (maximum change in nuclear/cytoplasmic signal over time) measured in (a). The p value of comparing the means distribution by a z-test is $p<0.0001$. CS, JF and MN.

RL25-NLS

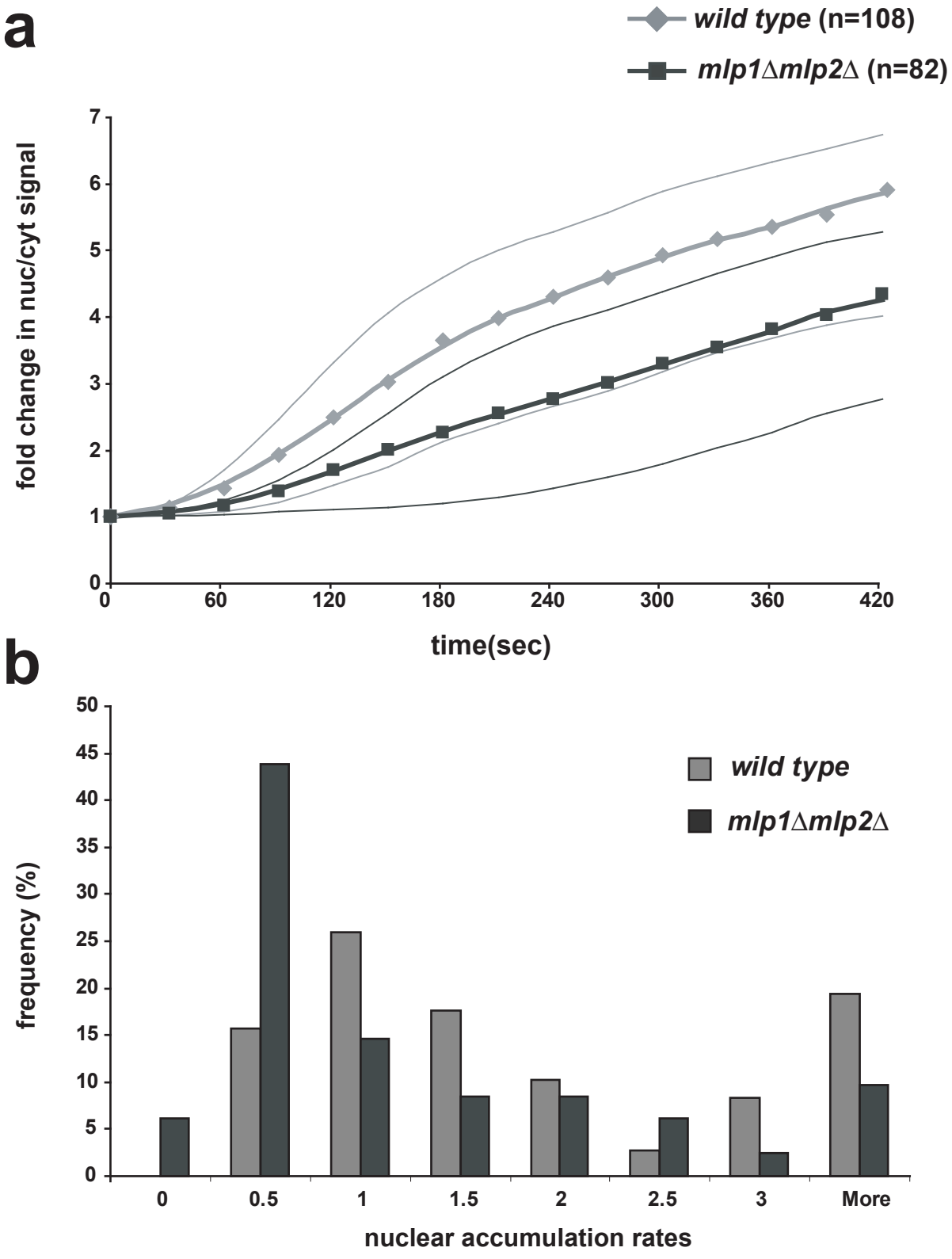
a
wild type (n=108)
mlp1Δmlp2Δ (n=82)
fold change in nuc/cyt signal
0
1
2
3
4
5
6
7
0
60
120
180
240
300
360
420
time(sec)
b
frequency (%)
0
5
10
15
20
25
30
35
40
45
50
wild type
mlp1Δmlp2Δ
0
0.5
1
1.5
2
2.5
3
More
nuclear accumulation rates

Figure 15: ***mlp1Δmlp2Δ* cells have a reduced nuclear accumulation rate of a RGG-NLS reporter.**

(a) Import assays as described in Figure 13 were carried out using an RGG-NLS-GFP reporter and the average change of nuclear/cytoplasmic signal is plotted over time (thick lines). For each cell measured the nuclear/cytoplasmic ratio was normalized to 1 at t=0sec. In addition, the 1st and 3rd quartile for each strain is plotted (thin lines). **(b)** Histogram of the nuclear accumulation rates (maximum change in nuclear/cytoplasmic signal over time) measured in (a). The p value of comparing the means distribution by a z-test is $p<0.0175$. CS, JF and MN.

RGG-NLS

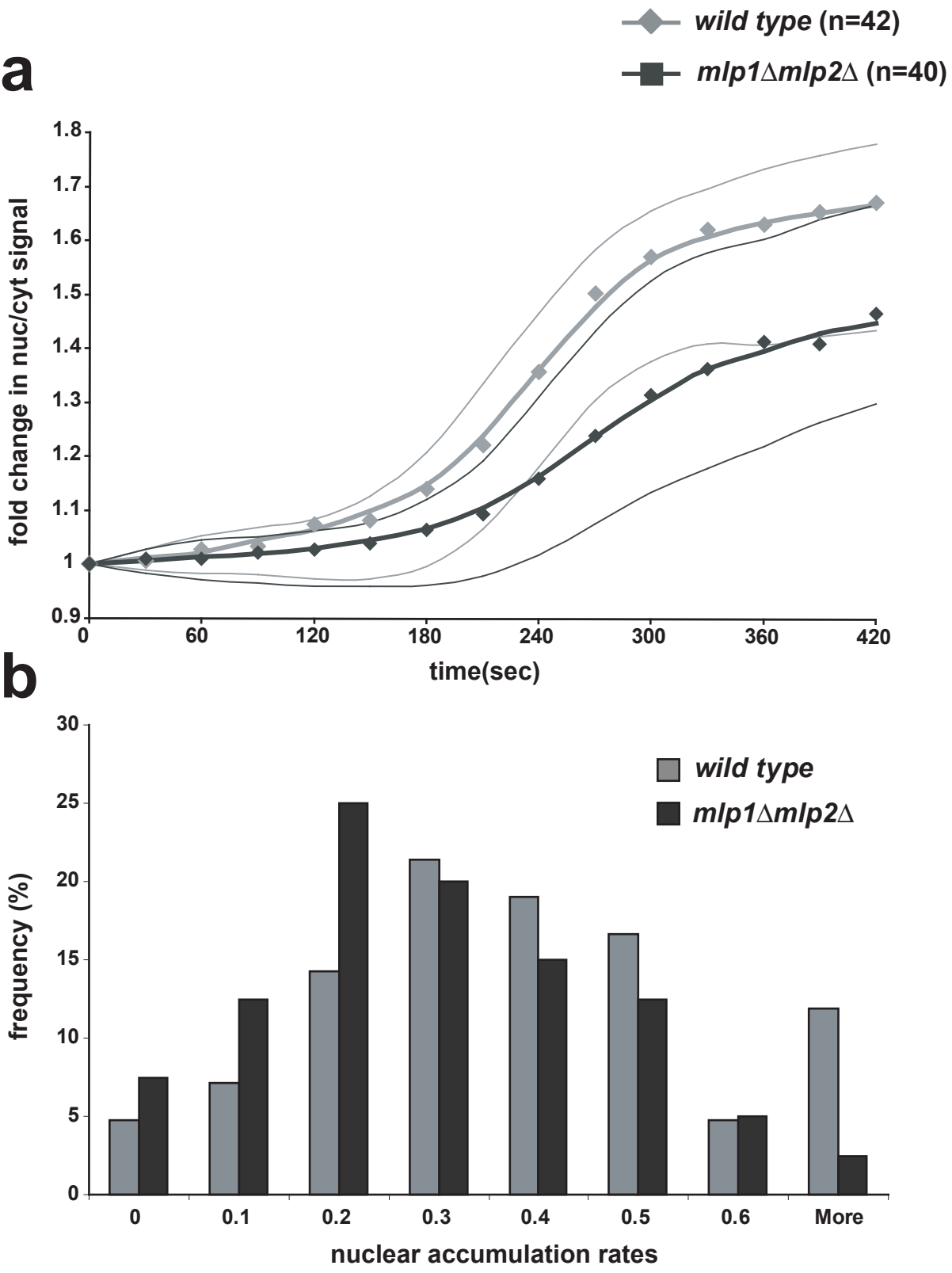
a
wild type (n=42)
mlp1Δmlp2Δ (n=40)
fold change in nuc/cyt signal
1.8
1.7
1.6
1.5
1.4
1.3
1.2
1.1
1
0.9
0
60
120
180
240
300
360
420
time(sec)
b
wild type
mlp1Δmlp2Δ
frequency (%)
30
25
20
15
10
5
0
0
0.1
0.2
0.3
0.4
0.5
0.6
More
nuclear accumulation rates

Figure 16: **Aberrant *mlp1*Δ*mlp2*Δ do not contribute disproportionally to reduced nuclear accumulation rates.**

(a) The data of the import assays presented in Figure 14 was plotted with the *mlp1*Δ*mlp2*Δ divided into two categories. Cells were categorized as aberrant if they had abnormal numbers of buds and enlarged cell size. As comparison, the *wild type* data from Figure 14 is plotted as a dashed line. **(b)** Histogram of the rates of nuclear accumulation (maximum change in nuclear/cytoplasmic signal over time) measured in (a). CS, JF and MN.

RL25-NLS

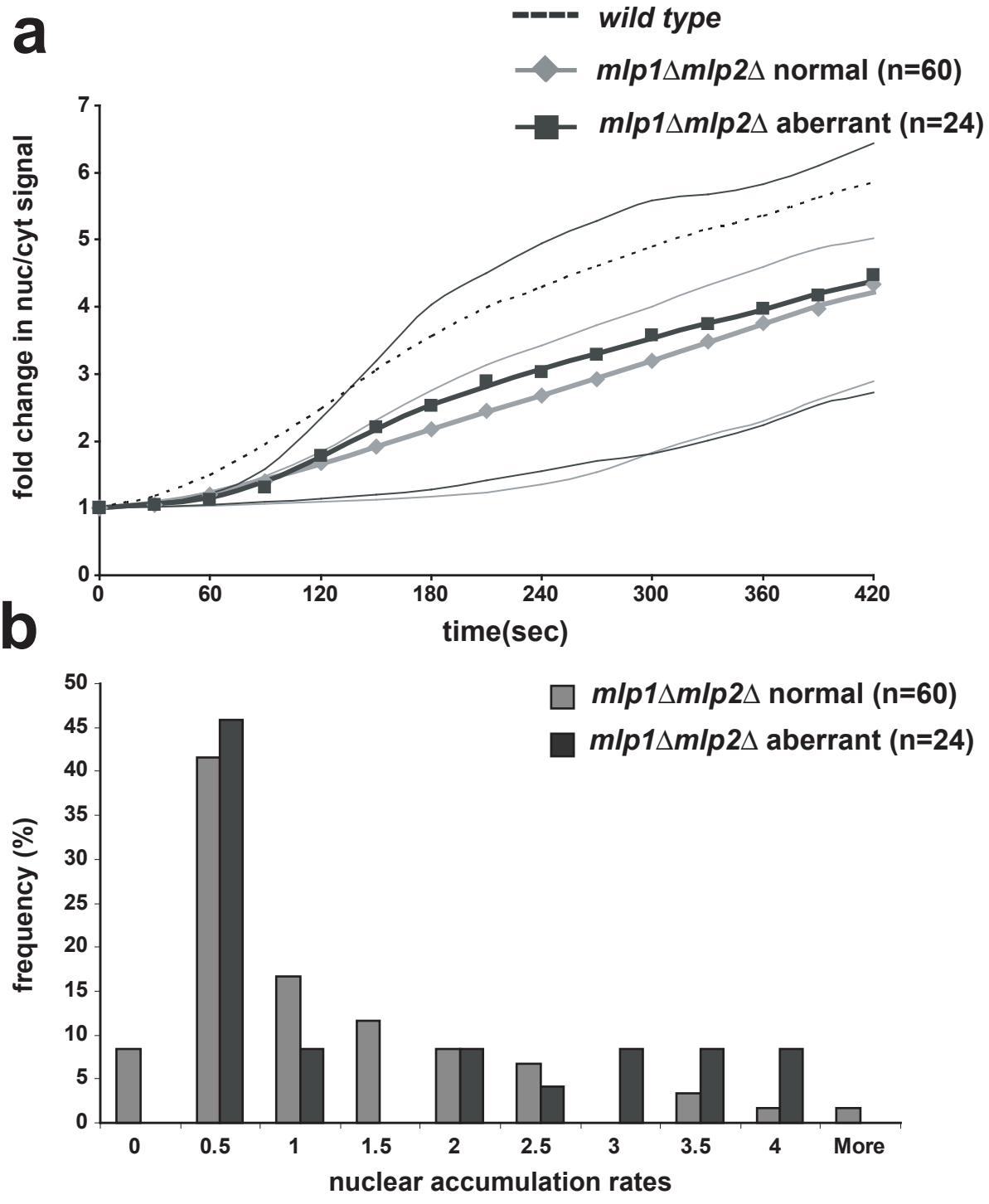
a
wild type
mlp1Δmlp2Δ normal (n=60)
mlp1Δmlp2Δ aberrant (n=24)
fold change in nuc/cyt signal
0
1
2
3
4
5
6
7
0
60
120
180
240
300
360
420
time(sec)
b
mlp1Δmlp2Δ normal (n=60)
mlp1Δmlp2Δ aberrant (n=24)
frequency (%)
0
5
10
15
20
25
30
35
40
45
50
0
0.5
1
1.5
2
2.5
3
3.5
4
More
nuclear accumulation rates

Figure 17: **The steady state distribution of import substrates is not significantly altered in *MLP* deletion strains.**

Nuclear versus cytoplasmic signal of the indicated NLS-GFP transport reporters was measured in *wild type* and *mlp* deletion strains. The averages are plotted with the standard deviation as error bars. CS, JF and MN.

Steady State Distribution

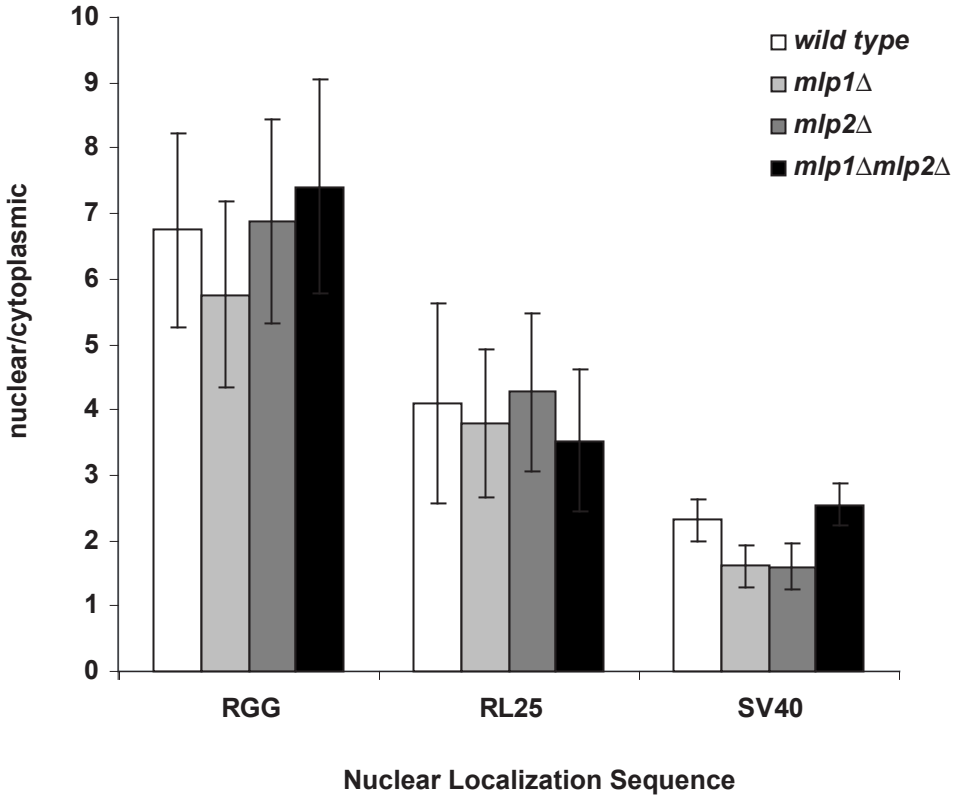

Figure 18: **Model of transport defects observed in *mlp1*Δ*mlp2*Δ.**

Model on how the import rate and diffusion rate influence the rate of nuclear accumulation and the steady state distribution of a transport substrate. Shown are a normal *wild type* cell **(a)**, a cell with fewer active NPCs **(b)** and a cell with an enlarged nucleus and **(c)**. For a further explanation of the models see also text. The import rate is indicated by the size of the black arrows and diffusion is indicated by the size of the white arrow.

Model of Transport Defects

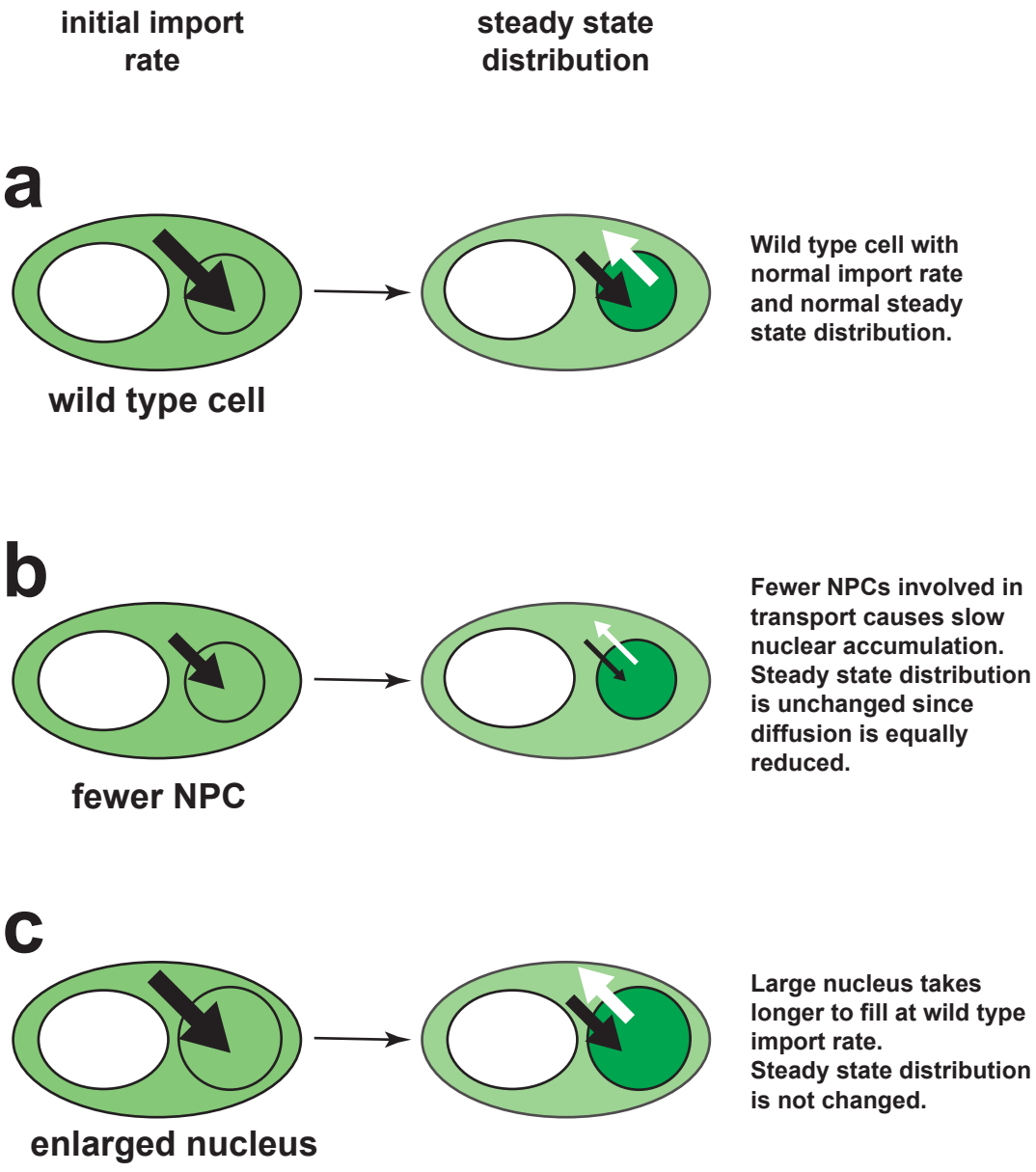

Chapter 5: Proteomic Analysis of Mlp1p and Mlp2p.

Background.

One of the difficulties in the study of the Mlp proteins has been the lack of a comprehensive analysis of the protein complexes it can participate in, which makes the interpretation of the phenotypes found in the Mlp deletion strains very difficult. To tackle this problem, we adapted proteomic techniques developed in our laboratory to purify Mlp in complex with its interacting partners and identify them. Cells expressing Mlp1p-PrA or Mlp2p-PrA were grown to mid-log phase in large scale cultures. The harvested cells were resuspended in protease inhibitors containing buffer, frozen in liquid nitrogen immediately, and the frozen cells were physically crushed in a motorized grinder. The resulting powder was thawed directly into protease inhibitor containing extraction buffer, cleared from cell debris by a short spin and used immediately for the affinity purification of Mlp complexes. The PrA containing complexes were captured by rabbit IgG antibodies immobilized on the surface of magnetic beads, washed and eluted. The resulting proteins were then separated by gel electrophoresis and identified by tandem mass spectrometry.

Our technique has a number of advantages over previously published attempts of biochemically identifying the complexes Mlp can form (Galy et al., 2004; Galy et al., 2000; Green et al., 2003; Kosova et al., 2000). The rapid freezing upon harvesting and the immediate contact with protease inhibitors upon thawing of the cell powder effectively

inhibits the degradation of the protease sensitive Mlp proteins (see Figure 19, high salt). The physical disruption of the cells into micrometer sized particles allows us to use mild extraction conditions, preserving low affinity interactions the Mlp proteins might form, while at the same time facilitating the release of Mlp complexes from the NE. The high speed of this process (it takes less than two hours from the point of thawing the cells to the elution of the purified complexes) also favors the preservation of low affinity interactions. Finally, the use of the surface-coated magnetic beads allows the efficient isolation of very large complexes (see also Figure 23). These significant improvements over other attempts have allowed us to reproducibly isolate and identify a number of proteins in complex with the Mlp proteins.

Purification of proteins associated with Mlp proteins.

We performed immunopurifications of Mlp1p-PrA, Mlp2p-PrA and PrA as a control in extraction buffers containing low, medium and high concentrations of salt (Figure 19; top). Looking at the general pattern of the bands purifying together with Mlp1p-PrA and Mlp2p-PrA, it is obvious that both proteins interact with overlapping yet different sets of proteins, suggesting overlapping yet different functions for Mlp1p and Mlp2p (see also Table 1). To control for non-specific binding of proteins to the affinity tag, PrA alone was expressed from a native yeast promoter and an amount similar to that of the Mlps was purified under identical conditions (Figure 19, control). Under mild extraction conditions, the PrA tag co-isolated with a number of faint bands, few of which appear to be present in the complexes purified with the Mlp proteins. Under more stringent

conditions, the PrA moiety did not bind to any native yeast proteins, suggesting that the proteins found in the Mlp purifications do not interact with the affinity tag.

It should be noted that even though a particular protein might co-isolate together with the PrA tagged Mlps, this does not prove that this protein is in direct physical contact with the Mlps. In fact, the majority of proteins found in the affinity purification might not form a direct interaction with the Mlps, but the interaction might be bridged by other proteins present in the Mlp complex. For the sake of clarity, in this work only direct, physical binding of one protein to another will be referred to as direct interaction. If the nature of the interaction is not determined, it will be referred to as an association or complex formation.

Multiple classes of proteins are in complex with the Mlps.

We were able to identify the majority of bands visible by Coomassie staining in the immunoprecipitations of Mlp1p-PrA and Mlp2p-PrA (Figure 19, bottom; Table 1). These proteins can be categorized in six classes, each of which is discussed below.

Mlp proteins

The most prominent band in each of the lanes was not surprisingly the protein carrying the PrA tagged bait. However, we also found Mlp2p in complex with Mlp1p. Likewise, Mlp1p is found in the Mlp2p-PrA co-immunoprecipitation, even though here the Mlp1p protein band was completely obscured by Mlp2p-PrA. In addition, we also found protein bands corresponding to bait that have lost their affinity tag. The fact that

both Mlp proteins are found in complex with each other supports the idea that they are part of a larger molecular assembly or network, at the nuclear periphery (Galy et al., 2000; Strambio-de-Castillia et al., 1999).

Nucleoporins

Both Mlp proteins are found in complex with a large subset of NPC components. It is unlikely that the Mlp proteins directly interact with all of the Nups found, but rather are tethered by a few Nups at the nuclear face of the NPC, which in turn bridge the interaction with other Nups. The Nups common to both Mlps were predominantly structural Nups lining the periphery and the inner transport channel of the pore and not the filamentous Nups thought to serve as docking sites for transport substrates. In complex with Mlp1p, we found all components of the Nup84p complex (Nup84p, Nup120p, Nup145Cp and Nup133p), all of which could be accessible to a peripherally binding Mlp protein, thus serving as a tethering site for Mlp1p. Virtually all Nups found in complex with Mlp2p have been identified as forming a complex with the peripheral Nup1p, which in turn might serve as tethering site for Mlp2p (Dokudovskaya, personal communications).

Interestingly, of the two Nups exclusively found at the nuclear face of the NPC, Nup60p was present in the Mlp1p complex, while Nup1p was present in the Mlp2p complex. Quite possibly, these two Nups act as anchor sites for the Mlp proteins, and bridge the interaction with the other Nups found in the complexes. We note that human Nup153, the homolog of Nup1p, has been identified as the anchor site for Tpr (Hase and Cordes, 2003), while the deletion of Nup60p has been reported to disrupt Mlp

localization to the NE (Galy et al., 2004). Furthermore, Nic96p, a Nup found in complex with both Mlp1p and Mlp2p has previously been shown to form a complex with Mlp2p (Kosova et al., 2000).

Protein import factors

The protein transport factors Kap60p was found in a complex with Mlp1p, while Kap95p was in a complex with both Mlps. This raises the possibility that the Mlp proteins might act as a terminal docking site for protein import, in accordance with the fact that an *mlp1*Δ*mlp2*Δ strain shows deficiencies in protein import (Strambio-de-Castillia et al., 1999). However, these factors are also commonly found in complex with a number of the Nups in complex with the Mlps, for example Nup60p and Nup1p. In addition, the Kap60p/Kap95p complex might be responsible for transporting the Mlp proteins into the nucleus, therefore binding them as a cargo and not as a docking site.

RNA processing/export factors

The RNA processing and export factors Sac3p, Mex67p and Yra1p were found in complex with both Mlp1p and Mlp2p. This result is entirely consistent with published findings: Sac3p has been found to be in complex with Mlp1p and Mex67p (Lei 2003), Mlp1p and Mlp2p have been shown to be in complex with Mex67p and Yra1p (Vinciguerra et al., 2005) and functional and genetic connections have been found between the Mlp proteins and the mRNA processing and export machinery (Galy et al., 2004; Green et al., 2003; Vinciguerra et al., 2005).

Deletion of MLP1 has also been found to be synthetically lethal with low expression levels of Yra1p, while the deletion of MLP2 slightly rescues cells with low Yra1p expression levels (Zhao, personal communications). We are currently collaborating to elucidate the function of this biochemical and genetic interaction.

SPB components/mitotic exit

Unexpectedly, we found a large number of SPB components and factors involved in regulating mitotic exit in complex with Mlp2p, but not with Mlp1p. This was the most striking difference between the complexes these proteins form, and will be discussed in greater detail in the following chapter. Interestingly, Bfa1p was present even in the medium salt extraction as a fairly strong band, while only traces of Spc110p and none of the other SPB components found in abundance in the high salt extraction are visible. This suggests that the complex formation of Mlp2p with Bfa1p is independent of the remaining SPB components and could point towards a specific role for Mlp2p in the regulation of the spindle orientation checkpoint.

Other proteins/contaminants

In particular in the low salt extractions, a number of proteins in complex with the Mlp proteins were not easily classified into a functional group. The known localization of these proteins and unpublished data from our laboratory suggested that the majority of these proteins might be contaminants. These include heat shock proteins (e.g. Ssa1p, Ssa2p), cytoplasmic metabolic enzymes (e.g. Adh1p, Eno1p) and other proteins known to

be ‘sticky’ (e.g. Tef2p). However, even though these considerations suggest that the proteins in this group are contaminants, we can not exclude that they might be in complex with the Mlp proteins in a functionally relevant way. Since other proteins found in our study suggest themselves as more promising candidates for further study, we did not investigate any of the proteins found in this class.

Deletion of one MLP gene does not significantly alter the complexes formed by their paralog.

Since the Mlp proteins are at least partially redundant, the deletion of one MLP gene might induce a change in the complexes the remaining paralog forms. To test if this is the case, we compared co-immunoprecipitations of PrA tagged Mlp proteins in the presence and absence of their paralogs (Figure 20a and 20c). The deletion of neither of the MLP genes significantly altered the proteins co-purifying together with Mlp1p-PrA or Mlp2p-PrA. This suggests that the functional redundancy of the Mlps does not depend on one Mlp protein replacing the other in the complexes it forms. In particular, even in the absence of MLP2, Mlp1p-PrA did not interact with SPB components under the same conditions as Mlp2p does (Figure 20b), suggesting that Mlp1p is not capable of substituting directly for functions Mlp2p may perform at the SPB. In addition, the fact that the complexes formed by Mlp1p and Mlp2p did not change in the absence of their respective paralogs suggests that one Mlp protein is not required for the other to properly localize to the nuclear periphery and form its appropriate interactions.

Figure 19: **Mlp1p and Mlp2p form extensive protein complexes.**

PrA containing complexes were affinity purified from cell lysates expressing Mlp1p-PrA, Mlp2p-PrA or PrA as a control using three different TBT based extraction buffers containing 0mM (*low*), 150mM (*medium*) and 300mM (*high*) NaCl as additional extractant. The complexes were separated by SDS-PAGE, visualized by Coomassie staining and identified by tandem mass spectrometry. Closed circles indicate identified proteins corresponding to the list below. Position of rabbit IgG heavy chain leaked from the DynaBeads is indicated (*open circles*). MN.

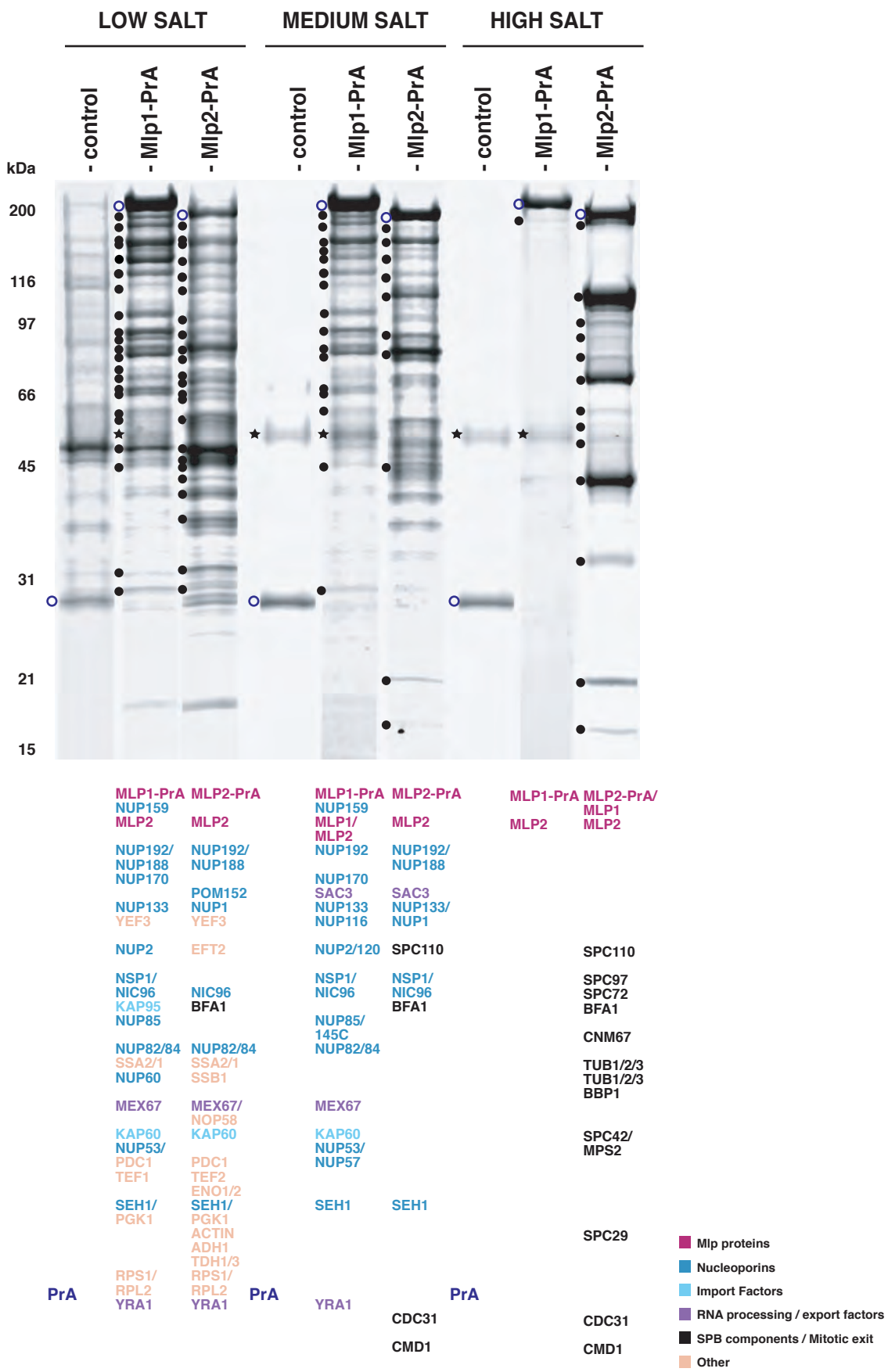
LOW SALT
MEDIUM SALT
HIGH SALT
- control
- Mlp1-PrA
- Mlp2-PrA
kDa
200
116
97
66
45
31
21
15
MLP1-PrA
NUP159
MLP2
NUP192/
NUP188
NUP170
NUP133
YEF3
NUP2
NSP1/
NIC96
KAP95
NUP85
NUP82/84
SSA2/1
NUP60
MEX67
KAP60
NUP53/
PDC1
TEF1
SEH1/
PGK1
RPS1/
RPL2
YRA1
PrA
MLP2-PrA
MLP2
NUP192/
NUP188
POM152
NUP1
YEF3
EFT2
NIC96
BFA1
NUP82/84
SSA2/1
SSB1
MEX67/
NOP58
KAP60
PDC1
TEF2
ENO1/2
SEH1/
PGK1
ACTIN
ADH1
TDH1/3
RPS1/
RPL2
YRA1
PrA
MLP1-PrA
NUP159
MLP1/
MLP2
NUP192
NUP170
SAC3
NUP133
NUP116
NUP2/120
NSP1/
NIC96
NUP85/
145C
NUP82/84
MEX67
KAP60
NUP53/
NUP57
SEH1
YRA1
PrA
MLP2-PrA
MLP2
NUP192/
NUP188
SAC3
NUP133/
NUP1
SPC110
NSP1/
NIC96
BFA1
SEH1
CDC31
CMD1
MLP1-PrA
MLP2
MLP2-PrA/
MLP1
MLP2
SPC110
SPC97
SPC72
BFA1
CNM67
TUB1/2/3
TUB1/2/3
BBP1
SPC42/
MPS2
SPC29
CDC31
CMD1
PrA
Mlp proteins
Nucleoporins
Import Factors
RNA processing / export factors
SPB components / Mitotic exit
Other

Table 1: **List of proteins found in complex with Mlp1p and Mlp2p.**

List of proteins found in complex with Mlp1p and Mlp2p. The proteins are divided into six classes. The protein description is based on information from the Proteome BioKnowledge Library and references therein.

Mlp1p Complex	Mlp2p-Complex	Protein description
Mlp Protein		
Mlp1p	**Mlp1p**	Myosin-like protein 1
Mlp2p	**Mlp2p**	Myosin-like protein 2
Nucleoporins		
Nic96p	**Nic96p**	non-FG Nucleoporin
Nsp1p	**Nsp1p**	FG Nucleoporin
	Nup1p	FG Nucleoporin; nuclear
Nup116p		FG Nucleoporin
Nup120p		non-FG Nucleoporin
Nup133p	**Nup133p**	FG-repeat Nucleoporin
Nup145Cp		non-FG Nucleoporin
Nup159p		FG Nucleoporin; cytoplasmic
Nup170p		non-FG Nucleoporin
Nup188p	**Nup188p**	non-FG Nucleoporin
Nup192p	**Nup192p**	non-FG Nucleoporin
Nup2p		dynamically associated with NPC
Nup53p		FG Nucleoporin
Nup57p		FG Nucleoporin
Nup60p		FG Nucleoporin; nuclear
Nup82p	**Nup82p**	non-FG Nucleoporin
Nup84p	**Nup84p**	non-FG Nucleoporin
Nup85p		non-FG Nucleoporin
	Pom152p	pore membrane protein
Seh1p	**Seh1p**	non-FG Nucleoporin

Mlp1p Complex	Mlp2p-Complex	Protein description
Transport factors		
Kap60p	**Kap60p**	in complex with Kap95p; binds NLS,; import
Kap95p		in complex with Kap60p; binds NLS,; import
mRNA export/processing		
Mex67p	**Mex67p**	mRNA export; Mex67p-Mtr2p binds Yra1p
Sac3p	**Sac3p**	mRNA export; binds Mex67p-Mtr2p
Yra1p	**Yra1p**	RNA bindg.; 3'formation; binds Mex67p-Mtr2p
SPB /mitotic exit		
	Bfa1p	spindle assembly checkpoint
	Bbp1p	SPB duplication; binds Cdc5p
	Cdc31p	calmodulin-like; SPB duplication; bridge
	Cmd1p	Calmodulin; multifunctional; SPB core
	Cnm67p	cytoplasmic face of SPB; SPB core
	Mps2p	insertion of nascent SPB into NE
	Spc110p	links nuclear microtubules to core; SPB core
	Spc29p	links Spc42p and Spc110p; SPB core
	Spc42p	major component central plaque; SPB core
	Spc72p	cytoplasmic plaque; forming astral microtubules
	Spc97p	nuclear/cytoplasmic microtubule organization
	Tub1/2/3p	tubulin

Mlp1p Complex	Mlp2p-Complex	Protein description
Contaminants/other		
	Actin	component of cytoskeleton
	Adh1p	Alcohol dehydrogenase I; cytoplasmic
	Eft1p	Translation elongation factor EF-2
	Eno1/2p	Enolase 1/2; cytoplasmic
Pdc1p	**Pdc1p**	Pyruvate decarboxylase isozyme 1; cytopl/nucl
Pck1p	**Pck1p**	Phosphoenolpyruvate carboxykinase; cytoplasm
Rpl1p	**Rpl1p**	Ribosomal protein L5
Rps2p	**Rps2p**	Ribosomal protein S2
Ssa1p	**Ssa1p**	chaperone and HS protein; Rad9p complex
Ssa2p	**Ssa2p**	chaperone and HS protein; Rad9p complex
	Ssb1p	rRNA processing
	Tdh1/3p	Glyceraldehyde-3-phosphate dehydrogenase
Tef1/2p	**Tef1/2p**	Translation elongation factor EF-1alpha
Yef3p	**Yef3p**	Translation elongation factor EF-3A
	Nop58p	rRNA processing; nucleolar

Figure 20: **Mlp1p and Mlp2p form complexes in the absence of their paralog.**

(a) Mlp1p-PrA containing complexes were purified as described in Figure 19 from control (+) or *mlp2*Δ (-) strains using the indicated extraction conditions. The complexes were separated by SDS-PAGE and visualized by Coomassie staining. **(b)** Mlp2p-PrA containing complexes were purified as in (a) from control (+) or *mlp1*Δ (-) strains. **(c)** Mlp1p-PrA was purified as described in (a) using the same conditions under which Mlp2p-PrA is in complex with SPB components. MN.

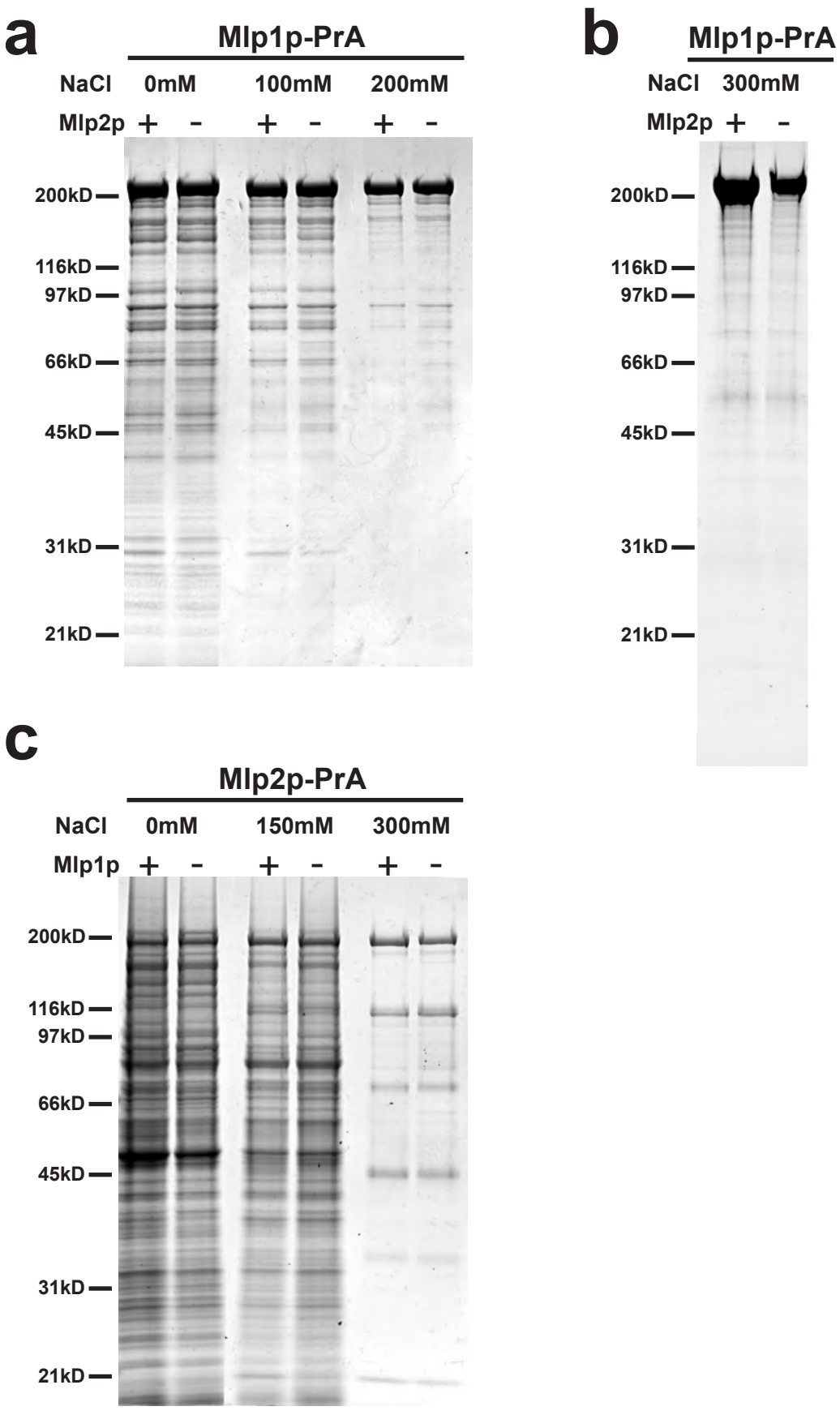
a
Mlp1p-PrA
NaCl 0mM 100mM 200mM
Mlp2p + - + - + -
200kD
116kD
97kD
66kD
45kD
31kD
21kD
b
Mlp1p-PrA
NaCl 300mM
Mlp2p + -
200kD
116kD
97kD
66kD
45kD
31kD
21kD
c
Mlp2p-PrA
NaCl 0mM 150mM 300mM
Mlp1p + - + - + -
200kD
116kD
97kD
66kD
45kD
31kD
21kD

Chapter 6: Mlp2 and the SPB.

Background.

In eukaryotes, the NE forms a barrier to free diffusion between the genetic material and the rest of the cell, thus necessitating a mechanism for RNA transcripts and translated proteins to be transported between the nucleus and the cytoplasm. This exchange is mediated by NPCs, octagonally symmetric cylindrical structures that span pores in the NE. However, during mitosis, the spindle microtubules must gain access to the nucleoplasm in order to segregate the daughter genomes. This can be achieved either by breaking down the NE (open mitosis), or by assembling the spindle inside the nucleus (closed mitosis) as occurs in both budding and fission yeast. In higher eukaryotes, the NE disassembles at the beginning of mitosis in a highly coordinated fashion, and recent evidence points to an active role for centrosomal microtubules in this process (Beaudouin et al., 2002; Salina et al., 2002). After the NE has broken down, large clusters of disassembled NE-derived vesicles remain in the vicinity of the spindle poles throughout cell division (Beaudouin et al., 2002). Even after mitosis the duplicated interphase centrioles are found in close proximity to the nucleus and are robustly associated to the cytoplasmic surface of the NE (Bornens, 1977; Nadezhdina et al., 1979). In the budding yeast *Saccharomyces*, the spindle is assembled by SPBs. SPBs are the sole yeast microtubule-organizing centers (MTOCs), and like NPCs are directly embedded within pores in the NE throughout the cell cycle. These observations suggest an active albeit ill-

defined role for the NE in coordinating different aspects of cell division, and underscore how the fate of the NE is intimately linked to the activity of the spindle.

In *Saccharomyces,* the SPB consists of a multi-layered disk structure embedded within the NE made of hundreds of copies of each of its core components (reviewed in Jaspersen and Winey, 2004). In actively dividing haploid cells, it has an average thickness of 150nm, a diameter of 110nm, and a molecular mass of ~1.5 GDa (Bullitt et al., 1997). The electron-dense central plaque is assembled around a two dimensional crystal of the coiled-coil protein Spc42p (Bullitt et al., 1997), and is flanked on either side by the inner and outer plaques. On the cytoplasmic side, Cnm67p connects Spc42p to the nucleation site of the astral microtubules, responsible for nuclear positioning and spindle alignment (Schaerer et al., 2001). The filamentous protein Spc110p acts as a spacer between the central and the inner plaques, from where the nuclear microtubules emanate to form the mitotic spindle responsible for SPB separation and for chromosome segregation (Kilmartin et al., 1993; Rout and Kilmartin, 1990). The spindle also plays a critical role in ensuring that nuclear migration and division occur in concert with DNA replication and bud formation. Once cells are committed to entering S phase, SPBs duplicate, separate and migrate along the circumference of the NE to form a short metaphase spindle. At the same time, the spindle positions itself at the bud-neck along the mother-daughter axis. When spindle assembly and chromosomal attachment is complete, anaphase ensues during which the spindle elongates and the nucleus divides. Finally, the spindle disassembles at telophase and cytokinesis (reviewed in Winey and O'Toole, 2001). Despite the observation that the SPBs are extremely resistant to disruption *in vitro*, recent results indicate that SPBs are dynamic *in vivo*. Both the newly synthesized and the

old SPB continue to grow in size from G2 to telophase (Bullitt et al., 1997; Yoder et al., 2003). At the same time, the old SPB is constantly renewed by the exchange of ~50% of old with newly made Spc110p (Yoder et al., 2003). A poorly understood element of SPB physiology is how this structure operates in the context of the NE as a whole, and in particular how it interacts with other NE components. Recent observations suggest a functional relationship between SPBs and NPCs. For example, some components are shared between the two structures, and proteins known to regulate spindle function are found to reside at the NPC (Chial et al., 1998; Iouk et al., 2002; Kerscher et al., 2001; Rout et al., 2000). Although these results suggest a possible role for the NE in aiding SPB function, they have not provided an explanation for the mechanism underlying this connection.

Mlp2p, but not Mlp1p, interacts with core components of the SPB.

We set out to identify the interacting partners of Mlp1p and Mlp2p by biochemically purifying these proteins from yeast lysates. As described above, using a variety of extraction conditions, we found striking differences between the proteins co-purifying with Mlp1p and Mlp2p (Figure 21a; see also Figure 19). Under stringent conditions, Mlp1p-PrA was reproducibly isolated in a complex exclusively with Mlp2p, indicating that the two proteins are able to bind directly to each other as previously proposed (Galy et al., 2000; Strambio-de-Castillia et al., 1999). By contrast, in addition to binding Mlp1p, Mlp2p-PrA formed a tight complex with at least six major proteins, which were identified by mass spectrometry as key SPB components. Five of these represent the components of

the SPB core: Spc110p, Cnm67p, Spc42p, Spc29p and Cmd1p. The sixth, Cdc31p, is a calmodulin-like calcium-binding protein that helps form the bridge structure involved in SPB duplication (Spang et al., 1993). With the exception of Nud1p and the addition of Cdc31p, these proteins match those identified as core components in a previous proteomic study (Adams and Kilmartin, 1999). Lower abundance bands present in the complex were identified to be the inner plaque components Spc98p, Spc97p and the outer plaque component Spc72p, as well as Mps2p and Bbp1p, two SPB-associated proteins with important roles in SPB duplication (reviewed in Jaspersen and Winey, 2004).

To determine which of the SPB components are capable of directly binding Mlp2p, we performed an *in vitro* blot binding experiment (Figure 21b). The Mlp2p-associated SPB proteins were separated by SDS-PAGE and immobilized on nitrocellulose. The immobilized proteins were then probed either with purified Mlp1p-PrA or Mlp2p-PrA (see also Figure 5a). While Mlp1p did not bind any SPB components, Mlp2p-PrA bound specifically to three SPB proteins (Spc110p, Spc42p and Spc29p), but failed to interact with a fourth (Cnm67p). These results are consistent with the immunopurification data, and indicate that Mlp2p interacts directly with at least three SPB components, all of which are exposed on the nuclear side of the SPB and so accessible to the Mlp proteins *in vivo*.

Core components of the SPB co-immunoprecipitate Mlp2p, but not Mlp1p.

To test the specificity of the Mlp2p-SPB interaction, we performed reciprocal co-immunoprecipitation experiments followed by immunoblotting. We used Spc110p-PrA,

Spc42p-PrA or Cnm67p-PrA as baits and Mlp1p-Myc or Mlp2p-Myc as targets (Figure 21c-e, *co-expressed*). Consistent with the results presented in Figure 21b, we found that Mlp2p-Myc was indeed co-immunoprecipitated by both Spc110p-PrA and Spc42p-PrA, and Mlp1p-Myc did not interact with either of the baits. This confirms the high specificity of the Mlp2p-SPB interaction, since Mlp1p (a protein similar in location, size and secondary structure to Mlp2p) is unable to interact either with Spc110p or Spc42p. Cnm67p-PrA failed to immunoprecipitate either Mlp1p-Myc or Mlp2p-Myc under the conditions used for Spc110p and Spc42. This is in agreement with the *in vitro* binding experiment, which suggests that Mlp2p only indirectly interacts with Cnm67p.

Long coiled-coil domains are common to Mlp2p and many SPB components. Since these domains have the potential to artifactually adhere to each other under non-physiological conditions, we set out to demonstrate the physiological relevance of the Mlp2p-SPB interactions. We performed the experiment described above under conditions in which the SPB-bait and the Mlp-targets were expressed independently and mixed only after cell lysis. Under these conditions we detected no interaction between Mlp2p and the tested SPB proteins (Figure 21c-e, *mixed*), showing that the Mlp2p/SPB interaction does not occur post-lysis in the extracts.

The Mlp2p-SPB complex is very stable.

To determine if we could further extract the Mlp2p-SPB complex into smaller subcomplexes, we increased the stringency of the extraction conditions. When increasing the NaCl concentration stepwise to 2M, we found that the complex formed by Mlp2p was

very stable (Figure 22a). Even at a concentration of 1.5M NaCl, Mlp2p-PrA purified together with the Cnm67p and the main components of the central plaque: Spc110p, Spc42p and Spc29p. However, using the detergent sodium N-lauroyl-sarcosine as an extractant, we were able to break apart the Mlp2p-SPB complex further (Figure 22b). At low concentrations, Spc29p, Cdc31p and Cmd1p were removed from the complex, with the core central plaque proteins remaining bound to Mlp2p. Increasing the detergent concentration further caused first Spc110p and then Cnm67p to dissociate from the complex, leaving behind only Mlp2p-PrA and Spc42p, confirming that Mlp2p can directly interact with the major component of the central plaque to form a binary complex.

Mlp2p binds the fully formed SPB.

It is possible that the interaction between Mlp2p and the SPB is limited to unassembled subcomplexes of the SPB or to certain stages during the spindle assembly cycle. To directly address this point, we visualized the complex associated with Mlp2p-PrA by transmission electron microscopy (TEM). Thin sections of beads from the Mlp1p-PrA immunoprecipitation (Figure 23a) and empty control beads (data not shown) were devoid of any visible protein structures. Conversely, the magnetic beads on which the Mlp2p-PrA complex was immobilized were covered with numerous discrete structures, ~80nm in diameter (Figure 23b, *small arrows*), which, at higher magnification, resembled isolated SPB cores (Adams and Kilmartin, 1999; Rout and Kilmartin, 1990; Rout and Kilmartin, 1991).

To confirm that Mlp2p-associated structures were indeed *bona fide* SPB cores, we also compared the isolated structures from either haploid or diploid cells (Figure 23e-d), as SPBs from diploid cells are characteristically larger than SPBs from haploid cells in diameter but not in thickness, and the layered morphology of diploid SPBs is more easily discernable than that of haploid SPBs (Bullitt et al., 1997; Byers and Goetsch, 1974; Byers and Goetsch, 1975b). The structures on the beads isolated from diploid cells were revealed to be morphologically identical to chemically extracted diploid SPB cores (Adams and Kilmartin, 1999). The layered appearance of SPBs was clearly visible in these structures, with the electron-dense central plaque flanked on either side by filamentous protein layers. Structures resembling the bridge, which connects recently duplicated SPBs during early S-phase, were also visible in some examples, accounting for the presence of Cdc31p in the Mlp2p-SPB complex (Spang et al., 1993). While the average width of the diploid layered structures was significantly larger than that of the haploid structures, their average thicknesses were the same (Figure 23e); all their measurements are consistent with previously published values for SPBs. Together, these data establish that the structures associated with Mlp2p are *S*PB-derived cores.

We observed filamentous protein structures emanating from the nuclear side of the SPB-derived cores, connecting them to the beads (Figure 23c, *large arrows*), consistent in size with Mlp2p coiled-coil homodimers. This suggests that a few Mlp2p molecules were sufficient to capture an SPB, which consists of hundreds copies of its core components. Thus, the stoichiometry observed in Figure 22a could be accounted for by only a small amount of peripheral Mlp2p interacting directly with the SPB, while the majority of Mlp2p is located elsewhere.

The SPB is localized in close proximity to Mlp2p throughout the cell cycle.

With their C-shaped distribution around the rim of the nucleus, the Mlps define a specific hemisphere of the NE, which only partially overlaps with the even distribution of NPCs around the rim of the nucleus and is excluded from the region juxtaposed to the nucleolus (Galy et al., 2004; Kosova et al., 2000; Strambio-de-Castillia et al., 1999). As illustrated previously (Figure 3d), the SPBs exhibit a significant preference to localize within the Mlp network. To further investigate the association between the Mlp distribution and the SPBs, we followed the localization of YFP-Mlp2p and Spc42p-CFP at different stages of the cell cycle. We separated actively growing haploid cells into individual phases of the cell cycle by differential elutriation (Miller and Cross, 2001). Using this method, G1 cells (i.e. un-budded) were reliably separated from S-phase cells (small-budded) and G2 or mitotic cells (large-budded). We observed that the connection between the Mlp-containing hemisphere and the SPBs was always conserved (Figure 24a). In particular, at the time of SPB duplication the association between the Mlps and the SPBs was exceptionally tight, with the SPBs often being engulfed inside the Mlp network. Following S phase, the SPBs migrated to opposite ends of the Mlp hemisphere. At anaphase the YFP-Mlp2p signal appeared to trail behind Spc42p-CFP, as the spindle and the nucleus extend. At telophase, upon spindle disassembly, the Mlps appeared to surround the SPBs once again in a pattern reminiscent of the interphase topology.

The SPB is continuously bound by Mlp2p.

To test if Mlp2p also physically remains associated with the SPB throughout the cell cycle, cells expressing Mlp2p-PrA were synchronized in metaphase and samples for PrA immunoprecipitations were removed at the indicated timepoints (Figure 24b). At metaphase (t=0) five proteins (Spc110p, Spc42p, Spc29p, Cdc31p and Cmd1p) were easily discernable in the Mlp2p-PrA complex, by comparison to their known migration patterns (see Figure 21). However, multiple bands were observed to migrate at the position corresponding to the molecular weight of Cnm67p. This could be explained either by a composition change in the SPB complex, with Cnm67p disassociating at this time or the multiple bands could correspond to alternative phosphorylation states of Cnm67p (Schaerer et al., 2001). As the cells progressed though mitosis, judged by the constant amounts of the major Coomassie stained protein bands, the gross composition of the complex which immunoprecipitated with Mlp2p remained the same. In late S phase (t=90) Cnm67p once again was visible as a discrete band, again signifying either a reassociation of Cnm67p with the complex, or a change in its phosphorylation pattern. At this time the complex was virtually indistinguishable from the control purified from asynchronous cells. The expression levels of Mlp2p-PrA remained roughly equal during the experiments as measured by immunoblotting (Figure 24c) and the cells appeared to progress normally though the cell cycle as monitored by the expression levels of Clp2p, FACS analysis and microscopic analysis (Figure 24c; data not shown).

Since Mlp2p interacts with intact cores of the SPB, this type of analysis does not allow us to discriminate whether any changes observed in the purified complex are due to specific changes in Mlp2p's affinity to SPB components over time or if the general

composition of the SPB changes over time. However, our data does demonstrates that Mlp2p remains tightly associated with the SPB throughout the course of the cell cycle, suggesting that a functional role of Mlp2p at the SPB is not limited to certain cell cycle stages.

Cells lacking Mlp2p have aberrant numbers of SPBs and cytokinesis defects

In order to explore the functional significance of the interaction between the SPB and Mlp2p, we determined the position and morphology of the SPBs in actively dividing haploid cells by following GFP-tagged Spc42p. Though we did not find any *wild type* and *mlp1Δ* cells with more than two SPBs, 8% of cells lacking *MLP2* carried abnormally high numbers of Spc42p-GFP-containing foci (3-6 per cell; Figure 25a). Cells that displayed this defect were predominantly found in chains of multiple cell bodies that had failed to complete cytokinesis (hereafter referred to as multi-cellular chains). Similar results were obtained with cells expressing Spc110p-GFP or GFP-tubulin (GFP-Tub1p) (data not shown). These results indicate that the aberrant Spc42p-GFP containing foci found in cells lacking Mlp2p also contain Spc110p and are able to nucleate microtubules.

To further study the nature of this defect, we enriched for multi-cellular chains and large-budded cells by elutriation. We found that *wild type* and *mlp1*Δ elutriation fractions contained no abnormal cell types (Figure 25c, *wild type* and *mlp1*Δ). In contrast, in cells that carried the *mlp2Δ* mutation, late elutriation fractions were enriched in multi-cellular chains, which also displayed abnormal numbers of microtubule organizers (Figure 25b and c, right panels). In all cases, the generation of the microtubule organizers appeared to

be coupled with the formation of an extra bud before completion of the previous cell division (Figure 25b, *mlp2*Δ, inset).

Since a number of the *mlp2*Δ cells develop abnormal numbers of microtubule organizers which appear in multi-budded cell chains, we further analyzed the elutriation fractions by FACS, to determine if these cells undergo additional rounds of DNA duplication, uncoupled from mitosis. Approximately 35% of the *mlp2*Δ cells in elutriation fraction 12 were in cell chains, yet only a very small number of cells actually had an abnormally high DNA content (Figure 25c). Gating cells by their size, we further tested if the abnormally large cell chains predominantly contribute to the small amount of cells with abnormal DNA content (Figure 25d). Yet, even in the fraction containing only the largest cells, the majority still had a normal DNA content. This suggests that these cells do not undergo multiple rounds of DNA replication, uncoupled from mitosis. The phenotypes observed in the elutriation fraction is similar to the phenotypes observed in a subpopulation of the *mlp1*Δ*mlp2*Δ cells. Approximately 20% of the *mlp1*Δ*mlp2*Δ cells have multiple Spc42p-GFP containing bodies and accumulate in multibudded cell chains (see also Figure 10a). This data suggests that Mlp1p, at least in the absence of Mlp2p aides in proper SPB function and that Mlp1p and Mlp2p might have at least partially overlapping functions at the SPB.

The presence of additional SPB protein-containing microtubule organizers could indicate either a defect in the regulation of SPB duplication (Haase et al., 2001) or a defect in SPB assembly and structural integrity (Sundberg et al., 1996). To distinguish between these two possibilities, we performed a detailed ultrastructural analysis on enriched defective cells using thin section transmission electron microscopy (Figure 25e).

For comparison, an equivalent elutriation fraction from a *wild type* culture was also analyzed (data not shown). In the nuclei of *mlp2*Δ cells we found numerous examples of aberrant amorphous, electron-dense structures that were absent from the control and were reminiscent of the intranuclear microtubule organizers found in spc110-220 mutant cells (Sundberg et al., 1996). These masses lacked the well-defined architecture characteristic of SPBs and appeared to reside primarily inside the nucleoplasm, although on occasion they were connected to an SPB at the NE. In addition they appeared to nucleate microtubules (Figure 25e, top left, *arrowheads)*. We also observed instances in which multiple microtubule bundles appeared to be emanating from MTOCs elsewhere in the nucleus and not forming a normal spindle (Figure 25e, bottom left, *arrows*). The *mlp2*Δ nuclei often appeared to be fragmented and lobulated and sometimes displayed deep invaginations of the NE carrying what appeared to be fully formed SPBs. These results likely explain the abnormal appearance of the DAPI stained nuclei shown in Figure 25b. Overall, these data are consistent with the results we obtained by fluorescent microscopy and suggest the formation of misassembled microtubule nucleating SPB-like masses inside the nucleus in *mlp2*Δ cells but not in *wild type* or *mlp1*Δ.

MLP2 interacts genetically with SPC110

To further investigate the functional interactions between the SPB and Mlp2p, we tested temperature sensitive mutations of various SPB components for genetic interactions with *MLP1* and *MLP2*. When a strain containing the *spc110-220* mutation was mated with the *mlp2Δ* strain we were unable to recover spores carrying both mutations, although we could generate double mutant strains from all other crosses tested

(see below). The *spc110-220* strain carries a C911R mutation in the Cmd1p-binding domain of Spc110p, which reduces the ability of Spc110p to bind Cmd1p at the restrictive temperature and impairs the incorporation of Spc110p into the central plaque of the SPB, leading to slow growth and the formation of intranuclear mitotic organizers (Sundberg et al., 1996). To study this genetic interaction, we created *spc110*Δ strains covered by plasmids expressing either *SPC110* or *spc110-C911R* (thereafter referred to as *spc110-220)*. In addition, we introduced a repressible promoter upstream of either a PrA tagged *MLP1* or *MLP2* gene. When grown in dextrose this promoter repressed the expression of *MLP1* or *MLP2* to levels below the detection limit as determined by immunoblotting.

While the *SPC110* control strains exhibited an equal viability at all temperatures tested, the strains carrying *spc110-220* had inhibited growth at 37ºC (Figure 26a). The additional depletion of *MLP2* from *spc110-220* cells led to them being inviable at this temperature. Even at permissive temperatures the depletion of *MLP2* decreased the viability of *spc110-220* strains significantly. The repression of *MLP1* also reduced viability in conjunction with *spc110-220*, but to a lesser extent than *MLP2*. This is consistent with the observation that the additional deletion of MLP1 worsens the phenotypes observed in the *mlp2*Δ strain and is consistent with partially overlapping functions of the Mlp proteins at the SPB. We measured the budding index, cellular morphology and nuclear migration, and found that the *spc110ts* mutation led to an accumulation of very large budded cells, with a high frequency of nuclei being trapped in the bud neck at 37ºC (Figure 26b, left); however, this phenotype was independent of *MLP2*. In contrast, we found that the depletion of *MLP2* led to a nearly 4-fold increase in

aberrant nuclear morphology in the *spc110-220* mutant at the restrictive temperature (Figure 26b, right). The nuclei appeared enlarged or fragmented with multiple intense DAPI stained areas distributed throughout the cell, in contrast to the discrete, round *wild type* nuclei. This morphology of the nucleus was reminiscent of the one we observed in multi-cellular chains present in *mlp2*Δ strains (Figure 25b). Other described defects associated with spc110-220 at the restrictive temperature were found to be independent of the expression level of *MLP2* (Sundberg et al., 1996).

We compared the strong synthetic effects of MLP depletion in the spc110-220 background with the effect of MLP deletion in other ts SPB protein mutants (Figure 27; Davis, 1992; Elliott et al., 1999; Geiser et al., 1991; Sundberg and Davis, 1997). When quantified, we found that most other mutants we tested showed either mild or no synthetic lethal interactions with MLP2. Interestingly, the deletion of MLP1 or MLP2 in the background of *cmd1-1*, a mutant thought to be involved in the same functional pathway as *spc110-220*, also causes lethality at the restrictive temperature (Geiser et al., 1993). These results suggest that a specific functional interaction exists between spc110-220, a mutant in a central plaque component affecting SPB assembly, and the Mlps *via* Mlp2p.

*Incorporation of components into the SPB occurs with reduced efficiency in mlp2*Δ *cells*

Our data are consistent with a model in which the connection of SPBs to the Mlp assembly *via* Mlp2p is necessary for the efficient incorporation of SPB components into the SPB core (see also Figure 29). This model may explain the binding of Mlp2p to the

SPB core, the stochastic failures in cell division in cells lacking Mlp2, the appearance of intranuclear microtubule organizers in *mlp2*Δ cells, and the synthetic interaction of Mlps with *spc110-220*. A prediction of this model is that cells lacking Mlp2p would have a defect in incorporating newly made components into SPBs, resulting in smaller SPBs. We tested this prediction by quantitating the fluorescence signal intensity associated with Spc42p-GFP labeled SPBs in *wild type* and mutant cells (Figure 28a). We observed a ~10% decrease in Spc42p-GFP signal intensity in *mlp2*Δ cells with respect to *wild type*. A smaller but equally significant reduction in SPB-associated fluorescence was observed in cells lacking Mlp1p. To exclude the possibility that the observed decrease in Spc42p-GFP fluorescent signal is due to a reduction of the Spc42p-GFP expression level in cells lacking Mlps, we performed an immunoblot analysis on whole cell lysates from mutant and *wild type* cell strains (Figure 28b). We did not observe any apparent variation in Spc42p-GFP expression due to the lack of either of the Mlps. The results presented in here show that the anchoring of SPBs to the Mlp assembly *via* Mlp2p promotes the ability of components to be incorporated into the SPB. In the absence of the Mlp connection, incorporation of components into the SPB occurs with a reduced efficiency, resulting in smaller and suboptimal SPBs.

Figure 21: **Mlp2p, but not Mlp1p, strongly interacts with SPB proteins.**

(a) PrA containing complexes were affinity purified from cell lysates expressing Mlp1p-PrA, Mlp2p-PrA or PrA alone as a control (see also Figure 19). The complexes were separated by SDS-PAGE, visualized by Coomassie staining and identified by tandem mass spectrometry. The position of rabbit IgG heavy chain leaked from the DynaBeads is indicated (*open circles*). (**b**) Mlp2p directly binds Spc110p, Spc42p and Spc29p, but not Cnm67p. Mlp2p-PrA associated SPB components were affinity purified as described above and eluted from IgG-Dynabeads using 1M $MgCl_2$ leaving Mlp2p-PrA attached to the beads. Proteins in the eluate were then separated on SDS-PAGE and transferred to nitrocellulose. The blot was probed with purified Mlp1-PrA or Mlp2p-PrA (see also Figure 5a), or with blocking buffer alone as control. Bound PrA probes were detected with rabbit IgG. **(c-e)** Spc110p-PrA and Spc42p-PrA co-immunoprecipitate Mlp2p, but not Mlp1p. PrA containing affinity purified complexes (*IP*) and whole cell lysates (*lysate*) of strains co-expressing combinations of the indicated PrA-tagged SPB components as baits and Myc-tagged Mlp1p or Mlp2p as targets, were probed by immunoblotting for Myc and PrA (*co-expressed*). To control for interactions occurring post-lysis, strains expressing either one PrA-tagged bait or one Myc-tagged target were mixed after cell lysis and analyzed as above (*mixed*). MN.

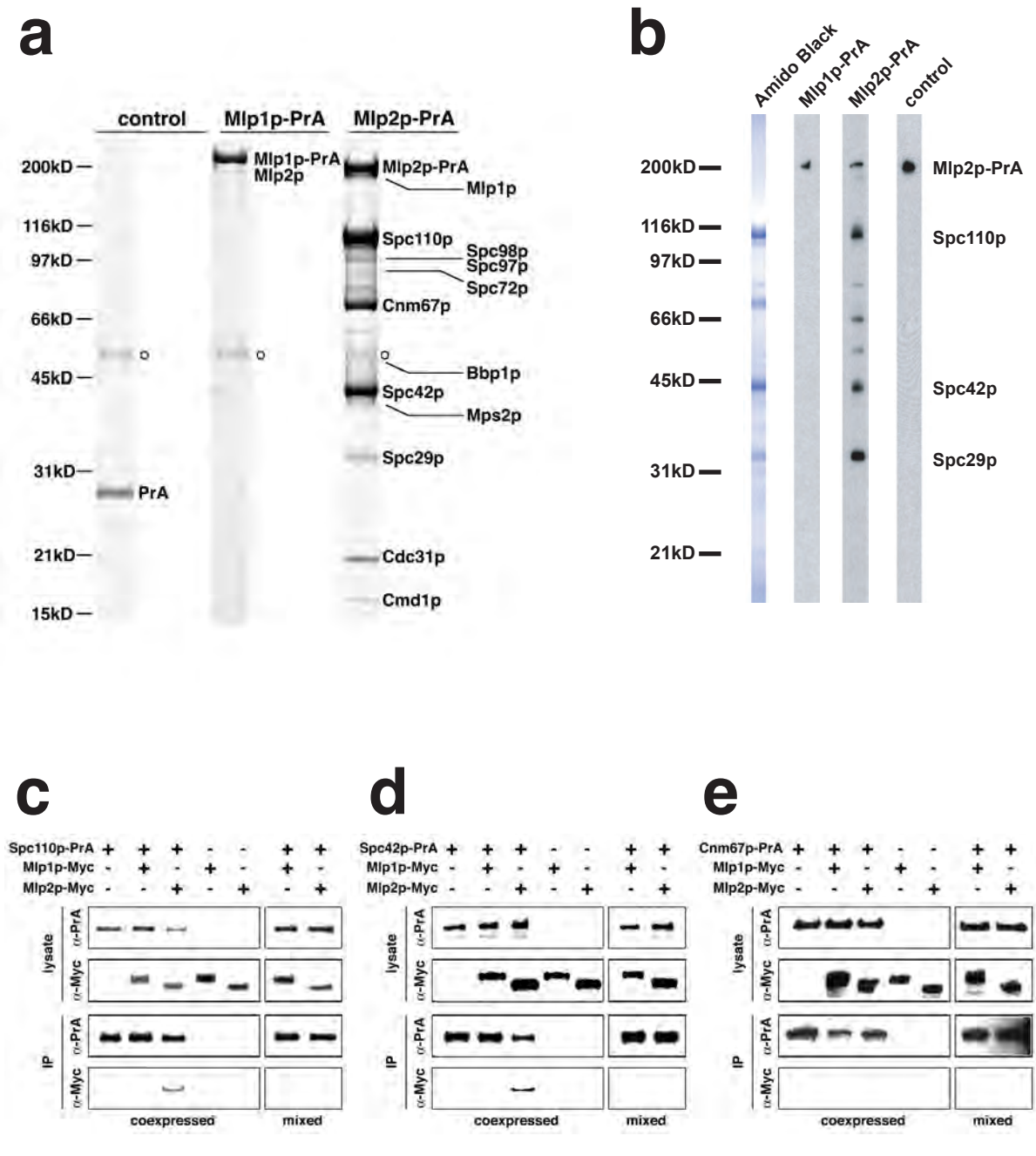
a
control
Mlp1p-PrA
Mlp2p-PrA
200kD
116kD
97kD
66kD
45kD
31kD
21kD
15kD
PrA
Mlp1p-PrA
Mlp2p
Mlp2p-PrA
Mlp1p
Spc110p
Spc98p
Spc97p
Spc72p
Cnm67p
Bbp1p
Spc42p
Mps2p
Spc29p
Cdc31p
Cmd1p
b
Amido Black
Mlp1p-PrA
Mlp2p-PrA
control
200kD
116kD
97kD
66kD
45kD
31kD
21kD
Mlp2p-PrA
Spc110p
Spc42p
Spc29p
c
Spc110p-PrA
Mlp1p-Myc
Mlp2p-Myc
lysate
IP
α-PrA
α-Myc
coexpressed
mixed
d
Spc42p-PrA
Mlp1p-Myc
Mlp2p-Myc
lysate
IP
α-PrA
α-Myc
coexpressed
mixed
e
Cnm67p-PrA
Mlp1p-Myc
Mlp2p-Myc
lysate
IP
α-PrA
α-Myc
coexpressed
mixed

Figure 22: **The complex of Mlp2p with SPB components is stable to extraction.**

PrA containing complexes from cells expressing Mlp2p-PrA were purified as in Figure 21a. The stringency of the extraction buffer was sequentially increased using higher concentrations of NaCl **(a)** or sodium N-lauroyl-sarcosine **(b)**. Protein bands were compared against Figure 21a and identified by their molecular weight. MN.

a

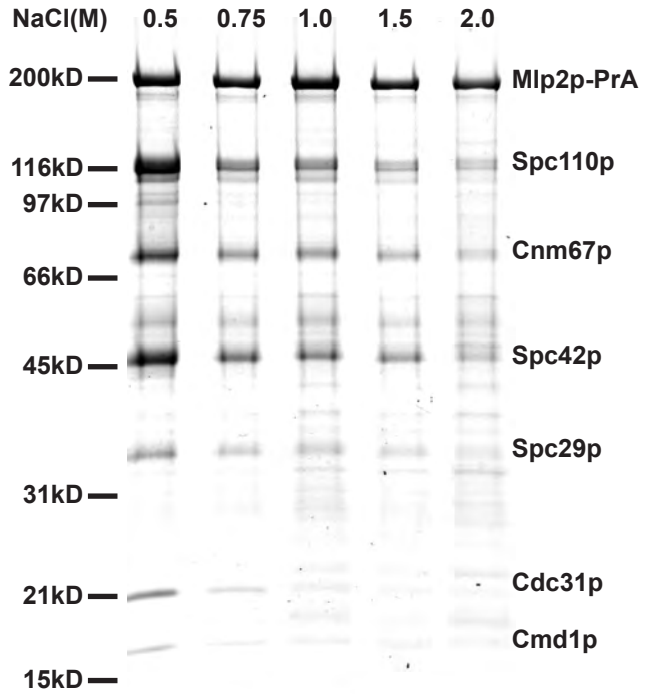
NaCl(M)
0.5
0.75
1.0
1.5
2.0
200kD
116kD
97kD
66kD
45kD
31kD
21kD
15kD
Mlp2p-PrA
Spc110p
Cnm67p
Spc42p
Spc29p
Cdc31p
Cmd1p

b

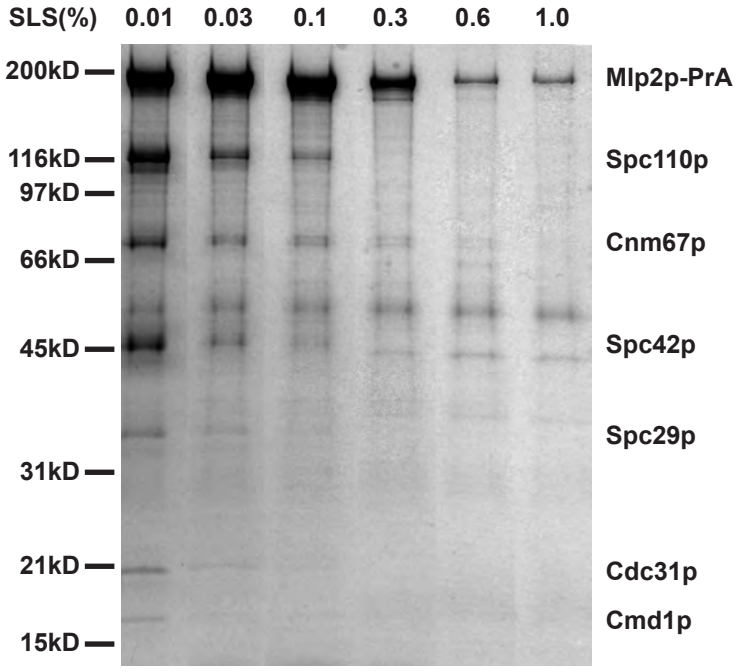
SLS(%)
0.01
0.03
0.1
0.3
0.6
1.0
200kD
116kD
97kD
66kD
45kD
31kD
21kD
15kD
Mlp2p-PrA
Spc110p
Cnm67p
Spc42p
Spc29p
Cdc31p
Cmd1p

Figure 23: **Mlp2p interacts with assembled SPB cores.**

DynaBeads carrying Mlp1p-PrA **(a)** or Mlp2p-PrA **(b, c** and **d)** containing complexes were prepared exactly as described above from either haploid **(a, b,** and **c)** or diploid **(d)** cells and visualized by TEM. The electron-dense globular particles visible in **(a)** and **(b)** are also present in empty control beads and are the magnetic material from the DynaBeads. **(c)** Three representative examples of haploid SPBs bound to Mlp2p-PrA beads at higher magnification. **(d)** Three examples of diploid SPBs bound to Mlp2p-PrA beads. **(e)** The diameter and thickness of the central plaque of both haploid and diploid Mlp2p-PrA bound SPBs were measured on calibrated digital images using the ImageJ software, presented as Tukey plots, and listed as the mean value +/- 1 standard deviation. Dots indicate data points lying outside 3/2 times the interquartile range, shown by the thin lines with horizontal bars. Also indicated (*) is the Student's t test P value obtained for the comparison of the distribution of diameters of haploid versus diploid SPBs. Clearly discernable haploid SPBs (*small arrows*). Mlp2p-PrA filaments attaching the SPBs to the beads (*Large arrows*). Bars, 500nm (a and b); 100nm (c and d). MN.

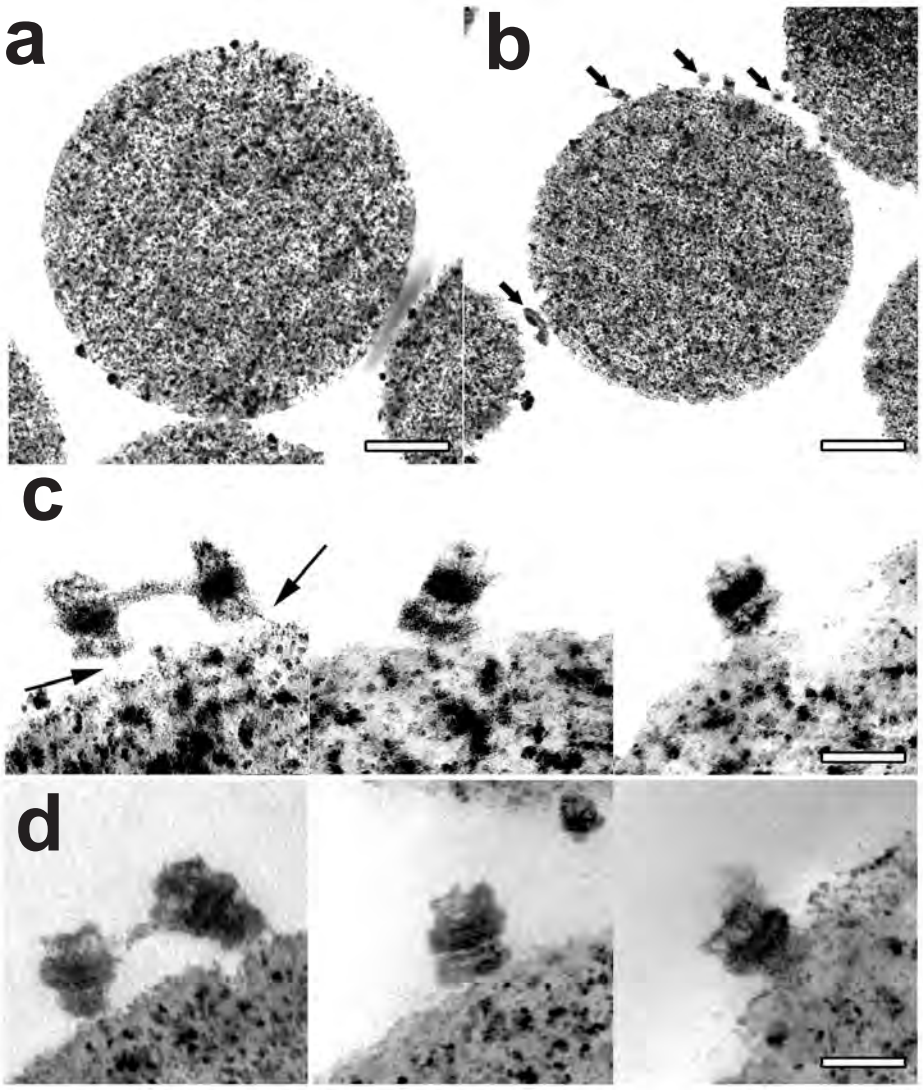

e

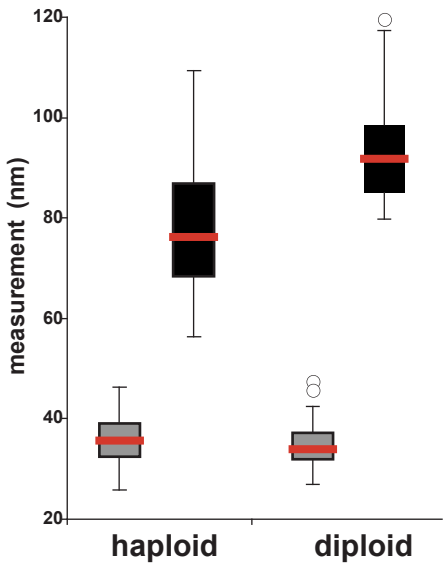

diameter
thickness

haploid (n = 54)
diameter* = 76.9nm +/- 11.9
thickness = 35.6nm +/- 4.5

diploid (n = 55)
diameter* = 93.1nm +/- 9.4
thickness = 35.3nm +/- 4.2

*p < 0.0001

Figure 24: **Mlp2p binds the SPB at all stages of the cell cycle.**

(a) YFP-Mlp2p (green), Spc42p-CFP (red) double-tagged haploid cells were subjected to differential elutriation to enrich for cells at different stages of the cell cycle. Representative fluorescence images for each cell cycle stage are displayed as indicated. *Merge*, two-dimensional image projections for both YFP and CFP were overlaid over a DIC images of each individual cell. *3D*, a three-dimensional rendition of each double-color image was obtained employing the Imaris software and overlaid over a digital outline of the whole cell. Bar, 1μm. **(b)** Mlp2p-PrA expressing cells were released from a metaphase arrest and PrA containing complexes were prepared from samples at the indicated timepoints as described in Figure 21a. A control sample was taken from an asynchronous culture (*AS*). **(c)** Samples collected in (b) were prepared for western blotting and FACS analysis. Blots were probed for Mlp2p-PrA, Clb2p and Pgk1p. FACS samples and Clb2p levels were used to determine the progression through the cell cycle in (b). (a) CS (b and c) MN.

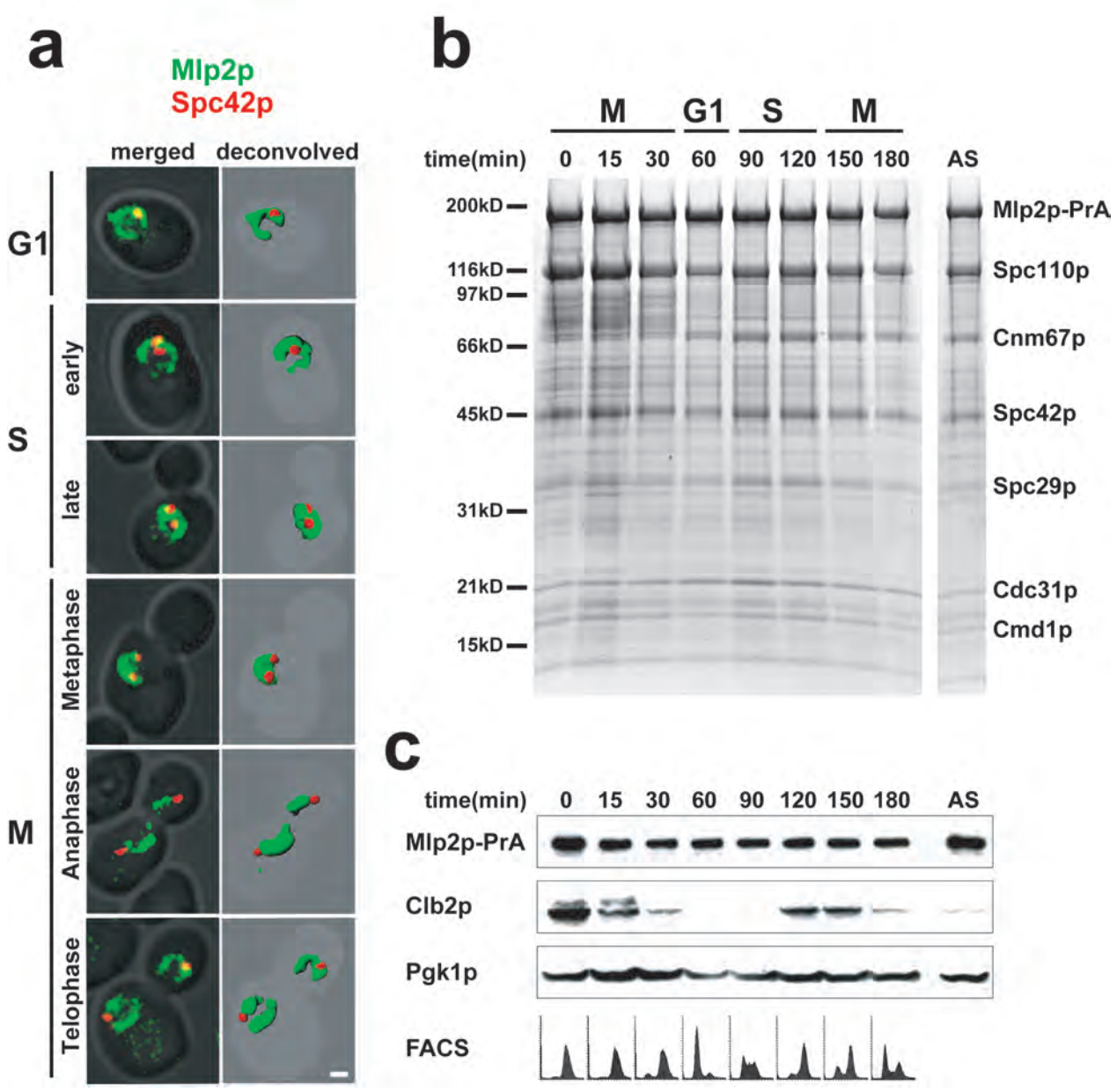
a
Mlp2p
Spc42p
merged
deconvolved
G1
S
early
late
M
Metaphase
Anaphase
Telophase
b
M
G1
S
M
time(min)
0
15
30
60
90
120
150
180
AS
200kD
116kD
97kD
66kD
45kD
31kD
21kD
15kD
Mlp2p-PrA
Spc110p
Cnm67p
Spc42p
Spc29p
Cdc31p
Cmd1p
c
time(min)
0
15
30
60
90
120
150
180
AS
Mlp2p-PrA
Clb2p
Pgk1p
FACS

Figure 25: ***mlp2*Δ cells accumulate multiple amorphous nuclear Spc42p-containing bodies.**

(a) Quantitative analysis of the number of Spc42p-GFP containing foci in *wild type*, *mlp1*Δ and *mlp2*Δ cells. Asynchronous Spc42p-GFP haploid cells were fixed and stained with DAPI to reveal the position of the nucleus. Two-dimensional image projections of 3D image stacks obtained for both GFP and DAPI were overlaid onto each respective DIC image for scoring multiple Spc42p-GFP signals (n>600). **(b)** *Wild type*, *mlp1*Δ and *mlp2*Δ cells expressing Spc42-GFP were separated by differential elutriation. Cells present in equivalent elutriation fractions were imaged as described in (a) for Spc42p-GFP (red) and DAPI stained nuclei (blue). Two representative fields are presented for *mlp2*Δ. Bar, 2μm. **(c)** Budding index (top panels) and FACS profile (bottom panels) of *wild type* and *mlp2*Δ cells separated by differential elutriation. **(d)** FACS analysis of elutriation fraction 12 gated by size (top panel) to reveal the DNA content of three sub-populations (bottom panels). **(e)** *Left panels*, thin section, TEM images of diploid mutant cells lacking Mlp2p, after enrichment for large-budded cells and cell-chains by elutriation. *Arrowheads*, amorphous electron-dense material presumably composed of mis-assembled SPB components. *Arrows*, spurious microtubules bundles emanating form MTOC positioned perpendicular to the visible SPB. Inset, two-fold magnification of an area presented in the bottom left panel, showing one of these bundle of microtubules. *Right panels*, line drawings of the panels shown on the left highlighting the position of microtubule bundles, the NE, SPBs and amorphous electron-dense SPB-like structures. Bars, 100 nm. CS.

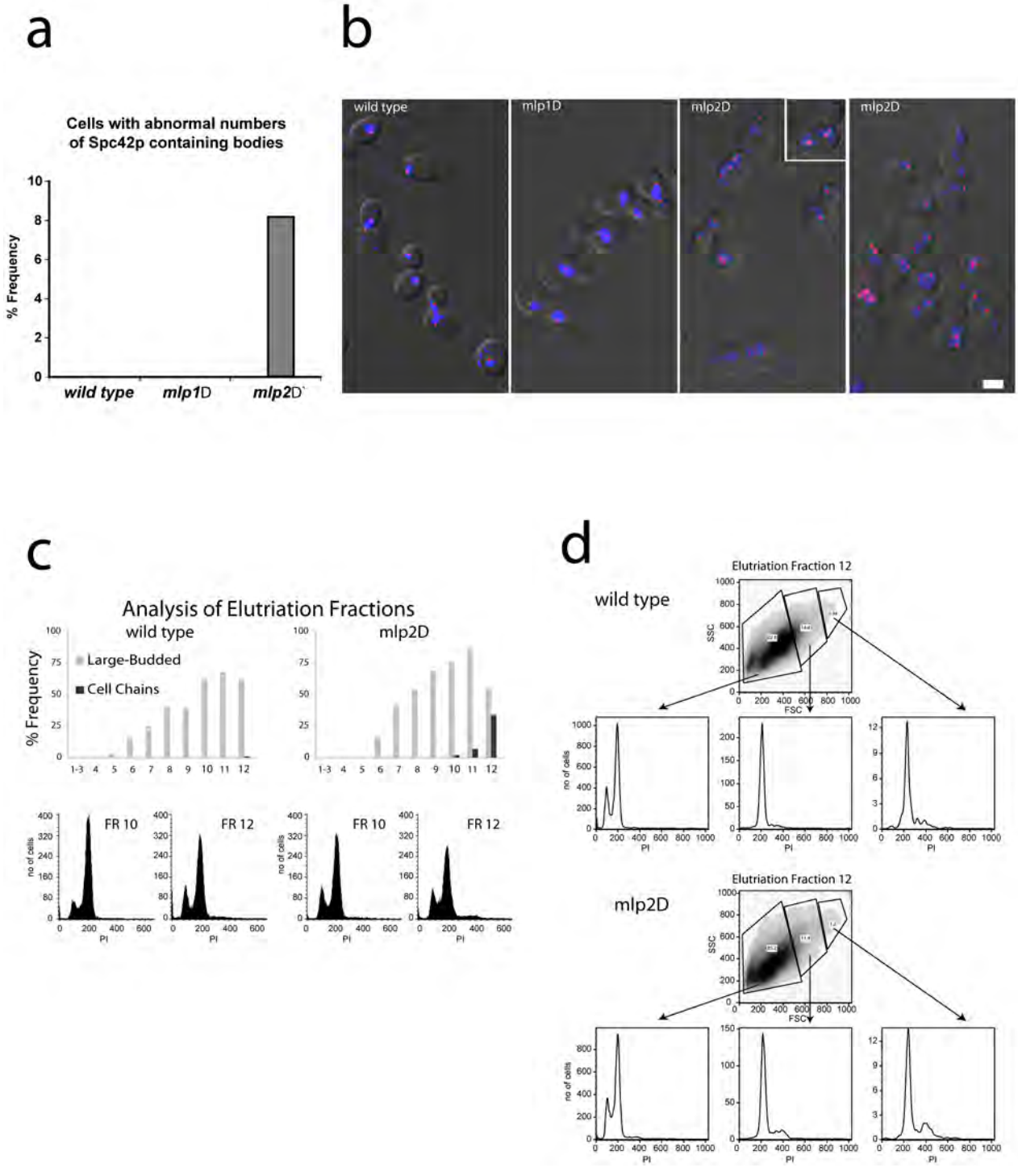
a
b
Cells with abnormal numbers of Spc42p containing bodies
% Frequency
wild type
mlp1D
mlp2D
wild type
mlp1D
mlp2D
mlp2D
c
d
Analysis of Elutriation Fractions
wild type
mlp2D
Large-Budded
Cell Chains
% Frequency
FR 10
FR 12
no of cells
PI
Elutriation Fraction 12
wild type
mlp2D
SSC
FSC

e

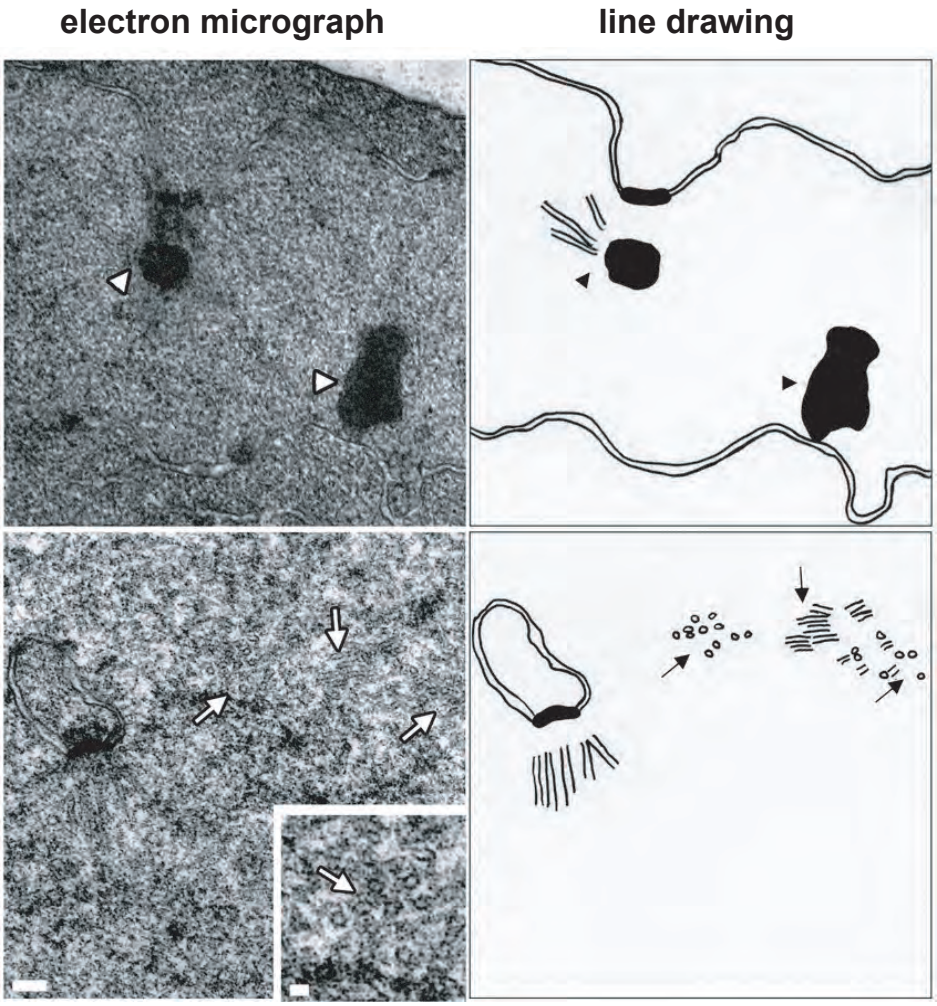

Figure 26: **Low expression levels of *MLP2* in conjunction with *spc110-220* cause lethality and loss of nuclear integrity at 37ºC.**

(a) Two individual clones of strains expressing either *SPC110* or the *spc110-220* allele alone (-) or in combination with either *MLP1* or *MLP2* under the control of the *GAL1-10* promoter (*Gal-MLP1* and *Gal-MLP2* respectively) were spotted in 10^{-1} dilution steps on dextrose-containing plates and grown for two days at the indicated temperatures. **(b)** Cells were scored for DAPI stained nuclei spanning the bud neck (left) and for grossly aberrant nuclear morphology (right; n>300). **(c)** The spindle (red) and DNA (blue) were visualized by indirect immunofluorescence and DAPI staining in formaldehyde-fixed cells (top). The DNA content of propidium iodide stained cells was measured by FACS (bottom). The indicated strains were grown at the indicated temperature 48 hours (a) or at room temperature to mid-log phase (b, *23ºC*) and shifted for 4 hours to the restrictive temperature (b, *37ºC*; c). Bar, 4µm. MN.

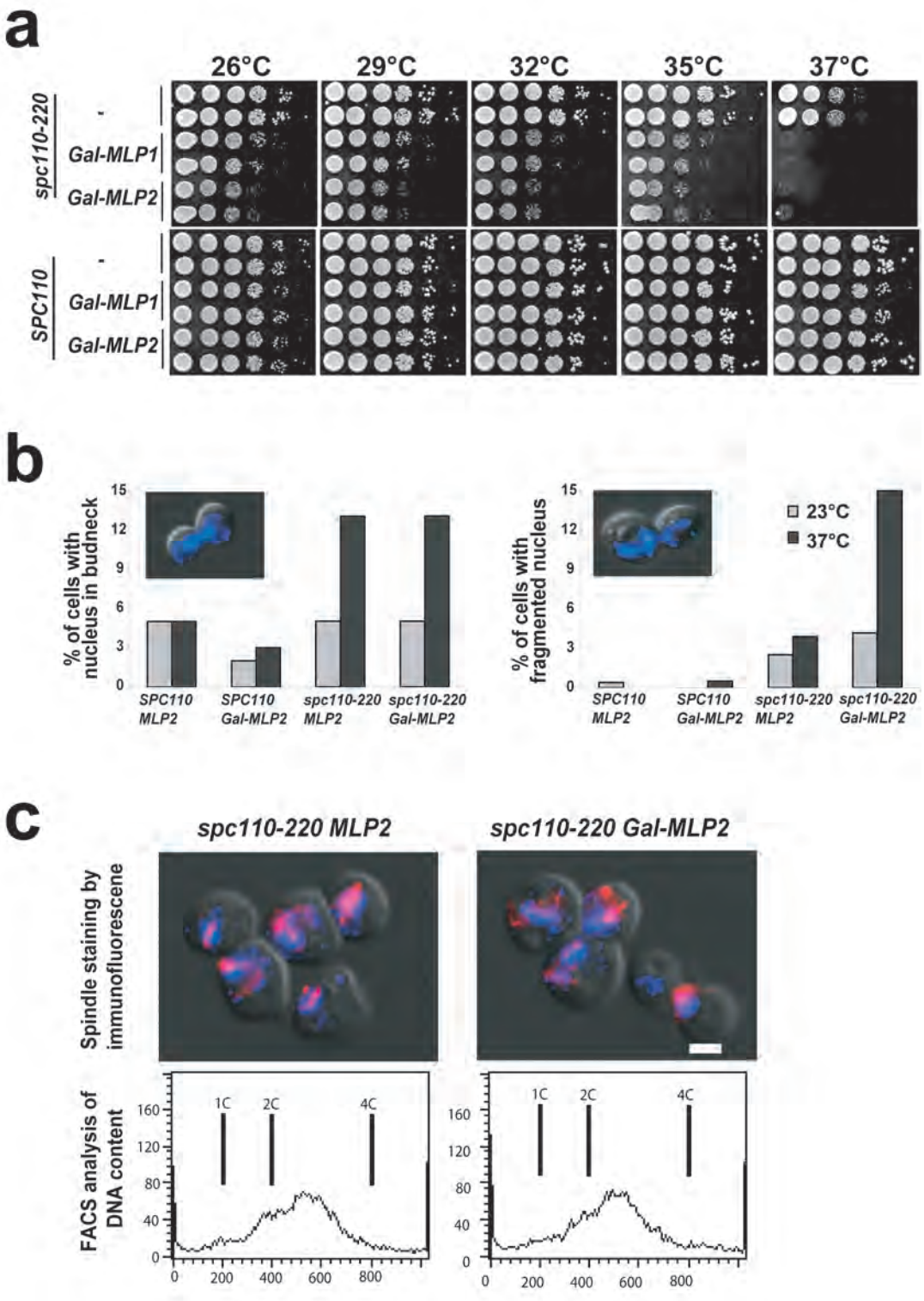
a
26°C
29°C
32°C
35°C
37°C
spc110-220
-
Gal-MLP1
Gal-MLP2
SPC110
-
Gal-MLP1
Gal-MLP2
b
% of cells with nucleus in budneck
15
12
9
6
3
0
SPC110 MLP2
SPC110 Gal-MLP2
spc110-220 MLP2
spc110-220 Gal-MLP2
% of cells with fragmented nucleus
23°C
37°C
c
spc110-220 MLP2
spc110-220 Gal-MLP2
Spindle staining by immunofluorescene
FACS analysis of DNA content
1C
2C
4C
160
120
80
40
0
0
200
400
600
800

Figure 27: **Other mutations of SPB components are not synthetically lethal with deletion *mlp2*Δ.**

(a) Semiquantitative relative measure of dilution-adjusted colony density from strains with the indicated genotype and their counterparts carrying the *wild type* SPB protein allele grown as described in Figure 26a. Data presented in Figure 26a and 27b-c was used for this analysis. **(b)** Two independent isolates of strains expressing the indicated temperature sensitive mutant genes or their *wild type* alleles either alone (-) or in combination with *mlp1*Δ or *mlp2*Δ were spotted in 10^{-1} dilution steps and grown for two days at the indicated temperatures. **(c)** Control strains for (b) were grown as described. Shown is the growth at the indicated temperatures, yet all temperatures tested gave identical results. MN.

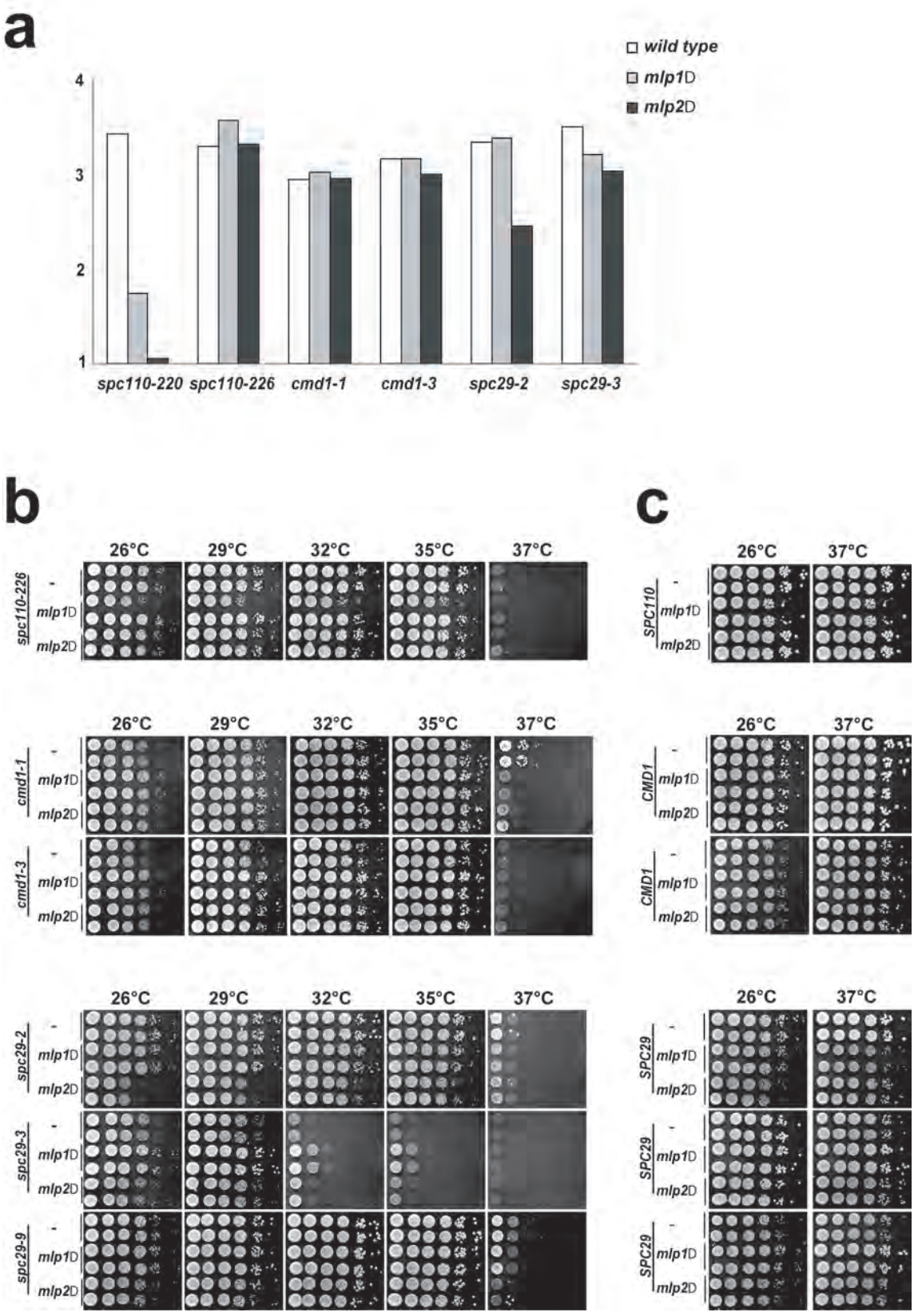
a
wild type
mlp1D
mlp2D
4
3
2
1
spc110-220
spc110-226
cmd1-1
cmd1-3
spc29-2
spc29-3
b
c
26°C
29°C
32°C
35°C
37°C
spc110-226
cmd1-1
cmd1-3
spc29-2
spc29-3
spc29-9
SPC110
CMD1
SPC29
-
mlp1D
mlp2D

Figure 28: ***mlp2*Δ has a defect in incorporating components into their SPBs, resulting in smaller SPBs.**

(**a**) Haploid *wild type* and mutant cells expressing genomically tagged Spc42p-GFP were analyzed by fluorescence microscopy as in Figure 10a. Projections of image stacks were utilized for quantitative analysis of the GFP signal associated with each individual SPB (n>100, 3 repetitions with similar results). Data was normalized to the average *wild type* intensity value and a combination of all data is presented. The distributions of SPB intensity measurements for each strain are displayed as "bee swarm" plots, in which individual data points are randomly spread out in the horizontal direction. Indicated is the mean intensity +/- standard deviation (*wild type* 1.00+/-0.128, *mlp1*Δ, 0.947+/-0.114, *mlp2*Δ, 0.915+/-0.114). P values of Student's t test pairwise comparisons are indicated. (**b**) Deletion of *MLP1* or *MLP2* does not influence the expression of Spc42p-GFP. Total cell lysates from mutant or *wild type* strains used in (a) were probed for Spc42p-GFP and Pgk1p by western blotting. The Spc42p-GFP signal was quantified using the OpenLab software, normalized against Pgk1p signals and plotted (top, error bars indicate standard deviation of 3 experiments). CS and MN.

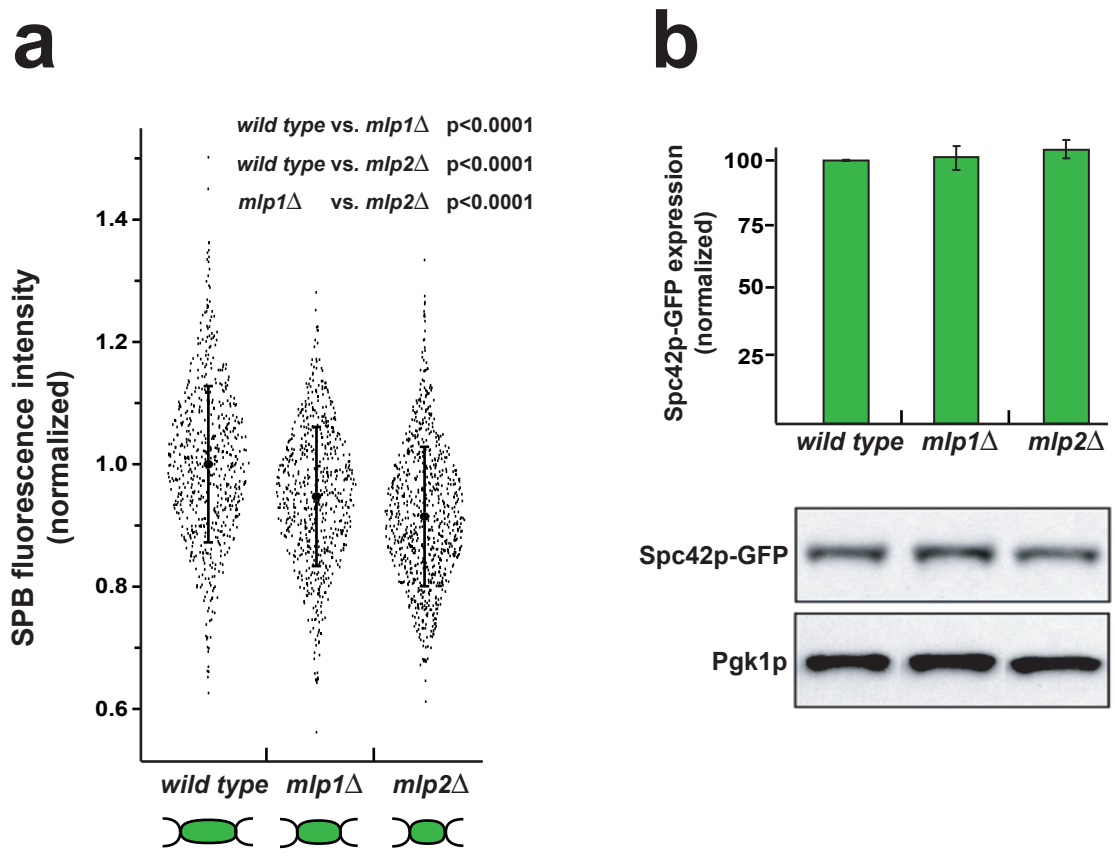
a
wild type vs. mlp1Δ p<0.0001
wild type vs. mlp2Δ p<0.0001
mlp1Δ vs. mlp2Δ p<0.0001
SPB fluorescence intensity (normalized)
1.4
1.2
1.0
0.8
0.6
wild type
mlp1Δ
mlp2Δ
b
Spc42p-GFP expression (normalized)
100
75
50
25
wild type
mlp1Δ
mlp2Δ
Spc42p-GFP
Pgk1p

Figure 29: **Mlp2p links the SPB into the nuclear peripheral Mlp layer and aids the incorporation of new components into its tightly packed core.**

A model depicting the turnover of components at the central plaque of the SPB facilitated by Mlp2p.

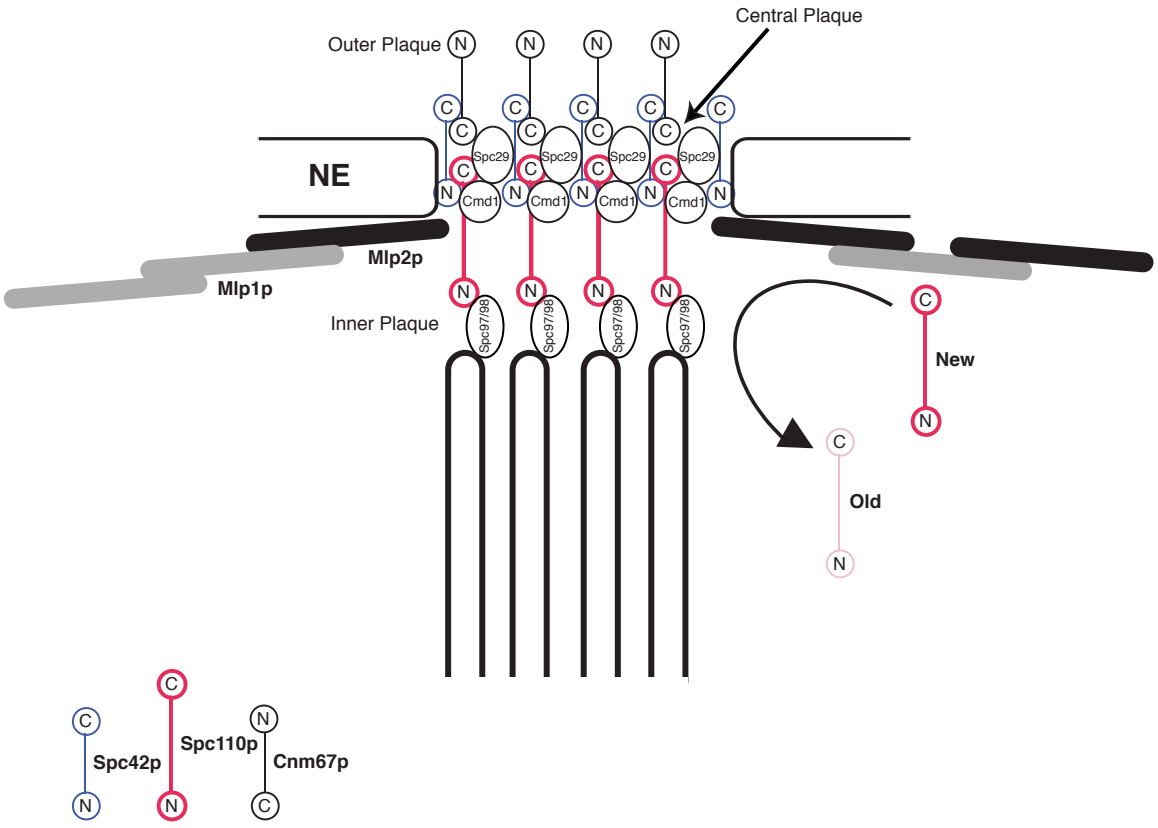
Central Plaque
Outer Plaque
NE
Spc29
Cmd1
Mlp2p
Mlp1p
Inner Plaque
Spc97/98
New
Old
Spc42p
Spc110p
Cnm67p

Chapter 7: Discussion.

Mlp proteins likely form the basket of the NPC.

Current data accumulated by us and others clearly indicates that the bulk of the Mlp proteins are anchored at the NPC. Mlp proteins are in complex with a large number of Nups (Kosova et al., 2000), Mlp proteins map to the NPC by both IEM (Strambio-de-Castillia et al., 1999) and fluorescence, Mlp proteins partially co-fractionate with the NPC in biochemical purifications (Strambio-de-Castillia et al., 1999), Mlp localization is altered by the deletion of Nups (Galy et al., 2004; Galy et al., 2000; Strambio-de-Castillia et al., 1999) and Mlp proteins are implicated in functions of the NPC (Green et al., 2003; Kosova et al., 2000; Strambio-de-Castillia et al., 1999; Vinciguerra et al., 2005).

Recent studies by the Cordes laboratory (Hase and Cordes, 2003; Krull et al., 2004) have convincingly shown that Tpr binds to the peripheral Nup153p to form the nuclear basket structure. Tpr binds as a coiled-coil homodimer forming a hairpin loop structure, with the NBD anchoring it to the NPC with the N- and C-terminus of Tpr located away from the NPC. This conformation suggests that the coiled-coil domains can fold back on each other to form the basket fibers and that the globular C-termini forms the basket ring. The measured size (40-60nm) of the basket and its distance from the NE midplane (60-80nm) (Goldberg and Allen, 1992; Ris, 1997) overlap perfectly with the size and localization of Tpr (Frosst et al., 2002; Krull et al., 2004). The nuclear basket in yeast is less well defined (Fahrenkrog et al., 1998; Rout and Blobel, 1993), but an elegant study

using field emission scanning EM by Kiseleva et al. (2004) has shown that it is very similar to the vertebrate basket. It consists of up to eight filaments, approximately 10nm in diameter, extending about 40nm away from the nucleoplasmic face of the NPC (Kiseleva et al., 2004).

Based on our data, we propose that the Mlp proteins form the nuclear basket in *S. cerevisiae*. Mlp proteins are attached to the NPC and their localization overlaps exactly with the proposed location of the yeast basket. The specific localization of both the N- and the C-terminus away from the pore is conserved between Mlp proteins and Tpr (this study). Purified Mlp1p has approximately the same sedimentation rate (and presumably the same tertiary structure) as purified Tpr. Finally, none of the Nups investigated in a comprehensive study localize far enough away from the pore into the nucleoplasm to form the basket (Rout et al., 2000).

If the Mlp proteins indeed form the nuclear basket structure in yeast, then the fact that not all NPCs are associated with Mlps is surprising. The Mlp layer covers only about 70% of the nuclear periphery and is excluded from the nucleolus this study (Galy et al., 2004), while the NPCs are distributed along the entire NE. This leads to the conclusion that about 30% of the NPCs do not have a nuclear basket and therefore differ in their composition. If the Mlp proteins do play a role in functions associated with the NPC, as our and other data indicates, then why are not all NPCs lined by the Mlp basket?

First, the nucleolus could form a diffusion barrier to mRNPs, excluding them from interacting with Mlp-free NPCs. Second, the Mlp proteins are not essential for yeast viability, so transport occurs even in their absence. Hence, the NPCs underlying the nucleolus must be functional, even without the Mlp basket. Third, Mlp proteins have

been suggested to act as a docking site for the export of mRNPs (Green et al., 2003; Vinciguerra et al., 2005) and to perform a quality control step (Galy et al., 2004). The very fact that mRNPs can bind to Mlp proteins could cause their specific accumulation at pores associated with the Mlps. By tracking individual fluorescently labeled mRNPs, Shav-Tal et al. (2004) determined that in higher eukaryotes, mRNPs traverse from the site of transcription to the NPCs by free diffusion. Since these particles diffuse at a speed of about 0.5μm/s (Shav-Tal et al., 2004) and the size of a haploid yeast nucleus is small (r=1μm), each mRNP will rapidly encounter multiple NPCs. Thereby, they can selectively accumulate at Mlp-associated pores. Fourth, recent evidence suggests that in yeast, there is a correlation between the transcriptional activity of a gene locus and its association with the NPC (Casolari et al., 2004; Ishii et al., 2002). Using chromatin immunoprecipitation, Casolari et al. have illustrated that both Mlp1p and Mlp2p preferentially associate with highly transcribed genes (2004). This hypothesis implies that mRNPs are created preferentially in the vicinity of Mlp-bound NPCs, increasing the probability of docking to such a pore. However, the rapid diffusion rate of mRNPs appears to make this process unnecessary. It should be pointed out that the tethering of actively transcribed chromatin to the NPCs was shown by chromatin immunoprecipitation experiments, which rely on the presence of crosslinkers (Casolari et al., 2004). Since transcripts are processed while they are still being transcribed (Jensen and Rosbash, 2003), these partially formed mRNPs might provide the link found between chromatin and the NPCs.

To determine which, if any, of these models is correct, further work needs to be carried out. In addition, the specific role of Mlp proteins in mRNA metabolism and the

mechanisms of the interaction need to be determined. Do Mlp proteins license mRNPs for export? Do Mlp proteins facilitate the initial transport steps? How do Mlp proteins determine which mRNPs are suitable for export? Likewise, it should be established if mRNPs are exported at all NPCs or preferentially translocate through pores with an Mlp basket. Also, the mechanism for how transcriptionally active chromatin might interact with the NPC is unclear.

Furthermore, it is not known which mechanism ensures that the regions of the NE associated with the Mlps and the nucleolus remain separated. Some evidence indicates that the nucleolus might indeed form a steric barrier to the movement of the Mlp proteins. Dissociation of Mlp1p from the pore by the deletion of Nup60p causes Mlp1p to accumulate within the nucleus, yet it remains largely excluded from the region of the nucleolus (Galy et al., 2004). This in turn means that any free Mlp within the nucleus will more likely encounter a pore that is not in the same region as the nucleolus. This simple sorting mechanism might also explain how other proteins like Esc1p (Andrulis et al., 2002) and Ulp1p (Zhao et al., 2004) accumulate specifically in the region excluded of the NE excluded from the nucleolus.

Mlp proteins form a peripheral nuclear network.

Increasing evidence indicates that the nuclear basket may not be the static and discrete structure most illustrations portray. In fact, the basket appears to be highly flexible, as evidenced by drastic conformational changes during the export of mRNPs (Kiseleva et al., 1998b) and it appears to be integrated into a continuous array of protein

filaments connecting neighboring pores (Kiseleva et al., 2004; Ris, 1997). Studies on Tpr confirm that its localization is not static relative to the pore (Krull et al., 2004) and can extend considerable distances away from the NPC (Cordes et al., 1997; Frosst et al., 2002).

Our data is consistent with the Mlp proteins forming a molecular assembly at the nuclear periphery, interlinking neighboring NPCs into a network. Mapping the localization of Mlp proteins at the NPC, we find that both the N- and C-terminus can spread along the NE for considerable distances. Given that the N- and C-terminus of the Mlp proteins project away from the pore for approximately 50nm (this study) and the distance to the nearest neighboring NPCs in yeast (Winey et al., 1997), two Mlp dimers could span the distance between two neighboring pores and physically link them together. Both Mlp proteins are found together in large complexes, containing multiple Nups. In addition, our data shows that Mlp1p and Mlp2p can directly interact with each other. Field emission scanning EM of the inner face of the nuclear envelope illustrates that there are protein filaments connecting neighboring pores which are continuous with the nuclear basket structure (Kiseleva et al., 2004). Neither the analysis of NPC associated proteins (Rout et al., 2000) nor the immunopurification of Mlp complexes (this study) has yielded any plausible candidate that might form these connections, other than the Mlp proteins itself. In higher eukaryotes, the NPCs are connected into a stable, elastic network with the underlying lamins (Daigle et al., 2001). Studies in yeast, using fluorescently labeled Nups, showed that their NPCs are considerably more mobile than in higher eukaryotes (Belgareh and Doye, 1997; Bucci and Wente, 1997), consistent with the fact that yeast do not contain a lamina. The Mlp network is much more dynamic and loosely associated

with the NPC than the lamina as evidenced by the great difficulty of fractionating NPCs away from the associated lamins (Aaronson and Blobel, 1975; Havre and Evans, 1983), while in contrast Mlps are easily stripped from the NPC fraction in yeast (Rout et al., 2000). It should be noted that the two studies on the mobility of NPCs might be misleading, since they were not performed on unperturbed *wild type* cells. Belgareh and Doye (1997) tested the mobility of pores in the background of a clustering mutant which alters the normal distribution of Mlp proteins (Strambio-de-Castillia et al., 1999). Bucci and Wente (1997) performed their mobility assay during karyogamy of mating yeast. We demonstrated that yeast downregulate their expression of both Mlp proteins to non-detectable levels when treated with alpha factor, released during a natural stage of the mating process (data not shown), possibly facilitating the easy distribution of pores in mating cells. So it remains to be seen how an intact Mlp network might influence the mobility of NPCs.

Our study of cells lacking Mlp proteins suggests that an important function of this network is to support the structure of the NE. Loss of Mlp proteins causes the nucleus to lose its regular shape and become less rigid. Furthermore, the *mlp1*Δ*mlp2*Δ strains are sensitive to further weakening of the NE. These phenotypes are surprisingly similar to those caused by defects in the nuclear lamina of higher eukaryotes (Lammerding et al., 2004; Muchir et al., 2003; Sullivan et al., 1999). Structural support might not be the sole function of the Mlp network. The connection of the NPCs by protein filaments not only ensures that pores are kept in close proximity to each other; it also guarantees that neighboring pores are separated by a minimum distance. Studying the distribution of NPCs in yeast, Winey and co-workers (1997) found that a region of about 120nm around

each NPC is completely free of neighboring pores. It is plausible that pores would need to be kept at a minimum distance to ensure their proper function, or that the close proximity of multiple channels through the NE might be detrimental to its stability.

Interestingly, in mitotic cells, NPCs cluster around the SPB at a distance of approximately 200nm, yet in closer proximity no NPCs are found (Winey et al., 1997). As discussed below, Mlp2p binds tightly to the central plaque of the SPB, which in turn might account for this spatial distribution of the NPCs. Interactions between Mlps bound to the NPCs and to the SPB might link the two structures together, while at the same time ensuring that a minimal distance is maintained at all times. Apart from the direct function on SPB assembly and turnover discussed below, this interaction might have additional functions. As suggested previously (Winey et al., 1997), it might aide in the even distribution of NPCs during mitosis. In fact, the close connection between the SPB, the NPCs and the Mlps may reflect a further cooperation between the structures of the nuclear periphery. The SPBs may actively promote segregation of the Mlp/NPC network to mother and daughter nuclei. Because the Mlp proteins are located asymmetrically along the nuclear periphery, a random bisection of the nucleus does not guarantee their equal distribution at karyokinesis. However, at metaphase the SPBs line up the Mlp layer perpendicular to the axis of nuclear division. This configuration may not only facilitate the segregation of the Mlps; the nucleolar components, which are also closely associated with the NE and excluded from the Mlps, would be aligned perfectly for equal partitioning to mother and daughter nuclei as well. The faithful distribution of the Mlp proteins and other interconnected NE structures to the opposite spindle poles ensure that each cell has a fully functional NE immediately upon entering G1.

Mlp proteins affect nucleo-cytoplasmic transport.

Due to their localization at the NPC and previous studies (Strambio-de-Castillia et al., 1999) we investigated in detail if the Mlp proteins are directly involved in the transport of proteins across the NE. Our results show that without the Mlp proteins, the import of certain cargoes into the nucleus is impaired. Interestingly, the steady state distribution of the very same cargo remains unchanged in comparison to *wild type* cells. These results postulate that in cells lacking Mlps there is a change in the rate of cargo being actively imported into the nucleus and an equal, but opposite change in the rate the same cargo diffuses out of the nucleus. This makes it very unlikely that the Mlp proteins are directly involved in a specific step of protein transport. As discussed previously, there are several models that could explain such a finding, most notably that less NPCs are available in the Mlp mutant, both for transport and for diffusion.

How might the absence of Mlp proteins affect such a change in the cells? Since the Mlp network ensures proper spacing between neighboring pores, in the *mlp1*Δ*mlp2*Δ strain neighboring pores could move too close to each other and obstruct proper function. The Mlp basket structure may function in keeping nuclear material away from the pore, thereby ensuring free access to the transport channel. Mlp proteins have also been implicated in the docking and transport of mRNPs across the pore. If this process is slowed in cells lacking Mlps, individual pores could get physically blocked by translocating mRNPs. Finally, the Mlp proteins may play a role in the biogenesis of NPCs, leading to a reduced number of pores in the Mlp mutant. None of these models are

mutually exclusive and further testing is required to determine the exact cause of impaired transport and diffusion rates in strains lacking Mlps.

A proteomic approach to study the Mlp proteins.

In the work described here, we purified and identified a large number of proteins in complex with Mlp1p and Mlp2p. Using techniques and conditions optimized for the Mlp proteins, we were able to overcome the challenges posed by working with these proteins. Cryolysis preserves native complexes and facilitates the extraction of the proteins associated with the NE. The immediate contact of protease inhibitors upon thawing of the cell powder allows for purification of full length Mlp proteins. The short timeframe the proteins are in contact with extraction and washing buffers aides in the isolation of low-affinity interactions. The methods used in previous studies to gather data on proteins in complex with the Mlps have considerable caveats. Most published interactions rely on the use of co-immunoprecipitations followed by western blotting, which can easily lead to false positives if not carefully controlled and give no indication on the scope of the complex purified (Galy et al., 2004; Galy et al., 2000; Lei et al., 2003; Vinciguerra et al., 2005). In addition, this technique, like the use of purified proteins for *in vitro* binding assays (Green et al., 2003; Kosova et al., 2000) requires prior knowledge about the interaction to be tested. This will in turn make the discovery of unsuspected interactions unlikely.

As described above, we were able to reproducibly purify extensive complexes formed by the Mlp proteins. We identified the majority of proteins in the complexes and found

that they fall into six different classes of proteins: Mlps, Nups, transport factors, mRNA processing factors, SPB components and a group of possible contaminants. The strength of our approach is apparent when we analyze the proteins found with respect to previously published data and our unpublished results.

It is now generally accepted that the bulk of the Mlp proteins in the cell are attached to the NPC. In agreement, the majority of proteins we find in complex with the Mlps are Nups. Specifically, both Mlp proteins are in complex with Nic96p, a Nup which has been reported to bind Mlp2p using a crosslinking study (Kosova et al., 2000). Mlp2p is in a complex with the peripheral Nup1p, the yeast homolog of Nup153p, which connects Tpr to the NPC (Hase and Cordes, 2003). Mlp1p is in a complex with peripheral Nup60p, deletion of which abrogates the association of Mlp1p with the nuclear periphery (Feuerbach et al., 2002). We find the transport factors Kap60p and Kap95p in complex with the Mlp proteins. Kosova et al. (2000) determined that both proteins can bind to Mlp2p *in vitro*, confirming our data. The mRNA transport and processing factors Yra1p, Sac3p and Mex67p we find in the Mlp complexes have all been reported to form complexes with the Mlp proteins using co-immunoprecipitation followed by western blotting (Lei et al., 2003; Vinciguerra et al., 2005). Also, a wealth of data indicates a role for the Mlps in mRNA metabolism (Galy et al., 2004; Green et al., 2003; Lei et al., 2003; Vinciguerra et al., 2005). Finally, we found SPB components associated with Mlp2p and our work established a functional basis for this connection (discussed below). Taken together, these studies provide strong evidence that the method utilized here is sound and provides useful data to study Mlp function.

Since the publication of the complete *S. cerevisiae* genome and the generation of a genetic map (Cherry et al., 1997), multiple high-throughput studies have been carried out to aide elucidating the function of the yeast proteome (Gavin et al., 2002; Huh et al., 2003; Lee et al., 2004; Troyanskaya et al., 2003). While these high throughput methods are a valuable tool in a rough, primary analysis of a specific protein, they often offer little more than a starting point for future research. The data provided by the yeast protein complex database is incomplete since only about 4% of the yeast proteome was tagged and successfully used for complex purification and analysis (Gavin et al., 2002). The available data suggests that Mlp1p is part of the SRB mediator complex, involved in transcription initiation and regulation from Pol II promoters (Gavin et al., 2002). This interaction is plausible, since a recent study supports a role for the Mlp proteins in the global regulation of transcription (Vinciguerra et al., 2005). However, it is surprising that the Mlp proteins were not found to participate in any other complexes. None of the SPB components, mRNA processing or transport factors, protein import factors or Nups tagged and analyzed in the large scale study were found to participate in complexes with the Mlp proteins (Gavin et al., 2002). It is possible that this is due to the extraction conditions used, which are mild and might therefore select against the purification of NE associated complexes (Rigaut et al., 1999). It will be interesting to see how the large scale interaction screens progress from here. Certainly, the tagging and subsequent purification of all yeast proteins should increase the amount of useful data.

Even though the complexes found with Mlp1p and Mlp2p are extensive, we can not be certain to have identified all the complexes of which the Mlps might be a part. Notably missing is, for example the Mlp1p containing SRB mediator complex (Gavin et al., 2002).

Although the Mlp proteins have been implicated in DNA silencing (Feuerbach et al., 2002; Galy et al., 2000), telomere anchoring (Galy et al., 2000), telomere maintenance (Hediger et al., 2002a), DNA repair (Galy et al., 2000; Kolling et al., 1993; Kosova et al., 2000; Zhao and Blobel, 2005) and the maintenance of 2 micron DNA circles (Zhao et al., 2004) we did not find a single protein directly involved in DNA metabolism. However, convincing data has yet to be published that establishes a direct physical connection between Mlp proteins and proteins involved in DNA metabolism. Since we have successfully utilized this technique to isolate chromatin bound complexes (Tacket et al., manuscript accepted for publication) and mRNPs (Oeffinger, personal communications), it seems unlikely that our conditions specifically selected against DNA associated proteins.

The possibility of further undiscovered interactions not withstanding, we decided to focus our efforts on investigating the most striking result of our immunoprecipitation data: the complex formed by Mlp2p and components of the SPB.

Mlp2p promotes the incorporation of components into the SPB.

Traditionally, SPBs and NPCs have been considered functionally separate entities. However, the recent findings that NPCs and SPBs share a small number of components point to potential functional links between the two. Our finding that Mlp2p physically interacts with the SPB core is therefore interesting, suggesting that Mlps, SPBs and NPCs are interconnected as part of a continuous functional unit at the nuclear periphery. Several lines of evidence indicate that one reason for the connection of SPBs to the peripheral

Mlp assembly is to aid the insertion of new components into the nuclear face of the SPB (Fig. 8). First, new SPBs are inserted normally into the NE in cells lacking Mlp2p, suggesting that the protein has no role in the initial stages of SPB assembly. Second, the nucleus migrates normally, a process associated with the cytoplasmically nucleated SPB microtubules, likely excluding Mlp2p from roles associated with the cytoplasmic face of the SPB. Third, Mlp2p is exclusively nuclear, and attaches to the SPB on its nuclear face via nucleoplasmically oriented SPB components, suggesting that Mlp2p is intimately involved in the function of the SPB -- but only after it has inserted into the NE. Fourth, *mlp2*Δ cells have an increased failure rate in SPB separation and in progression past early mitosis, indicating that the nuclear face of SPBs is occasionally compromised in forming proper spindles. Fifth, a significant fraction of the *mlp2*Δ population accumulates aberrant intranuclear microtubule organizers, indicating a failure in the proper targeting of components to the SPB. This is similar to the phenotype of the *spc110-220* mutant, which also fails to properly target SPB components. Here the defect is in the C-terminus of the Spc110p protein, where it tightly interdigitates with the Spc42p crystalline layer (Adams and Kilmartin, 1999; Kilmartin et al., 1993). The synthetic lethality we observe in cells lacking Mlp2p and carrying the *spc110-220* allele suggests that Mlp2p and the C-terminus of Spc110p act synergistically in the maturation and maintenance of the SPB. Sixth, SPBs in the *mlp2Δ* mutant are smaller on average in comparison to SPBs of a *wild type* strain, as indicated by relative SPB fluorescence intensity. Since the thickness of the individual SPB layers is constant, this reduction in fluorescence intensity represents roughly a 10% decrease in surface area. Even though this appears to be only a minor reduction, the surface area of the SPB in yeast limits the number of microtubules

emanating from it. A haploid *wild type* SPB can nucleate the sixteen required kinetochore microtubules and approximately two to four pole-to-pole microtubules (O'Toole et al., 1999). Since we neither observe chromosome loss nor increased lethality with spindle checkpoint mutants in the *mlp2Δ* strain (data not shown), it appears that capturing of the kinetochores is unimpaired. Thus, the 10% reduction in SPB size might lead to a greater than 50% reduction in the number of pole-to-pole microtubules, consistent with an increase in cells with duplicated but not completely separated SPBs in the *mlp2*Δ strain. The requirement for Mlp2p in SPB function is not absolute, as *mlp2*Δ cells are viable. Yet, a significant number of *mlp2*Δ cells fail to execute mitosis normally. Given that loss of Mlp2p can lead to sub-optimal SPBs, each new round of SPB duplication might cause the introduction of additional defects due to the dynamic nature of the SPB during S-phase. This in turn would lead to stochastic failures of individual SPBs at different stages of the cell cycle. Equally diverse mitotic defects are observed with other (more penetrant) mutants involved in SPB assembly, such as *cmd1-1* and *SPC110* C-terminal mutants (Stirling et al., 1996; Stirling and Stark, 2000).

We hypothesize that Mlp2p helps to incorporate new SPB components into both the mother and daughter SPBs, by recruiting them for exchange or by facilitating their integration into the central plaque. It may be that Mlp2p accomplishes this either by providing additional binding sites for SPB components at the SPB, or by anchoring the edges of the SPB to the surrounding Mlp layer, providing the necessary tension to keep the central plaque crystal "open" for the exchange and addition of proteins. Surprisingly, even though Mlp1p does not appear to bind to the SPB, some phenotypes, like a smaller SPB or synthetic lethality with *spc110-220* found in the *mlp2*Δ strain, are also present in

the *mlp1*Δ strain. Since Mlp1p and Mlp2p directly interact with each other, it is possible that the presence of Mlp1p is required for proper Mlp2p at the SPB, yet, an undiscovered interaction between Mlp1p and SPB components may also be the cause of the phenotypes observed. However, it is also possible that a role of Mlp proteins in organizing the nuclear periphery might be the cause of the phenotypes detected in the *mlp1*Δ strain. For example, the proper distribution and spacing of the NPCs might be required for SPB function and assembly. This would indeed be consistent with the strong phenotypes exhibited by the *mlp1*Δ*mlp2*Δ strain.

Yeast are the only known eukaryotes for which two different Mlps have been identified in the same organism (Kellis et al., 2004; Kellis et al., 2003; Kuznetsov et al., 2002). Although in both *S. cerevisiae* and its close relatives the second copy arose because of a whole-genome duplication event (Kellis et al., 2003), detailed sequence analyses reveal that in fission yeast this second copy of the Mlp protein arose independently. Alm1p/TC80, the *Schizosaccharomyces pombe MLP2* homolog, localizes to the nuclear rim and appears to accumulate at the SPB and at the medial region MTOC (Ding et al., 2000). Since both budding and fission yeast undergo closed mitosis, with the NE remaining intact throughout the cell cycle, it is conceivable that this kind of direct communication between the NE and spindle organizer may facilitate closed mitosis. Even though many eukaryotes dispense with their NE during mitosis, the distinction between open and closed mitosis appears to be less than absolute. Thus, the MTOC is linked with the NE during nuclear migration and positioning, and varying amounts of NE stay in the vicinity of the MTOCs during spindle assembly, even in cells with open mitosis (Beaudouin et al., 2002; Malone et al., 2003; Nadezhdina et al., 1979). While there is no

direct evidence that Mlp/Tpr homologs in vertebrates play a role similar to that of yeast Mlp2p, in *Drosophila* it appears to aid the formation of a spindle matrix, supporting this idea (Qi et al., 2004). This suggests that the close relationship between the NE, Mlp/Tpr and the MTOC might be universal and an essential feature of the cell division process.

A novel method to purify morphologically intact SPB cores.

An unexpected side product of studying the interaction between Mlp2p and the SPB has been the surprising result of visualizing the complex by electron microscopy. Without any specific optimization steps we were able to purify SPB structures virtually indistinguishable from extracted SPB cores purified by traditional methods (Rout and Kilmartin, 1990). However, the method used by Rout and Kilmartin is time consuming and cumbersome (1990). Its reliance on a long enzymatic digestion step and the difficulties of a small scale preparation render a number of interesting experiments to examine the SPB impractical or impossible.

In our purification protocol, cells are frozen immediately upon harvesting, thus preserving the specific state of the SPB at this point. To purify a sufficient quantity of SPBs to analyze their components by SDS-PAGE and their morphology by electron microscopy, only about 1g of cells are required, the equivalent of about 0.5l of liquid culture. Finally, the preparation time for multiple samples is manageable, taking less than six hours to prepare 10 samples from frozen cells to purified SPBs on the magnetic beads ready for analysis. These features of our protocol could enable researchers to perform experiments that were previously virtually impossible. SPBs from synchronized cell

cultures could be purified analyzed for changes of their composition and structure over time. Likewise, SPB mutants could be incubated at multiple temperatures for multiple periods of time or cells could be treated with inhibitors of specific aspects of cell function, and the effects on the SPB in each case could be rapidly observed.

A caveat to the usefulness of this strategy is the fact that we were only able to purify SPB cores. However, by optimizing the extraction conditions, possibly using the same buffers used in the original protocol, we might be able to actually isolate intact SPBs. Likewise, the use of other PrA tagged SPB components, like Spc110p or Spc42p, might lead to a further improvement of the SPB preservation. We hope that the publication of this method will encourage others to utilize our protocol to further unravel the structure and function of the SPB and possibly other organelles.

Mlps: Multifunctional structural components of the nuclear periphery.

Our work presented here has illustrated that the Mlp proteins are structural components of the NE. They form both the basket structure of the NPC as well as an interconnection between neighboring NPCs. Mlp2p integrates the SPB into this Mlp/NPC network. This structural assembly and the complexes it forms with soluble factors determine the function of the Mlp proteins (Figure 30).

As an example I would like to illustrate a model on how the Mlp proteins may perform their role in the retention of improperly processed mRNAs (Galy et al., 2004; Green et al., 2002; Vinciguerra et al., 2005). Translocation of mRNPs through the NPC has been shown to be dependent on factors associated with the 5' end (Visa et al., 1996)

and the 3' end of mRNPs (Strasser et al., 2002; Zenklusen et al., 2001). EM studies have determined that transport occurs sequentially from the 5' end to the 3' end (Mehlin et al., 1995) and that the nuclear basket is intimately involved in this process (Kiseleva et al., 1998a). mRNPs come into contact with the nuclear basket, inducing conformational changes in the basket fibers and the distal ring, in turn allowing mRNPs to unfold from a globular particle into a linear form which can translocate through the pore (Kiseleva et al., 1998a). A correctly processed 3' end of an mRNP destined for export will contain multiple proteins known to form complexes with the Mlps (Green et al., 2002; Lei et al., 2003; Strasser et al., 2002; Vinciguerra et al., 2005). Thereby mRNPs are able to dock to the Mlp basket and induce a conformational change, which in turn allows the 5' end of the mRNP to gain access to the transporter. This two step process could effectively function as a gatekeeping mechanism to sort mRNPs for export or retention in the nucleus depending on their processing state. Only mRNPs with a properly formed 3' end will be able to bind to the Mlp basket to gain access to the transporter, and only mRNPs with a properly formed 5' end will be able to translocate to the cytoplasm. Thus, improperly or incompletely processed mRNPs will be retained in the nucleoplasm either until their processing is completed, or until they are degraded.

This model can account for a number of the mRNA related phenotypes observed in strains lacking the Mlp proteins. First, overexpressed of Mlp1p accumulates both at the periphery and the interior of the nucleus (Strambio-de-Castillia et al., 1999) and causes the retention of poly(A)+ RNA within the nucleus (Green et al., 2003; Kosova et al., 2000). The excess and mislocalized amount of Mlp1p might simply prevent the mRNPs from reaching the site of export efficiently. Second, deletion of MLP1 is synthetically

lethal with a mutant defective in splicing, leading to an increase in the amount of improperly spliced RNA in the nucleus and the cytoplasm (Galy et al., 2004). Consequently, in this background of a splicing mutant, the gatekeeping function of the Mlp proteins becomes more vital for cell survival. Third, the deletion of MLPs rescues the growth defect of *GFP-yra1-8*, a mutant which causes increased accumulation of Poly(A)+ RNA within the nucleus and has an increased binding affinity to Mlps (Vinciguerra et al., 2005). This increased affinity might effectively trap *GFP-yra1-8* containing mRNPs at the Mlp basket. Therefore, the deletion of Mlp proteins would allow more of the *GFP-yra1-8* associated mRNPs to reach the cytoplasm. Lastly, differences in affinity of the mRNP associated proteins for either Mlp1p or Mlp2p may account for the differences observed between the Mlps in their genetic interactions with different mRNA metabolism mutations (Galy et al., 2004; Vinciguerra et al., 2005). Of course the interpretation of some of these results might not be as simple as laid out in this model, since the Mlp proteins have also been implicated in regulating global transcription in response to faulty mRNA processing, which would likewise influence the rate at which transcripts translocate across the NE (Vinciguerra et al., 2005).

Interestingly, the function of mRNP gatekeeping may also explain why nucleo-cytoplasmic transport is impaired in strains lacking the Mlp proteins. An inefficient export of mRNPs in the *mlp1*Δ*mlp2*Δ strain might block individual pores for other transport substrates trying to gain access to the nucleus. This would lead to effectively fewer pores available for protein import, consistent with the observed unchanged steady state distribution but reduced rate of import and diffusion of transport substrates (Strambio-de-Castillia et al., 1999).

The function of the Mlp structure appears not to be limited to the role of the basket structure itself. Disruption of the Mlp network causes global alterations of the nucleus, presumably unrelated to defects in mRNA metabolism. A striking example is the loss of NE stability leading to deformed and weakened nuclei in the *mlp1*Δ*mlp2*Δ strain. However, the alterations in the structure of the NE may lead to a number of further defects. If actively transcribed genes are associated with NPCs (Casolari et al., 2004) then the overall organization of the chromatin within the nucleus may depend on appropriate spacing of the NPC, and thereby on the presence of the Mlps. This may account for some phenotypes observed in the strains lacking Mlp proteins, like their role in global transcription regulation (Vinciguerra et al., 2005), telomere length maintenance (Hediger et al., 2002a) and the more controversial effects on telomere anchoring (Galy et al., 2000) and the establishment of silencing (Feuerbach et al., 2002). However, until the nature of chromatin organization at the periphery, in particular with respect to the NPCs, is better understood, the interpretation of these phenotypes will remain highly speculative. Since a large scale study suggested that Mlp1p is also part of the transcriptional SRB mediator complex, alternative causes for the same observed phenotypes can be devised.

Similar to the difficulties of studying other structural proteins (e.g. lamins, actin) it is difficult to separate the function of the overall structure formed by the Mlps from their direct roles in specific aspects of the biology of the cell. In particular, since the disruption of the Mlp proteins leads to overall changes in the organization of the NE and its associated structures, the SPB and the NPC, the consequences of this gross alteration can effectively mask other functions of the Mlp proteins.

This is illustrated in the analysis of the mitotic defect of the *mlp1*Δ*mlp2*Δ strain detailed in Chapter 6. The data presented shows that cells without Mlp proteins form large and multi-budded cells, often with higher than 2C DNA content. This phenotype is associated with the formation of abnormal spindles that accumulate close to the budneck, the frequent occurrence of multiple intranuclear microtubule organizers and a decrease in genomic stability. What might be the primary cause of this defect? The similarity to the more subtle phenotypes uncovered in the *mlp2*Δ strain suggest that the primary function may lie in the maintenance of the SPB. Yet, a supporting structure underlying the NE might be required for proper SPB and spindle function in yeast. It may also be that due to the lack of the basket structure, defects in mRNA metabolism (Galy et al., 2004; Vinciguerra et al., 2005), transcription (Vinciguerra et al., 2005) or protein transport lead to secondary defects due to altered expression levels. Another hypothesis could be that the global organization of the chromatin is perturbed by the lack of Mlp proteins (Casolari et al., 2004; Galy et al., 2000) which might cause difficulties in forming a proper metaphase spindle. Spindle checkpoint proteins located at the NPC (Iouk et al., 2002) or in complex with Mlp2p (this study) might depend on the Mlps for their function. And of course other factors even less well defined might be involved in this process. For example excess of 2 micron circles in the *mlp1*Δ*mlp2*Δ strain (Zhao et al., 2004) may cause interference with kinetochore function (Mehta et al., 2002).

The difficulty interpreting the phenotypes found in the *mlp1*Δ*mlp2*Δ strain is a compelling reason to study the biochemical properties of the Mlp proteins in greater detail. By determining the exact domains at which specific proteins bind to the Mlps, we should be able to separately study the function of a particular interaction, without the

multitude of effects caused by the disruption of the structural Mlp network. Investigating the Mlp proteins on the level of its individual protein/protein interactions should allow us to reach a better understanding how the Mlp structure performs its functions at the nuclear periphery.

Figure 30: **Model of the Mlp proteins at the NE.**

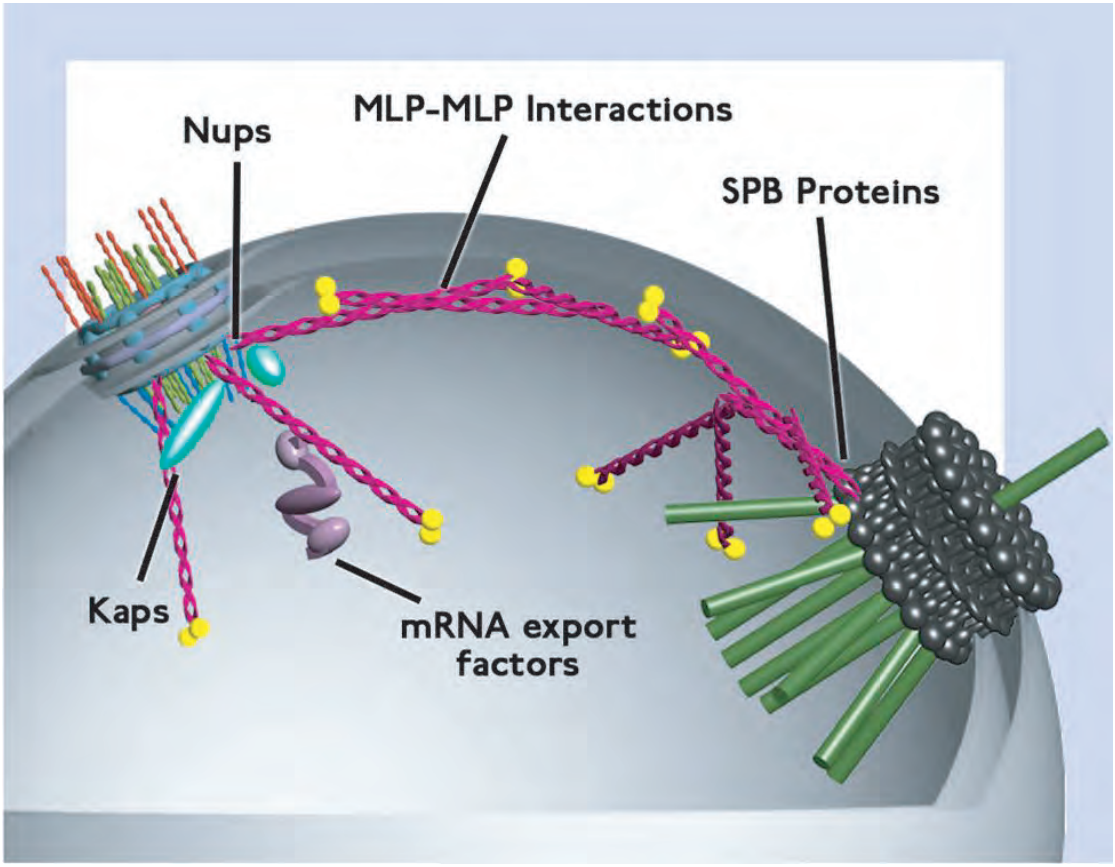
Nups
MLP-MLP Interactions
SPB Proteins
Kaps
mRNA export factors

Chapter 8: Materials and Methods.

Plasmids and Strains.

Strains are isogenic to W303 unless otherwise specified. All yeast strains were constructed using standard genetic techniques (Table 2). C-terminal genomically tagged strains were generated using the PCR method previously described (Aitchison et al., 1995; Reid et al., 2002; Rout et al., 2000). For the N-terminal yellow fluorescent protein (YFP)-, cyan fluorescent protein (CFP)- or Protein A (PrA) tagging of Mlp1p and Mlp2p we used the "pop-in / pop-out" method previously described (Reid et al., 2002). In all cases correct integration was verified by PCR analysis, immunoblotting and, in the case of fluorescent tags, by direct *in vivo* fluorescence microscopy. All tagged Mlp proteins are functional as judged by the absence of any obvious phenotypes in the tagged strains. The *GAL1-10* promoter was inserted upstream of *MLP2-PrA* in strain yCS115 using the vector pFA6a-kanMX6-PGAL1 (Longtine et al., 1998) to create yMN437. *Wild type SPC110* (pHS29) and *spc110-220* (*C911R;* pHS38) expressing plasmids (Sundberg et al., 1996) were transformed into yMN290 to create yMN443 and yMN444. yMN443 and yMN444 were crossed with yMN437 and sporulated to create strains yMN439-442. A similar strategy was followed to construct the corresponding *MLP1* strains.

pRS314-DsRed-Nop1 (Gadal et al., 2001) and pXYNup49-CFP (see below) were used in strains expressing either Mlp1p-YFP or YFP-Mlp2p. For pXYNup49-CFP, the enhanced-CFP (eCFP) open reading frame was PCR amplified from pECFP-N1 (BD

Biosciences-Clonetech) and inserted into the HindIII and SalI sites of pYX242 (Novagen) to produce pYX242-CFP. The *NUP49* open reading frame was PCR amplified from the pET28b-NUP49 plasmid (generous gift from S. Dokudovskaya) and inserted into the unique BamHI and HindIII sites of pXY242-CFP to produce pXYNup49-CFP. All nuclear localisation sequences were cloned N-terminal to eGFP in the pYX242 (Novagen, discontinued) multi-copy yeast expression plasmid, under control of the triosephosphate isomerase promotor. Rpl25NLS (Schaap et al., 1991) and SV40NLS (Nelson and Silver, 1989) were amplified by PCR of eGFP with primers encoding the respective NLS sequences, which were inserted between the EcoRI and SalI restriction sites of pYX242, generating plasmids pYX242- RL25NLS-GFP and pYX242- SV40NLS-GFP (Timney B et al, manuscript in preparation). The RGG rich NLS of Nab2p (Truant et al., 1998) was inserted between the EcoRI and HindIII sites of a modified pYX242, in which eGFP had been inserted between the HindIII and SalI restriction sites, generating plasmid pYX242-RGG-GFP (Timney B et al, manuscript in preparation). In all cases the plasmid sequence was verified by DNA sequencing.

Polyploid cells were created by forcing a mating type switch in diploid cells through the expression of HO endonuclease. The resulting a/a or alpha/alpha diploid cells were mated with haploid cells to form the triploid strains and with each other to form the tetraploid strains.

Affinity PrA purification.

The protocol for the purification of PrA-containing complexes was modified from published methods (Aitchison et al., 1996; Rout et al., 1997; Schultz et al., 1997). Briefly,

frozen cells were ground with a motorized grinder (Retsch) and 1g (PrA control, Mlp1p-PrA) or 2g (Mlp2p-PrA) were thawed into 9ml of extraction buffer (EB; 20mM Na-HEPES, pH 7.4, 0.5% TritonX-100, 1mM DTT, 4µg/ml pepstatin, 0.2mg/ml PMSF) supplemented with the indicated concentrations of NaCl or other extractants. Different amounts of frozen cell powder had to be used in order to recover comparable amounts of Mlp-PrA. Cell lysates were homogenized with a Polytron for 25sec (PT 10/35; Brinkman Instruments) and cleared by centrifugation at $2000g_{av}$ for 10min. 7.5mg of epoxy-activated DynaBeads (Dynal) cross-linked to rabbit IgG (ICN) were added to each lysate and rotated for 2 hours at 4ºC. The IgG-DynaBeads were collected with a magnet, washed 5 times with 1ml of EB and once with 1ml of 100mM ammonium acetate pH 7.4, 1mM $MgCl_2$. For sodium N-lauroyl-sarcosine preparations, 500mM NaCl and increasing concentrations of sodium N-lauroyl-sarcosine (0.01-1.00% w/vol) were added to EB and immunoaffinity isolations were performed as above. The PrA containing complexes were eluted off the beads in 1ml of 0.5M NH_4OH, 0.5mM EDTA at 25ºC for 20min and lyophilized in a SpeedVac (Thermo Savant). Protein samples were resolved by SDS-PAGE with Novex 4-20% Tris-glycine polyacrylamide gels (Invitrogen) and visualized by Coomassie blue staining. Protein bands were identified by mass.

For the purification of the Mlp2/SPB complex through the cell cycle eighteen liters of strain yMN410, expressing Mlp2p-PrA and the cdc20 gene under the control of the GAL promoter was grown to early log phase in galactose containing media and harvested. The cells were transferred to 18l of dextrose containing media and incubated at 30ºC for 3 hours until >95% showed the typical dumbbell shape of mitotic cells. The yeast were harvested again and transferred to 18l of galactose containing media. 2l samples were

taken at each timepoint for PrA affinity purification, immunoblotting, FACS and microscopic analysis.

For the preparation of purified Mlp1p- and Mlp2p-PrA for use as probes in the *in vitro* blot binding assay and sedimentation gradient centrifugation, the procedure described above was modified as follows. The ground cell powder (1.2g for Mlp1p-PrA and 4g for Mlp2p-PrA) was resuspended in 10ml of extraction buffer II (EB II; 20mM Hepes/KOH, pH 7.4, 1% TritonX-100, 0.5% Na-Deoxycholate, 0.3% sodium N-lauroyl-sarcosine, 0.1mM $MgCl_2$, 1mM DTT, 4µg/ml pepstatin, 0.2mg/ml PMSF) per gram. After homogenization and clarification, the lysate was incubated over night at 4ºC with IgG-Sepharose resin (10µl of bed volume per gram of cell powder). After extensive washing in EB II without DTT, bound material was eluted off the resin using a competing peptide. The eluting peptide was removed on a G25 sizing column (Amersham Biosciences) and the probe was quantified by running an aliquot on SDS-PAGE alongside BSA standards.

Co-immunoprecipitation immuoblot experiments.

For analysis of SPB-Mlp interactions, 0.5g of cell powder was used for each strain. To adjust for total protein amount, 0.5g of untagged cell powder was added to strains marked 'co-expressed'. The powder was thawed into 5ml of EB supplemented with 300mM NaCl, 1mg/ml Heparin for Spc42p-PrA and 150mM NaCl, 1mg/ml Heparin for Spc110p-PrA and Cnm67p-PrA, cleared by centrifugation and bound to 7.5mg of rabbit-IgG conjugated DynaBeads. For Mlp-Mlp interactions, cell lysates were prepared from

roughly 100 µl of cell-paste of each indicated strains with their cell walls weakened by digestion with 5mM DTT, 10% glusulase, 0.1% zymolyase T100, 0.1% Mutinase in 1.1M Sorbitol for 15 min at 30ºC. To adjust for total protein amounts, 100 µl of untagged cell-paste were added to strains marked 'co-expressed'. After digestion the cells were washed twice in 1.1 M sorbitol and broken by vortexing for 5 min at 4ºC with 300µl of acid washed glass beads in 1ml EB supplemented by 150 mM NaCl. Lysates were cleared and 2.5mg of rabbit-IgG conjugated DynaBeads were added.

In all cases the lysates were rotated with the beads for 2 hours at 4ºC and subsequently treated as described earlier. Samples of each cell lysate and each isolated complex were resolved in duplicate by SDS PAGE and transferred onto nitrocellulose. The presence of PrA and Myc in the samples was detected by immuno-blotting using a 1:1000 dilution of a rabbit IgG (ICN) and a mouse monoclonal anti-Myc antibody (Santa Cruz Biotechnology).

Identification of Proteins by mass spectrometry.

Protein bands were excised and tryptic digestions were prepared according to standard protocols (Krutchinsky et al., 2001). Extracted peptides were analyzed by a modified matrix-assisted laser desorption/ionization (MALDI) ion trap mass spectrometer (Krutchinsky et al., 2001) based on a LCQ Deca XP ion trap mass spectrometer (Thermo Finnigan). An automated protocol was used to perform tandem mass spectrometry and proteins were identified searching the National Center for Biotechnology Information

non-redundant protein database with the program Sonar (Genomic Solutions) to identify proteins from the tryptic peptide fragmentation masses (Field et al., 2002).

In vitro blot binding assay.

The Mlp2p-complex was immobilized on IgG-Dynabeads as described in Methods. After binding, Dynabeds were incubated using 1M $MgCl_2$, 20mM Hepes/KOH pH 7.4, 0.5% Tween-20 in order to preserve the binding of Mlp2p-PrA to IgG and selectively elute the Mlp2p-PrA bound proteins off the beads. The eluate was subsequently incubated with fresh IgG-Dynabeads to remove contaminating Mlp2p-PrA and with PrA-Sepharose beads to remove IgG moieties that might have bled through from the IgG-Dynabeads. Proteins were then recovered by TCA precipitation, separated on SDS-PAGE and transferred to nitrocellulose. After amido black staining the blot was cut into three 0.2cm wide identical strips. The strips were blocked for 1hr at 25ºC in 5% milk, 2% BSA, 20mM Hepes/KOH, 110mM KOAc, 2mM $MgCl_2$, 0.1% Tween-20, 1mM DTT, 4µg/ml pepstatin, 0.2mg/ml PMSF, before incubation with 1.2µg of purified Mlp probes in 500µl of the same buffer at 4ºC over night. After four brief washes with the same buffer at 25ºC, the strips were incubated with 1:2000 rabbit IgG-HRP conjugate (Jackson ImmunoResearch Laboratories) in binding buffer for 1hr at 25ºC. The presence of bound HRP was detected by chemiluminescence.

Microscopy.

For *in vivo* fluorescence experiments cells expressing DsRed-, GFP-, CFP- or YFP-tagged proteins were grown over night in YPD or the appropriate selective medium containing 200µg/ml Adenine to reduce auto-fluorescence. The next morning cells were diluted in the same medium and grown to mid-log phase for 4-5 hrs. When ready, cells were harvested and concentrated in SC medium with 200µg/ml Adenine. A small drop (1-2µl) of the concentrated cell suspension was spotted on a poly-L-lysine coated slides before immobilization using a cover slip. Cells were observed immediately after immobilization at 25ºC. Cell were visualized with a with a 100x 1.4 numerical aperture Planapochromat objective using an inverted Carl Zeiss Axiovert 200 wide-field confocal microscope fitted with a Perkin-Elmer Ultra-View spinning disk confocal head on side-port optimized for real-time confocal imaging. The microscope was equipped with a Hamamatsu Orca ER cooled CCD camera. Image analysis was performed using the MetaMorph software provided by Univeral Imaging. For 3D volume and surface reconstruction we used the Imaris and Imaris-Surpass (Bitplane AG) software.

For DAPI staining cells were grown to mid-log phase in YPD containing Adenine as above. Cells were fixed in 4% parafomaldehyde, 3.4% sucrose and 0.1M KPO_4 for 5-15min at 25ºC. Cells were washed with 1.2M sorbitol, 0.1M KPO_4 pH 7.5 sonicated and subsequently permeabilized with 0.1% Triton-X-100 in the same buffer for 1 min at 25ºC. Cells were stained with 0.06µg/ml DAPI in sorbitol/KPO for 10 min at 25ºC, washed in the same buffer and immobilized on slides as described above. For image acquisition we used an Axioplan 2 microscope (Carl Zeiss), with a 100x 1.4 numerical aperture Planapochromat objective, fitted with a Hamamatsu C4742-95 cooled charge-coupled

device camera (Sciscope Instrument) interfaced with the OpenLab software (Improvision). Indirect immuno-fluorescence (IF) was performed essentially as described (Strambio-de-Castillia et al., 1999). Cells were fixed for 1 hour on ice and the spindle was visualized using a 1/100 dilution of the monoclonal rat anti-tubulin antibody, YOL1/34 (Accurate Chemicals and Scientifics) and a 1/200 dilution of Cy3-conjugated donkey anti-rat (Jackson ImmunoResearch Laboratories) antibodies.

Samples were prepared for thin-section TEM and IEM essentially as described (Rout and Blobel, 1993, Rout 2000).

Nucleocytoplasmic transport assays were performed on a Zeiss AxioPlan 2 microscope fitted with a 63x (1.4 NA) objective lens and a Hamamatsu Orca II cooled CCD camera. GFP, Texas Red and AlexaFluor A350 images were collected using Chroma filter sets for FITC, CY3 and DAPI, respectively. The imaging system was controlled using Improvision's OpenLab software.

Quantitative Image Analyses.

All the quantitative analyses were performed on digital images. Scoring of SPB numbers, size and position and of DAPI stained nuclei was performed on two-dimensional projections of 3D image stacks containing 8 0.35μm optical sections, were overlaid onto DIC images for clearer positioning of SPB-signals and nuclei. All other analyses were performed directly utilizing Z-calibrated 3D digital image stacks, which contained 15-20 0.27μm optical sections. Scoring of spindle configuration frequencies in live cells expressing GFP-Tub1p was performed using the Manually Count Objects

module included in the MetaMorph software. All length measurements were obtained using the Measure XYZ Distance module of the same software. The spindle migration index of a cell is proportional to the proximity of its spindle to the bud neck and is calculated as the distance between the neck and the nearest edge of spindle, divided by the distance between the neck and the most distal edge of the cell (DeZwaan et al., 1997; Jacobs et al., 1988) The shape factor was determined using the Morphometric Analysis module of MetaMorph software.

Differential Elutriation.

Haploid strains yMN291 and yMN293 and diploid strains yCS101 and yCS251 were subjected to differential elutriation as previously described (Miller and Cross, 2001). 12 fractions were collected from each experiment. Cells were harvested by filtration and prepared for either DAPI staining and fluorescence microscopy (yMN291 and yMN293) or for EM analysis (yCS101 and yCS251). Progression of cells through the cell cycle was monitored by budding-index and by FACS as described previously (Epstein and Cross, 1992).

Chromosome Loss Assay.

The rate of chromosome III missegregation was carried out as described (Chi and Shore, 1996). Homozygous diploid colonies arising from single cells were collected and the cell viability was determined. Half of each colony was mated with excess haploid

tester strains for each mating type. The chromosome loss rate is determined as 0.434*(median mating frequency)/log(viable cell number).

Covalent Cell Wall Staining for Same-Slide Imaging.

Yeast cell pellets from 15mL log-phase cultures were washed and incubated at room temperature for 10 minutes in 500µL of 50mM sodium carbonate/bicarbonate buffer (pH 9.0) containing either 10µg/ml of Texas Red or 100µg/mL of AlexaFluor A350 respectively (Molecular Probes). Cells were washed and left to recover for 30min at room temperature. No dye transfer was observed from one cell to another or to daughter cells. Addition of neither dye effected the distribution of any cargo tested.

Nucleocytoplasmic Import Assay.

We modified a published yeast nucleocytoplasmic import assay (Shulga et al., 1996) to make data collection automatic and quantitative. Cell walls of *wild type* and *mlp1*Δ*mlp2*Δ strains expressing the indicating NLS reporters were stained as described above and mixed together in equal cell numbers. Cells were thoroughly washed with water and left at room temperature in 400µL of the transport poison (synthetic complete media without a carbon source, containing 10mM deoxyglucose and 10mM sodium azide). After 15 minutes the NLS-GFP cargoes diffused through the NPC and were fully equilibrated between nucleus and cytoplasm. A 100µL sample of poisoned cells was harvested, quickly washed once with water and resuspended in water to give an

appropriate density of cells for microscopy. On a poly-lysine coated microscope slide 1.5µL of cells were mixed with 1.5µL of synthetic media, containing glucose. A field of cells was located as quickly as possible and images of the NLS-GFP reporter were collected every 30 seconds for 7min. At each timepoint 8 images were taken at 0.35µm z-steps of the GFP fluorescence channel. After collection of the timecourse reference images of the fluorescent cell wall dyes and a DIC image were taken.

Yeast longevity assay.

The assay was performed as described (Kennedy et al., 1995). Cells were taken from log-phase cultures, plated at low density and incubated at 30ºC for 3h. Newly formed daughter cells were isolated and moved with a micro-manipulator to uninhabited parts of the plate. All future buds produced by these daughter cells were then micro-manipulated away. The positions of mother cells relative to newly formed buds were noted to distinguish mothers from daughters during symmetric division. The plates were grown at 30°C while not being worked on.

Sedimentation gradient centrifugation.

A mixture of purified Mlp proteins and standards with known S-values was overlayed on top of a continuous 5-20% sucrose/TBT gradient (BioComp Gradient Master) and centrifuged (Beckman SW55 rotor) at 40.000rpm speed for 13.5h and 12h respectively. Approximately 27 gradient fractions were collected (BioComp Piston Gradient

Fractionator) and a sample of each fraction was separated by SDS-PAGE and proteins were visualized by immunoblotting. Signal intensities for each protein band were determined using OpenLab software, plotted against the fraction number and peak curves were fitted using Excel (Microsoft). A standard curve was prepared by plotting the known S-values of the standard proteins against their determined peak fraction and used to determine the experimental S-value of the purified Mlp protein.

Table 2: **List of strains used in this study.**

Name	Descriptive Name	Genotype	Derivation
yCS101/ W303	W303 2n	*Mat a/alpha; leu2-3,112/l eu2-3,112; his3-11,15/his3-11,15; trp1-1/trp1-1; can1-100/can1-100; ade2-1/ade2-1; ura3-1/ura3-1*	Thomas and Rothstein, 1989
yMN164	W303 a	*Mat a; leu2-3,112; his3-11,15; trp1-1; can1-100; ade2-1; ura3-1*	Thomas and Rothstein, 1989
yMN165	W303 alpha	*Mat alpha; leu2-3,112; his3-11,15; trp1-1; can1-100; ade2-1; ura3-1*	Thomas and Rothstein, 1989
yCS108	Mlp1p-PrA	*W303; Mata; MLP1-PrA (HIS2; URA3)*	Strambio-de-Castillia et al., 1999
yCS115	Mlp2p-PrA	*W303; Mata; MLP2-PrA (HIS2; URA3)*	Strambio-de-Castillia et al., 1999
yMN135	PrA-Mlp1p	*W303; Mata; PrA-MLP1*	this study
yMN137	PrA-Mlp2p	*W303; Mata; PrA-MLP2*	this study
yCS135	Δmlp1Δmlp2	*W303; Mat alpha; mlp1::URA; mlp2::HIS*	Strambio-de-Castillia et al., 1999
yCS230	Δmlp1Δmlp2	*W303;mat a; mlp1::ura3::TRP1; mlp2::his3::LEU2*	this study
yCS241	Mlp1p-YFP	*W303; Mat alpha; MLP1-EYFP (KLURA3)*	this study
yCS249	mlp1Δmlp2Δ	*W303; Mat alpha; mlp1::ura3::TRP1; mlp2::his3::LEU2*	mating type switch of yCS230
yCS250	mlp1Δ	*W303; Mat a/alpha; mlp1::TRP1/mlp1::TRP1*	this study
yCS251	mlp2Δ	*W303; Mat a/alpha; mlp2::HIS3 / mlp2::KANMX6*	this study
yCS276/ AFS475	wild type, GFP-TUB1	*W303; Mata; his3::GFP-TUB1(HIS3)*	A. F. Straight, generous gift
yCS278	mlp1Δ, GFP-TUB1	*W303; Mata; mlp1::TRP; GFP-TUB1(HIS3)*	segregant of diploid derived from mating of yCS276 with yCS249; this study

Name	Descriptive Name	Genotype	Derivation
yCS280	mlp2Δ, GFP-TUB1	*W303; Mata; mlp2::LEU; GFP-TUB1(HIS3)*	segregant of diploid from mating of yCS276 and yCS249; this study
yCS327	Zpr1-PrA	*W303; Mata; ZPR1-PrA(TRP1; HIS2)*	G. Greco, generous gift
yCS348	CFP-Mlp1p	*W303; Mata; ECFP-MLP1*	genomic tagging; this study
yCS401	Mlp2p-PrA h.d.	*W303; Mata/Matalpha; MLP2-PrA-HIS; URA/MLP2-PrA-HIS; URA; pRS425-LEU; pRS424-TRP*	this study
yCS436	YFP-Mlp2p	*W303; Matalpha; EYFP-MLP2*	genomic tagging; this study
yCS437	YFP-Mlp2p	*W303; Mata; EYFP-MLP2*	genomic tagging; this study
yCS439	Spc42p-CFP	*V.2567; Matalpha; SPC42-CFP (Kan)*	mating type switch of yMN326; this study
yCS444	Mlp1p-YFP, Spc42p-CFP	*Mata; MLP1-EYFP(KLURA3); SPC42-CFP (Kan)*	segregant of diploid from mating yCS241 with yMN326
yCS450	YFP-Mlp2p, Spc42p-CFP	*Mata; EYFP-MLP2; SPC42-CFP (Kan)*	segregant of diploid from mating yCS437 with yCS439
yCS451	Mlp1p-YFP / pDsRed-Nop1	*W303; Mat alpha; MLP1-YFP / pRS314-DsRed-Nop1(TRP1)*	yCS241 transformed with pRS314-DsRed-Nop1; this study
yCS452	YFP-Mlp2p / pDsRed-Nop1	*W303; Mat alpha; YFP-MLP2 / pRS314-DsRed-Nop1(TRP1)*	yCS436 transformed with pRS314-DsRed-Nop1; this study
yCS476	Mlp1p-YFP / pYX242-NUP49-CFP	*W303; Mat alpha; MLP1-YFP / pYX242-NUP49-CFP(LEU2)*	yCS241 transformed with pYX242-NUP49-CFP; this study
yCS477	YFP-Mlp2p / pYX242-NUP49-CFP	*W303; Mat alpha; YFP-MLP2 / pYX242-NUP49-CFP(LEU2)*	yCS436 transformed with pYX242-NUP49-CFP; this study

Name	Descriptive Name	Genotype	Derivation
yCS465	CFP-Mlp1p, YFP-Mlp2p	*W303; Mata; ECFP-MLP1; YFP-MLP2*	segregant of diploid from mating yCS348 with yCS346; this study
yCS469	CFP-Mlp1p, YFP-Mlp2p	*W303; Mat a/alpha; ECFP-Mlp1/ ECFP-Mlp1; YFP-MLP2 / YFP-MLP2*	mating yCS464 with yCS465; this study
yCS476	YFP-Mlp2p / pNup49-CFP	*W303; Mat alpha; YFP-MLP2 / pYX242NUP49CFP(LEU2)*	yCS436 transformed with pYXNUP49-CFP; this study
yMN172	Mlp1p-MYC	*W303; Mata; MLP1-Myc (TRP1)*	genomic tagging; this study
yMN173	Mlp1p-MYC	*W303; Mat alpha; MLP1-MYC (TRP1)*	mating type switch of yMN172; this study
yMN178	Mlp2p-MYC	*W303; Mat a; MLP2-MYC (TRP1)*	genomic tagging; this study
yMN179	Mlp2p-MYC	*W303; Mat alpha; MLP2-MYC (TRP1)*	mating type switch of yMN178; this study
yMN189	Mlp1p-PrA, Mlp1p-MYC	*W303; Mat a/alpha; MLP1-PrA (HIS2; URA3)/MLP1-MYC (TRP1)*	mating of yCS108 with yMN173; this study
yMN190	Mlp2p-PrA, Mlp2p-MYC	*W303; Mat a/alpha; MLP2-PrA (HIS2; URA3)/MLP2-MYC (TRP1)*	mating yCS115 with yMN179; this study
yMN290/ 1141	PrA-Spc110p	*Mat a; spc110::LEU2; TRP1::PrA-SPC110*	J. Kilmartin, generous gift
yMN291/ IAY18	Spc42p-GFP	*K699; Mat a; spc42::LEU2; TRP1::SPC42-GFP 3x*	Adams and Kilmartin, 1999
yMN292	mlp1Δ, Spc42p-GFP	*spc42::LEU2; TRP1::SPC42-GFP 3x; mlp1::URA3*	segregant of diploid from mating yCS135 with yMN291; this study
yMN293	mlp2Δ, Spc42p-GFP	*spc42::LEU2; TRP1::SPC42-GFP 3x; mlp2::HIS2*	segregant of diploid from mating yCS135 with yMN291; this study

Name	Descriptive Name	Genotype	Derivation
yMN300	Mlp1p-PrA, Mlp2p-MYC	*W303; Mat a; MLP1-PrA (HIS2; URA3); MLP2-MYC (TRP1)*	segregant of mating yCS108 with yMN179; this study
yMN302	Mlp1p-MYC, Mlp2p-PrA	*W303; Mat a; MLP1-MYC (TRP1); MLP2-PrA (HIS2; URA3)*	segregant of mating yCS115 with yMN173; this study
yMN326/ SLJ941	Spc42p-CFP	*V.2567; Mat a; SPC42-CFP (Kan); ade2-1oc; ade3Δ100; can1-100; his3-11,15; leu13,112; ura3-1*	S. L. Jaspersen and M. Winey, generous gift
yMN331	Mlp1p-MYC, PrA-Spc110p	*Mat alpha; MLP1-MYC (TRP); spc110::LEU2; TRP1::PrA-Spc110*	segregant from mating yMN290 with yMN173; this study
yMN332	Mlp2p-MYC, PrA-Spc110p	*Mat alpha; MLP2-MYC (TRP); spc110::LEU2; TRP1:PrA-Spc110*	segregant from mating yMN290 with yMN179; this study
yMN367	Mlp1p-MYC, Spc42p-PrA	*W303; Mat a; MLP1-MYC (TRP); SPC42-PrA (HIS5)*	segregant from mating yMN173 with yMN412; this study
yMN369	Mlp2p-MYC, Spc42p-PrA	*W303; Mat a; MLP2-MYC (TRP); SPC42-PrA (HIS5)*	segregant from mating yMN179 with yMN412; this study
yMN412	Spc42p-PrA	*W303; Mat a; SPC42-PrA (HIS5)*	genomic tagging; this study
yMN476	Mlp1p-MYC, Cnm67p -PrA	*W303; Mat a; MLP1-MYC (TRP); CNM67-PrA (HIS5)*	segregant from mating yMN173 with yMN474; this study
yMN478	Mlp2p-MYC, Cnm67p -PrA	*W303; Mat a; MLP2-MYC (TRP); CNM67-PrA (HIS5)*	segregant from mating yMN179 with yMN474; this study
yMN474	Cnm67p-PrA	*W303; Mat a; CNM67-PrA (HIS5)*	genomic tagging; this study
yMN415/ ESM527-1	spc29-2	*YPH499; Mat a; spc29-2; ade2-110oc; his3Δ200,15; leu2Δ1; lys2-801am; trp1Δ63; ura3-52*	Elliott et al., 1999

Name	Descriptive Name	Genotype	Derivation
yMN417/ ESM530-1	spc29-9	*YPH499; Mat alpha; spc29-9; ade2-110oc; his3Δ200,15; leu2Δ1; lys2-801am; trp1Δ63; ura3-52*	Elliott et al., 1999
yMN420/ JGY44-2A	cmd1-1	*W303; Mat a; cmd1-1; ade2-1oc; ade3Δ; can1-100; his3-11,15; leu13,112; trp1-1; ura3-1*	Davis, 1992
yMN426/ HSY57-20A	spc110-226	*CRY1; Mat a; spc110-226; ade2-1oc; ade3Δ; can1-100; his3-11,15; leu13,112; trp1-1; ura3-1*	Sundberg and Davis, 1997
yMN428/ JGY41	cmd1-3	*W303; Mat a; cmd1-3; ade2-1oc; ade3Δ; can1-100; his3-11,15; leu13,112; trp1-1; ura3-1*	Geiser et al., 1991
yMN435	GAL1-10::Mlp1p-PrA	*W303; Mat a; KanMX6-GAL1,10-MLP1-PrA(HIS2-URA3)*	genomic tagging; this study
yMN437	GAL1-10::Mlp2p-PrA	*W303; Mat a; KanMX6-GAL1,10-MLP2-PrA(HIS2-URA3)*	genomic tagging; this study
yMN439	Mlp2p / pHS29-SPC110	*W303; Mat a; spc110::LEU2; MLP2 / pHS29-SPC110(URA3)*	segregant of mating yMN437 with yMN443; this study
yMN440	GAL1-10::Mlp2p-PrA / pHS29-SPC110	*W303; Mat a; spc110::LEU2; KanMX6-GAL1,10-MLP2-PrA(HIS2-URA3) / pHS29-SPC110(URA3)*	segregant of mating yMN437 with yMN443; this study
yMN441	Mlp2p / pHS38-spc110C911R	*W303; Mat alpha; spc110::LEU2; MLP2 / pHS38-spc110C911R(URA3)*	segregant of mating yMN437 with yMN444; this study
yMN442	GAL1-10::Mlp2p-PrA / pHS38-spc110C911R	*W303; Mat alpha; spc110::LEU2; KanMX6-GAL1,10-MLP2-PrA(HIS2-URA3) / pHS38-spc110C911R(URA3)*	segregant of mating yMN437 with yMN444; this study
yMN443	PrA-Spc110p / pHS29-SPC110	*W303; Mat alpha; spc110::LEU2; TRP1::PrA-SPC110 / pHS29-SPC110(URA3)*	yMN290 transformed with pHS29; this study
yMN444	PrA-Spc110p / pHS38-spc110C911R	*W303; Mat alpha; spc110::LEU2; TRP1::PrA-SPC110/ pHS38-spc110C911R(URA3)*	yMN290 transformed with pHS38; this study
yMN461	cmd1-1, mlp1Δ, mlp2Δ heterozygous diploid	*Mat a/alpha; cmd1-1/ CMD1; mlp1::URA3/ MLP1; mlp2::HIS3/ MLP2; ade2-1/ ade2-1; leu2-3,112/leu2-3,112; his3-11,15/ his3-11,15; trp1-1 / trp1-1; can1-100/ can1-100; ura3-1/ ura3-1*	mating of yMN420 with yCS135; this study

Name	Descriptive Name	Genotype	Derivation
yMN468	cmd1-3, mlp1Δ, mlp2Δ heterozygous diploid	*Mat a/alpha; cmd1-3/ CMD1;mlp1::URA3/ MLP1; mlp2::HIS3/ MLP2; ade2-1 / ade2-1; leu2-3,112/ leu2-3,112; his3-11,15 / his3-11,15; trp1-1 / trp1-1; can1-100 / can1-100; ura3-1/ ura3-1*	mating of yMN428 with yCS135; this study
yMN469	spc29-2, mlp1Δ, mlp2Δ heterozygous diploid	*Mat a/alpha; spc29-2/ SPC29; mlp1::URA3/ MLP1; mlp2::HIS3/ MLP2; ade2-110oc/ ade2-1; can1-100 / can1-100; his3Δ200/ his3-11,15; leu2Δ1/ leu2-3,112; lys2-801am/ LYS1; trp1Δ63/ trp1-1; ura3-52/ ura3-1*	mating of yMN415 with yCS135; this study
yMN472	spc29-3, mlp1Δ, mlp2Δ heterozygous diploid	*Mat a/alpha; spc29-3/ SPC29; mlp1::URA3/ MLP1; mlp2::HIS3/ MLP2; ade2-110oc/ ade2-1; can1-100 / can1-100; his3Δ200/ his3-11,15; leu2Δ1/ leu2-3,112; lys2-801am/ LYS1; trp1Δ63/ trp1-1; ura3-52/ ura3-1*	mating of yMN416 with yCS230; this study
yMN471	spc29-9, mlp1Δ, mlp2Δ heterozygous diploid	*Mat a/alpha; spc29-9/ SPC29; mlp1::URA3/ MLP1; mlp2::HIS3/ MLP2; ade2-110oc/ ade2-1; can1-100 / can1-100; his3Δ200/ his3-11,15; leu2Δ1/ leu2-3,112; lys2-801am/ LYS1; trp1Δ63/ trp1-1; ura3-52/ ura3-1*	mating of yMN417 with yCS230; this study
yMN161	mad1Δ	*W303; mad1::URA3*	generous gift F.Cross
yMN162	bub2Δ	*W303; bub2::HIS3*	generous gift F.Cross
yMN160	mad1Δ, bub2Δ	*W303; Mat a; mad1::URA3; bub2::HIS3*	segregant of mating yMN161 with yMN162; this study
yMN204	mlp1Δmlp2Δ	*W303; Mat alpha; mlp1::URA3::TRP1; mlp2::HIS3::LEU2*	this study
yMN170	mlp1Δmlp2Δ, mad1Δ, bub2Δ	*W303; Mat a/alpha; MLP1/mlp1::URA3::TRP1; MLP2/mlp2::HIS3::LEU2; MAD1/mad1::URA3; BUB2/bub2::HIS3*	mating of yMN4160 with yCS204; this study
yMN118/ U953-61D	mec1Δ, sml1Δ	*W303; Mat alpha; mec1::TRP1; sml1::HIS3*	generous gift X. Zhao
yMN457	mlp1Δmlp2Δ	*W303; Mat a; mlp1::URA3; mlp2::his3::LEU2*	this study
yCS231	mlp1Δmlp2Δ, mec1Δ, sml1Δ	*W303; Mat a; mlp1::URA3; mlp2::his3::LEU2; mec1::TRP1; sml1::HIS3*	segregant of mating yCS457 with yMN118; this study

Name	Descriptive Name	Genotype	Derivation
yMN410	Mlp2p-PrA, cdc20Δ, GAL-CDC20	*W303; Mat a; cdc20::LEU2; ADE2-Gal1,10-CDC20; MLP2-PrA (HIS2; URA3)*	segregant of mating yMN358 with yCS115; this study
yMN535	W303 2n a/a	*W303; Mat a/a*	forced mating type switch of yCS101, this study
yMN536	W303 2n alpha/alpha	*W303; Mat alpha/alpha*	forced mating type switch of yCS101, this study
yMN543	W303 3n	*W303; Mat a/alpha/alpha*	mating of yMN536 with yMN164
yMN549	W303 4n	*W303; Mat a/a/alpha/alpha*	mating of yMN536 with yMN535
yMN445	mlp1Δmlp2Δ	*W303; Mat a; mlp1::URA3::TRP1; mlp2::HIS3*	this study
yMN447	mlp1Δmlp2Δ	*W303; Mat alpha; mlp1::URA3::TRP1; mlp2::HIS3*	this study
yMN437	mlp1Δmlp2Δ	*W303; Mat a/a; mlp1::URA3::TRP1/ mlp1::URA3::TRP1; mlp2::HIS3/mlp2::HIS3/ mlp2::HIS3/mlp2::HIS3*	forced mating type switch of mating yMN445 and yMN447, this study
yMN438	mlp1Δmlp2Δ	*W303; Mat alpha/alpha; mlp1::URA3::TRP1/ mlp1::URA3::TRP1; mlp2::HIS3/mlp2::HIS3/ mlp2::HIS3/mlp2::HIS3*	forced mating type switch of mating yMN445 and yMN447, this study
yMN547	mlp1Δmlp2Δ, 3n	*W303; Mat a/alpha/alpha; mlp1::URA3::TRP1/ mlp1::URA3::TRP1/ mlp1::URA3::TRP1; mlp2::HIS3/mlp2::HIS3/ mlp2::HIS3/mlp2::HIS3/ mlp2::HIS3/mlp2::HIS3*	mating of yMN438 and yMN445, this study
yMN549	mlp1Δmlp2Δ, 4n	*W303; Mat a/a/alpha/alpha; mlp1::URA3::TRP1/ mlp1::URA3::TRP1/ mlp1::URA3::TRP1/ mlp1::URA3::TRP1; mlp2::HIS3/mlp2::HIS3/ mlp2::HIS3/mlp2::HIS3/ mlp2::HIS3/mlp2::HIS3/ mlp2::HIS3/mlp2::HIS3*	mating of yMN438 and yMN445, this study
yMN523	GAL1-10::Mlp1p-PrA / pHS29-SPC110	*W303; Mat a; spc110::LEU2; KanMX6-GAL1,10-MLP1-PrA(HIS2-URA3) / pHS29-SPC110(URA3)*	segregant of mating yMN435 with yMN443; this study
yMN525	GAL1-10::Mlp1p-PrA / pHS38-spc110C911R	*W303; Mat alpha; spc110::LEU2; KanMX6-GAL1,10-MLP1-PrA(HIS2-URA3) / pHS38-spc110C911R(URA3)*	segregant of mating yMN435 with yMN444; this study

Name	Descriptive Name	Genotype	Derivation
yCS282	mlp1Δmlp2Δ, GFP-TUB1	*W303; Mata; mlp1::TRP; mlp2::LEU; GFP-TUB1(HIS3)*	segregant from mating of yCS276 and yCS249; this study
yMN294	mlp1Δmlp2Δ, Spc42p-GFP	*spc42::LEU2; TRP1::SPC42-GFP 3x; mlp1::URA3; mlp2::HIS2*	segregant from mating yCS135 with yMN291; this study

Chapter 9: References.

Aaronson, R.P., and G. Blobel. 1975. Isolation of nuclear pore complexes in association with a lamina. *Proc. Natl. Acad. Sci. U. S. A.* 72:1007-1011.

Adam, S.A. 2001. The nuclear pore complex. *Genome Biol*. 2:REVIEWS0007.

Adams, I.R., and J.V. Kilmartin. 1999. Localization of core spindle pole body (SPB) components during SPB duplication in *Saccharomyces cerevisiae*. *J Cell Biol*. 145:809-23.

Aitchison, J.D., G. Blobel, and M.P. Rout. 1995. Nup120p: a yeast nucleoporin required for NPC distribution and mRNA transport. *J. Cell Biol.* 131:1659-75.

Aitchison, J.D., G. Blobel, and M.P. Rout. 1996. Kap104p: a karyopherin involved in the nuclear transport of messenger RNA binding proteins. *Science*. 274:624-7.

Andrulis, E.D., D.C. Zappulla, A. Ansari, S. Perrod, C.V. Laiosa, M.R. Gartenberg, and R. Sternglanz. 2002. Esc1, a nuclear periphery protein required for Sir4-based plasmid anchoring and partitioning. *Mol Cell Biol*. 22:8292-301.

Askjaer, P., A. Bachi, M. Wilm, F.R. Bischoff, D.L. Weeks, V. Ogniewski, M. Ohno, C. Niehrs, J. Kjems, I.W. Mattaj, and M. Fornerod. 1999. RanGTP-regulated interactions of CRM1 with nucleoporins and a shuttling DEAD-box helicase. *Mol Cell Biol*. 19:6276-85.

Bangs, P., B. Burke, C. Powers, R. Craig, A. Purohit, and S. Doxsey. 1998. Functional analysis of Tpr: identification of nuclear pore complex association and nuclear localization domains and a role in mRNA export. *J Cell Biol*. 143:1801-12.

Beaudouin, J., D. Gerlich, N. Daigle, R. Eils, and J. Ellenberg. 2002. Nuclear envelope breakdown proceeds by microtubule-induced tearing of the lamina. *Cell*. 108:83-96.

Belgareh, N., and V. Doye. 1997. Dynamics of nuclear pore distribution in nucleoporin mutant yeast cells. *J Cell Biol*. 136:747-59.

Bitterman, K.J., O. Medvedik, and D.A. Sinclair. 2003. Longevity regulation in *Saccharomyces cerevisiae*: linking metabolism, genome stability, and heterochromatin. *Microbiol Mol Biol Rev*. 67:376-99.

Bodoor, K., S. Shaikh, D. Salina, W.H. Raharjo, R. Bastos, M. Lohka, and B. Burke. 1999. Sequential recruitment of NPC proteins to the nuclear periphery at the end of mitosis. *J Cell Sci*. 112:2253-64.

Bornens, M. 1977. Is the centriole bound to the nuclear membrane? *Nature*. 270:80-2.

Bucci, M., and S.R. Wente. 1997. In vivo dynamics of nuclear pore complexes in yeast. *J. Cell Biol.* 136:1185-99.

Bullitt, E., M.P. Rout, J.V. Kilmartin, and C.W. Akey. 1997. The yeast spindle pole body is assembled around a central crystal of Spc42p. *Cell*. 89:1077-86.

Byers, B., and L. Goetsch. 1974. Duplication of spindle plaques and integration of the yeast cell cycle. *Cold Spring Harb Symp Quant Biol*. 38:123-31.

Byers, B., and L. Goetsch. 1975a. Behavior of spindles and spindle plaques in the cell cycle and conjugation of *Saccharomyces cerevisiae*. *J Bacteriol*. 124:511-23.

Byers, B., and L. Goetsch. 1975b. Electron microscopic observations on the meiotic karyotype of diploid and tetraploid *Saccharomyces cerevisiae*. *Proc Natl Acad Sci U S A*. 72:5056-60.

Byrd, D.A., D.J. Sweet, N. Pante, K.N. Konstantinov, T. Guan, A.C. Saphire, P.J. Mitchell, C.S. Cooper, U. Aebi, and L. Gerace. 1994. Tpr, a large coiled coil protein whose amino terminus is involved in activation of oncogenic kinases, is localized to the cytoplasmic surface of the nuclear pore complex. *J. Cell Biol.* 127:1515-26.

Casolari, J.M., C.R. Brown, S. Komili, J. West, H. Hieronymus, and P.A. Silver. 2004. Genome-wide localization of the nuclear transport machinery couples transcriptional status and nuclear organization. *Cell*. 117:427-39.

Cherry, J.M., C. Ball, S. Weng, G. Juvik, R. Schmidt, C. Adler, B. Dunn, S. Dwight, L. Riles, R.K. Mortimer, and D. Botstein. 1997. Genetic and physical maps of *Saccharomyces cerevisiae*. *Nature*. 387:67-73.

Chi, M.-H., and D. Shore. 1996. *SUM1-1*, a Dominant Suppressor of *SIR* Mutations in *Saccharomyces cerevisiae*, Increases Transcriptional Silencing at Telomeres and HM Mating-Type Loci and Decreases Chromosome Stability. *Mol. Cell. Biol.* 16:4281-4294.

Chial, H.J., M.P. Rout, T.H. Giddings, and M. Winey. 1998. *Saccharomyces cerevisiae* Ndc1p is a shared component of nuclear pore complexes and spindle pole bodies. *J Cell Biol*. 143:1789-800.

Chook, Y.M., and G. Blobel. 1999. Structure of the nuclear transport complex karyopherin-beta2-Ran x GppNHp. *Nature*. 399:230-7.

Collas, P. 1999. Sequential PKC- and Cdc2-mediated phosphorylation events elicit zebrafish nuclear envelope disassembly. *J Cell Sci*. 112 (Pt 6):977-87.

Cordes, V.C., S. Reidenbach, H.R. Rackwitz, and W.W. Franke. 1997. Identification of protein p270/Tpr as a constitutive component of the nuclear pore complex-attached intranuclear filaments. *J. Cell Biol.* 136:515-29.

Daigle, N., J. Beaudouin, L. Hartnell, G. Imreh, E. Hallberg, J. Lippincott-Schwartz, and J. Ellenberg. 2001. Nuclear pore complexes form immobile networks and have a very low turnover in live mammalian cells. *J Cell Biol*. 154:71-84.

Daum, J.R., N. Gomez-Ospina, M. Winey, and D.J. Burke. 2000. The spindle checkpoint of Saccharomyces cerevisiae responds to separable microtubule-dependent events. *Curr Biol*. 10:1375-8.

Davis, T.N. 1992. A temperature-sensitive calmodulin mutant loses viability during mitosis. *J Cell Biol*. 118:607-17.

De Sandre-Giovannoli, A., R. Bernard, P. Cau, C. Navarro, J. Amiel, I. Boccaccio, S. Lyonnet, C.L. Stewart, A. Munnich, M. Le Merrer, and N. Levy. 2003. Lamin a truncation in Hutchinson-Gilford progeria. *Science*. 300:2055.

DeZwaan, T.M., E. Ellingson, D. Pellman, and D.M. Roof. 1997. Kinesin-related KIP3 of *Saccharomyces cerevisiae* is required for a distinct step in nuclear migration. *J Cell Biol*. 138:1023-40.

Dilworth, D.J., A. Suprapto, J.C. Padovan, B.T. Chait, R.W. Wozniak, M.P. Rout, and J.D. Aitchison. 2001. Nup2p dynamically associates with the distal regions of the yeast nuclear pore complex. *J Cell Biol*. 153:1465-78.

Ding, D.Q., Y. Tomita, A. Yamamoto, Y. Chikashige, T. Haraguchi, and Y. Hiraoka. 2000. Large-scale screening of intracellular protein localization in living fission yeast cells by the use of a GFP-fusion genomic DNA library. *Genes Cells*. 5:169-90.

Dingwall, C., S.V. Sharnick, and R.A. Laskey. 1982. A polypeptide domain that specifies migration of nucleoplasmin into the nucleus. *Cell*. 30:449-58.

Doye, V., R. Wepf, and E.C. Hurt. 1994. A novel nuclear pore protein Nup133p with distinct roles in poly(A)+ RNA transport and nuclear pore distribution. *EMBO J.* 13:6062-75.

Ellenberg, J., E.D. Siggia, J.E. Moreira, C.L. Smith, J.F. Presley, H.J. Worman, and J. Lippincott-Schwartz. 1997. Nuclear membrane dynamics and reassembly in living cells: targeting of an inner nuclear membrane protein in interphase and mitosis. *J Cell Biol*. 138:1193-206.

Ellenberg, P., M. Edreira, M. Lozano, and L. Scolaro. 2002. Synthesis and expression of viral antigens in Vero cells persistently infected with Junin virus. *Arch Virol*. 147:1543-57.

Elliott, S., M. Knop, G. Schlenstedt, and E. Schiebel. 1999. Spc29p is a component of the Spc110p subcomplex and is essential for spindle pole body duplication. *Proc Natl Acad Sci U S A*. 96:6205-10.

Epstein, C.B., and F.R. Cross. 1992. CLB5: a novel B cyclin from budding yeast with a role in S phase. *Genes Dev.* 6:1695-706.

Eriksson, M., W.T. Brown, L.B. Gordon, M.W. Glynn, J. Singer, L. Scott, M.R. Erdos, C.M. Robbins, T.Y. Moses, P. Berglund, A. Dutra, E. Pak, S. Durkin, A.B. Csoka, M. Boehnke, T.W. Glover, and F.S. Collins. 2003. Recurrent de novo point mutations in lamin A cause Hutchinson-Gilford progeria syndrome. *Nature*. 423:293-8.

Fahrenkrog, B., E.C. Hurt, U. Aebi, and N. Pante. 1998. Molecular architecture of the yeast nuclear pore complex: localization of Nsp1p subcomplexes. *J Cell Biol*. 143:577-88.

Feuerbach, F., V. Galy, E. Trelles-Sticken, M. Fromont-Racine, A. Jacquier, E. Gilson, J.C. Olivo-Marin, H. Scherthan, and U. Nehrbass. 2002. Nuclear architecture and spatial positioning help establish transcriptional states of telomeres in yeast. *Nat Cell Biol*. 4:214-21.

Field, H.I., D. Fenyo, and R.C. Beavis. 2002. RADARS, a bioinformatics solution that automates proteome mass spectral analysis, optimises protein identification, and archives data in a relational database. *Proteomics*. 2:36-47.

Floer, M., and G. Blobel. 1999. Putative reaction intermediates in Crm1-mediated nuclear protein export. *J Biol Chem*. 274:16279-86.

Floer, M., G. Blobel, and M. Rexach. 1997. Disassembly of RanGTP-karyopherin beta complex, an intermediate in nuclear protein import. *J. Biol. Chem.* 272:19538-46.

Fontoura, B.M., S. Dales, G. Blobel, and H. Zhong. 2001. The nucleoporin Nup98 associates with the intranuclear filamentous protein network of TPR. *Proc Natl Acad Sci U S A*. 98:3208-13.

Frasch, M., M.R. Paddy, and H. Saumweber. 1988. Developmental and mitotic behavior of two novel groups of nuclear envelope antigens. *J. Cell Sci.* 90:247-264.

Frosst, P., T. Guan, C. Subauste, K. Hahn, and L. Gerace. 2002. Tpr is localized within the nuclear basket of the pore complex and has a role in nuclear protein export. *J Cell Biol*. 156:617-30.

Gadal, O., D. Strauss, J. Kessl, B. Trumpower, D. Tollervey, and E. Hurt. 2001. Nuclear export of 60s ribosomal subunits depends on Xpo1p and requires a nuclear export sequence-containing factor, Nmd3p, that associates with the large subunit protein Rpl10p. *Mol Cell Biol*. 21:3405-15.

Galitski, T., A.J. Saldanha, C.A. Styles, E.S. Lander, and G.R. Fink. 1999. Ploidy regulation of gene expression. *Science*. 285:251-4.

Galy, V., O. Gadal, M. Fromont-Racine, A. Romano, A. Jacquier, and U. Nehrbass. 2004. Nuclear retention of unspliced mRNAs in yeast is mediated by perinuclear Mlp1. *Cell*. 116:63-73.

Galy, V., J.C. Olivo-Marin, H. Scherthan, V. Doye, N. Rascalou, and U. Nehrbass. 2000. Nuclear pore complexes in the organization of silent telomeric chromatin. *Nature*. 403:108-12.

Gavin, A.C., M. Bosche, R. Krause, P. Grandi, M. Marzioch, A. Bauer, J. Schultz, J.M. Rick, A.M. Michon, C.M. Cruciat, M. Remor, C. Hofert, M. Schelder, M. Brajenovic, H. Ruffner, A. Merino, K. Klein, M. Hudak, D. Dickson, T. Rudi, V. Gnau, A. Bauch, S. Bastuck, B. Huhse, C. Leutwein, M.A. Heurtier, R.R. Copley, A. Edelmann, E. Querfurth, V. Rybin, G. Drewes, M. Raida, T. Bouwmeester, P. Bork, B. Seraphin, B. Kuster, G. Neubauer, and G. Superti-Furga. 2002. Functional organization of the yeast proteome by systematic analysis of protein complexes. *Nature*. 415:141-7.

Geiser, J.R., H.A. Sundberg, B.H. Chang, E.G. Muller, and T.N. Davis. 1993. The essential mitotic target of calmodulin is the 110-kilodalton component of the spindle pole body in Saccharomyces cerevisiae. *Mol Cell Biol*. 13:7913-24.

Geiser, J.R., D. van Tuinen, S.E. Brockerhoff, M.M. Neff, and T.N. Davis. 1991. Can calmodulin function without binding calcium? *Cell*. 65:949-59.

Gerace, L., and G. Blobel. 1980. The nuclear envelope lamina is reversibly depolymerized during mitosis. *Cell*. 19:277-87.

Gindullis, F., A. Rose, S. Patel, and I. Meier. 2002. Four signature motifs define the first class of structurally related large coiled-coil proteins in plants. *BMC Genomics*. 3:9.

Goldberg, M.W., and T.D. Allen. 1992. High resolution scanning electron microscopy of the nuclear envelope: demonstration of a new, regular, fibrous lattice attached to the baskets of the nucleoplasmic face of the nuclear pores. *J. Cell Biol.* 119:1429-40.

Greco, A., M.A. Pierotti, I. Bongarzone, S. Pagliardini, C. Lanzi, and G. Della Porta. 1992. TRK-T1 is a novel oncogene formed by the fusion of TPR and TRK genes in human papillary thyroid carcinomas. *Oncogene*. 7:237-42.

Green, D.M., C.P. Johnson, H. Hagan, and A.H. Corbett. 2003. The C-terminal domain of myosin-like protein 1 (Mlp1p) is a docking site for heterogeneous nuclear ribonucleoproteins that are required for mRNA export. *Proc Natl Acad Sci U S A*. 100:1010-5.

Green, D.M., K.A. Marfatia, E.B. Crafton, X. Zhang, X. Cheng, and A.H. Corbett. 2002. Nab2p is required for poly(A) RNA export in *Saccharomyces cerevisiae* and is regulated by arginine methylation via Hmt1p. *J Biol Chem*. 277:7752-60.

Haase, S.B., M. Winey, and S.I. Reed. 2001. Multi-step control of spindle pole body duplication by cyclin-dependent kinase. *Nat Cell Biol*. 3:38-42.

Hase, M.E., and V.C. Cordes. 2003. Direct interaction with Nup153 mediates binding of Tpr to the periphery of the nuclear pore complex. *Mol Biol Cell*. 14:1923-40.

Hase, M.E., N.V. Kuznetsov, and V.C. Cordes. 2001. Amino acid substitutions of coiled-coil protein Tpr abrogate anchorage to the nuclear pore complex but not parallel, in-register homodimerization. *Mol Biol Cell*. 12:2433-52.

Havre, P.A., and D.R. Evans. 1983. Disassembly and characterization of the nuclear pore complex-lamina fraction from bovine liver nuclei. *Biochemistry*. 22:2852-60.

Hector, R.E., K.R. Nykamp, S. Dheur, J.T. Anderson, P.J. Non, C.R. Urbinati, S.M. Wilson, L. Minvielle-Sebastia, and M.S. Swanson. 2002. Dual requirement for yeast hnRNP Nab2p in mRNA poly(A) tail length control and nuclear export. *EMBO J*. 21:1800-10.

Hediger, F., K. Dubrana, and S.M. Gasser. 2002a. Myosin-like proteins 1 and 2 are not required for silencing or telomere anchoring, but act in the Tel1 pathway of telomere length control. *J Struct Biol*. 140:79-91.

Hediger, F., F.R. Neumann, G. Van Houwe, K. Dubrana, and S.M. Gasser. 2002b. Live Imaging of Telomeres. yKu and Sir Proteins Define Redundant Telomere-Anchoring Pathways in Yeast. *Curr Biol*. 12:2076-89.

Hilleren, P., T. McCarthy, M. Rosbash, R. Parker, and T.H. Jensen. 2001. Quality control of mRNA 3'-end processing is linked to the nuclear exosome. *Nature*. 413:538-42.

Hopper, A.K., H.M. Traglia, and R.W. Dunst. 1990. The yeast RNA1 gene product necessary for RNA processing is located in the cytosol and apparently excluded from the nucleus. *J Cell Biol*. 111:309-21.

Huh, W.K., J.V. Falvo, L.C. Gerke, A.S. Carroll, R.W. Howson, J.S. Weissman, and E.K. O'Shea. 2003. Global analysis of protein localization in budding yeast. *Nature*. 425:686-91.

Iouk, T., O. Kerscher, R.J. Scott, M.A. Basrai, and R.W. Wozniak. 2002. The yeast nuclear pore complex functionally interacts with components of the spindle assembly checkpoint. *J Cell Biol*. 159:807-19.

Iovine, M.K., J.L. Watkins, and S.R. Wente. 1995. The GLFG repetitive region of the nucleoporin Nup116p interacts with Kap95p, an essential yeast nuclear import factor. *J Cell Biol*. 131:1699-713.

Iovine, M.K., and S.R. Wente. 1997. A nuclear export signal in Kap95p is required for both recycling the import factor and interaction with the nucleoporin GLFG repeat regions of Nup116p and Nup100p. *J. Cell Biol.* 137:797-811.

Ishii, K., G. Arib, C. Lin, G. Van Houwe, and U.K. Laemmli. 2002. Chromatin boundaries in budding yeast: the nuclear pore connection. *Cell*. 109:551-62.

Izaurralde, E., U. Kutay, C. von Kobbe, I.W. Mattaj, and D. Gorlich. 1997. The asymmetric distribution of the constituents of the Ran system is essential for transport into and out of the nucleus. *EMBO J.* 16:6535-47.

Jacobs, C.W., A.E. Adams, P.J. Szaniszlo, and J.R. Pringle. 1988. Functions of microtubules in the *Saccharomyces cerevisiae* cell cycle. *J Cell Biol*. 107:1409-26.

Jaspersen, S.L., and M. Winey. 2004. The budding yeast spindle pole body: Structure, Duplication, and Function. *Annu Rev Cell Dev Biol*. 20:1-28.

Jensen, T.H., and M. Rosbash. 2003. Co-transcriptional monitoring of mRNP formation. *Nat Struct Biol*. 10:10-2.

Kalderon, D., B.L. Roberts, W.D. Richardson, and A.E. Smith. 1984. A short amino acid sequence able to specify nuclear location. *Cell*. 39:499-509.

Kellis, M., B.W. Birren, and E.S. Lander. 2004. Proof and evolutionary analysis of ancient genome duplication in the yeast *Saccharomyces cerevisiae*. *Nature*. 428:617-24.

Kellis, M., N. Patterson, M. Endrizzi, B. Birren, and E.S. Lander. 2003. Sequencing and comparison of yeast species to identify genes and regulatory elements. *Nature*. 423:241-54.

Kennedy, B.K., N.R. Austriaco, Jr., J. Zhang, and L. Guarente. 1995. Mutation in the silencing gene SIR4 can delay aging in *S. cerevisiae*. *Cell*. 80:485-96.

Kerscher, O., P. Hieter, M. Winey, and M.A. Basrai. 2001. Novel role for a *Saccharomyces cerevisiae* nucleoporin, Nup170p, in chromosome segregation. *Genetics*. 157:1543-53.

Kilmartin, J.V., S.L. Dyos, D. Kershaw, and J.T. Finch. 1993. A spacer protein in the *Saccharomyces cerevisiae* spindle poly body whose transcript is cell cycle-regulated. *J Cell Biol*. 123:1175-84.

Kiseleva, E., T.D. Allen, S. Rutherford, M. Bucci, S.R. Wente, and M.W. Goldberg. 2004. Yeast nuclear pore complexes have a cytoplasmic ring and internal filaments. *J Struct Biol*. 145:272-88.

Kiseleva, E., M. Goldberg, T. Allen, and C. Akey. 1998a. Active nuclear pore complexes in chironomus: visualization of transporter configurations related to mRNP export. *J. Cell Sci.* 111:223-36.

Kiseleva, E., M.W. Goldberg, T.D. Allen, and C.W. Akey. 1998b. Active nuclear pore complexes in Chironomus: visualization of transporter configurations related to mRNP export. *J Cell Sci*. 111:223-36.

Klemm, J.D., C.R. Beals, and G.R. Crabtree. 1997. Rapid targeting of nuclear proteins to the cytoplasm. *Curr Biol*. 7:638-44.

Kolling, R., T. Nguyen, E.Y. Chen, and D. Botstein. 1993. A new yeast gene with a myosin-like heptad repeat structure. *Mol. Gen. Genet.* 237:359-369.

Kosova, B., N. Pante, C. Rollenhagen, A. Podtelejnikov, M. Mann, U. Aebi, and E. Hurt. 2000. Mlp2p, a component of nuclear pore attached intranuclear filaments, associates with Nic96p. *J Biol Chem*. 275:343-50.

Krull, S., J. Thyberg, B. Bjorkroth, H.R. Rackwitz, and V.C. Cordes. 2004. Nucleoporins as components of the nuclear pore complex core structure and Tpr as the architectural element of the nuclear basket. *Mol Biol Cell*. 15:4261-77.

Krutchinsky, A.N., M. Kalkum, and B.T. Chait. 2001. Automatic identification of proteins with a MALDI-quadrupole ion trap mass spectrometer. *Anal Chem*. 73:5066-77.

Kuznetsov, N.V., L. Sandblad, M.E. Hase, A. Hunziker, M. Hergt, and V.C. Cordes. 2002. The evolutionarily conserved single-copy gene for murine Tpr encodes one prevalent isoform in somatic cells and lacks paralogs in higher eukaryotes. *Chromosoma*. 111:236-55.

Lammerding, J., P.C. Schulze, T. Takahashi, S. Kozlov, T. Sullivan, R.D. Kamm, C.L. Stewart, and R.T. Lee. 2004. Lamin A/C deficiency causes defective nuclear mechanics and mechanotransduction. *J Clin Invest*. 113:370-8.

Lee, I., S.V. Date, A.T. Adai, and E.M. Marcotte. 2004. A probabilistic functional network of yeast genes. *Science*. 306:1555-8.

Lei, E.P., C.A. Stern, B. Fahrenkrog, H. Krebber, T.I. Moy, U. Aebi, and P.A. Silver. 2003. Sac3 is an mRNA export factor that localizes to cytoplasmic fibrils of nuclear pore complex. *Mol Biol Cell*. 14:836-47.

Longtine, M.S., A. McKenzie, 3rd, D.J. Demarini, N.G. Shah, A. Wach, A. Brachat, P. Philippsen, and J.R. Pringle. 1998. Additional modules for versatile and economical PCR-based gene deletion and modification in *Saccharomyces cerevisiae*. *Yeast*. 14:953-61.

Macaulay, C., E. Meier, and D.J. Forbes. 1995. Differential mitotic phosphorylation of proteins of the nuclear pore complex. *J. Biol. Chem.* 270:254-62.

Malone, C.J., L. Misner, N. Le Bot, M.C. Tsai, J.M. Campbell, J. Ahringer, and J.G. White. 2003. The *C. elegans* hook protein, ZYG-12, mediates the essential attachment between the centrosome and nucleus. *Cell*. 115:825-36.

Mancini, M.A., B. Shan, J.A. Nickerson, S. Penman, and W.H. Lee. 1994. The retinoblastoma gene product is a cell cycle-dependent, nuclear matrix-associated protein. *Proc Natl Acad Sci U S A*. 91:418-22.

Mehlin, H., B. Daneholt, and U. Skoglund. 1995. Structural interaction between the nuclear pore complex and a specific translocating RNP particle. *J Cell Biol*. 129:1205-16.

Mehta, S., X.M. Yang, C.S. Chan, M.J. Dobson, M. Jayaram, and S. Velmurugan. 2002. The 2 micron plasmid purloins the yeast cohesin complex: a mechanism for coupling plasmid partitioning and chromosome segregation? *J Cell Biol*. 158:625-37.

Miller, M.E., and F.R. Cross. 2001. Mechanisms controlling subcellular localization of the G(1) cyclins Cln2p and Cln3p in budding yeast. *Mol Cell Biol*. 21:6292-311.

Moir, R.D., M. Montag-Lowy, and R.D. Goldman. 1994. Dynamic properties of nuclear lamins: lamin B is associated with sites of DNA replication. *J Cell Biol*. 125:1201-12.

Moir, R.D., M. Yoon, S. Khuon, and R.D. Goldman. 2000. Nuclear lamins A and B1: different pathways of assembly during nuclear envelope formation in living cells. *J Cell Biol*. 151:1155-68.

Moroianu, J., G. Blobel, and A. Radu. 1996. Nuclear protein import: Ran-GTP dissociates the karyopherin alphabeta heterodimer by displacing alpha from an overlapping binding site on beta. *Proc. Natl. Acad. Sci. USA*. 93:7059-62.

Mounkes, L.C., and C.L. Stewart. 2004. Aging and nuclear organization: lamins and progeria. *Curr Opin Cell Biol*. 16:322-7.

Muchir, A., B.G. van Engelen, M. Lammens, J.M. Mislow, E. McNally, K. Schwartz, and G. Bonne. 2003. Nuclear envelope alterations in fibroblasts from LGMD1B patients carrying nonsense Y259X heterozygous or homozygous mutation in lamin A/C gene. *Exp Cell Res*. 291:352-62.

Nadezhdina, E.S., D. Fais, and Y.S. Chentsov. 1979. On the association of centrioles with the interphase nucleus. *Eur J Cell Biol*. 19:109-15.

Nelson, M., and P. Silver. 1989. Context affects nuclear protein localization in *Saccharomyces cerevisiae*. *Mol Cell Biol*. 9:384-9.

Nigg, E.A. 1989. The nuclear envelope. *Curr Opin Cell Biol*. 1:435-40.

O'Toole, E.T., M. Winey, and J.R. McIntosh. 1999. High-voltage electron tomography of spindle pole bodies and early mitotic spindles in the yeast *Saccharomyces cerevisiae*. *Mol Biol Cell*. 10:2017-31.

Ogbadoyi, E., K. Ersfeld, D. Robinson, T. Sherwin, and K. Gull. 2000. Architecture of the *Trypanosoma brucei* nucleus during interphase and mitosis. *Chromosoma*. 108:501-13.

Ohtsubo, M., H. Okazaki, and T. Nishimoto. 1989. The RCC1 protein, a regulator for the onset of chromosome condensation locates in the nucleus and binds to DNA. *J. Cell Biol.* 109:1389-97.

Park, M., M. Dean, C.S. Cooper, M. Schmidt, S.J. O'Brien, D.G. Blair, and G.F. Vande Woude. 1986. Mechanism of *met* oncogene activation. *Cell*. 45:895-904.

Qi, H., U. Rath, D. Wang, Y.Z. Xu, Y. Ding, W. Zhang, M.J. Blacketer, M.R. Paddy, J. Girton, J. Johansen, and K.M. Johansen. 2004. Megator, an essential coiled-coil protein that localizes to the putative spindle matrix during mitosis in *Drosophila*. *Mol Biol Cell*.

Radu, A., M.S. Moore, and G. Blobel. 1995. The peptide repeat domain of nucleoporin Nup98 functions as a docking site in transport across the nuclear pore complex. *Cell*. 81:215-22.

Reid, R.J., M. Lisby, and R. Rothstein. 2002. Cloning-free genome alterations in Saccharomyces cerevisiae using adaptamer-mediated PCR. *Methods Enzymol*. 350:258-77.

Rickwood, D. 1984. Centrifugation: a practical approach. 354 pp.

Rigaut, G., A. Shevchenko, B. Rutz, M. Wilm, M. Mann, and B. Seraphin. 1999. A generic protein purification method for protein complex characterization and proteome exploration. *Nat Biotechnol*. 17:1030-2.

Ris, H. 1997. High-resolution field-emission scanning electron microscopy of nuclear pore complex. *Scanning*. 19:368-75.

Rout, M.P., and J.D. Aitchison. 2000. Pore relations: nuclear pore complexes and nucleocytoplasmic exchange. *Essays Biochem*. 36:75-88.

Rout, M.P., J.D. Aitchison, M.O. Magnasco, and B.T. Chait. 2003. Virtual gating and nuclear transport: the hole picture. *Trends Cell Biol*. 13:622-8.

Rout, M.P., J.D. Aitchison, A. Suprapto, K. Hjertaas, Y. Zhao, and B.T. Chait. 2000. The yeast nuclear pore complex: composition, architecture, and transport mechanism. *J Cell Biol*. 148:635-51.

Rout, M.P., and G. Blobel. 1993. Isolation of the yeast nuclear pore complex. *J Cell Biol*. 123:771-83.

Rout, M.P., G. Blobel, and J.D. Aitchison. 1997. A distinct nuclear import pathway used by ribosomal proteins. *Cell*. 89:715-25.

Rout, M.P., and M.C. Field. 2001. Isolation and characterization of subnuclear compartments from *Trypanosoma brucei*. Identification of a major repetitive nuclear lamina component. *J Biol Chem*. 276:38261-71.

Rout, M.P., and J.V. Kilmartin. 1990. Components of the yeast spindle and spindle pole body. *J. Cell Biol.* 111:1913-1927.

Rout, M.P., and J.V. Kilmartin. 1991. Yeast spindle pole body components. *In* Cold Spring Harbor Symposia on Quantitative Biology. Vol. 56. Cold Spring Harbor Laboratory Press, Cold Spring Harbor, New York. 687-692.

Salina, D., K. Bodoor, D.M. Eckley, T.A. Schroer, J.B. Rattner, and B. Burke. 2002. Cytoplasmic dynein as a facilitator of nuclear envelope breakdown. *Cell*. 108:97-107.

Schaap, P.J., J. van't Riet, C.L. Woldringh, and H.A. Raue. 1991. Identification and functional analysis of the nuclear localization signals of ribosomal protein L25 from *Saccharomyces cerevisiae*. *J Mol Biol*. 221:225-37.

Schaerer, F., G. Morgan, M. Winey, and P. Philippsen. 2001. Cnm67p is a spacer protein of the *Saccharomyces cerevisiae* spindle pole body outer plaque. *Mol Biol Cell*. 12:2519-33.

Schultz, M.C., D.J. Hockman, T.A. Harkness, W.I. Garinther, and B.A. Altheim. 1997. Chromatin assembly in a yeast whole-cell extract. *Proc Natl Acad Sci U S A*. 94:9034-9.

Shah, S., S. Tugendreich, and D. Forbes. 1998. Major binding sites for the nuclear import receptor are the internal nucleoporin Nup153 and the adjacent nuclear filament protein Tpr. *J. Cell Biol.* 141:31-49.

Shav-Tal, Y., X. Darzacq, S.M. Shenoy, D. Fusco, S.M. Janicki, D.L. Spector, and R.H. Singer. 2004. Dynamics of single mRNPs in nuclei of living cells. *Science*. 304:1797-800.

Shibata, S., Y. Matsuoka, and Y. Yoneda. 2002. Nucleocytoplasmic transport of proteins and poly(A)+ RNA in reconstituted Tpr-less nuclei in living mammalian cells. *Genes Cells*. 7:421-34.

Shulga, N., P. Roberts, Z. Gu, L. Spitz, M.M. Tabb, M. Nomura, and D.S. Goldfarb. 1996. In vivo nuclear transport kinetics in *Saccharomyces cerevisiae*: a role for heat shock protein 70 during targeting and translocation. *J. Cell Biol.* 135:329-39.

Sinclair, D.A., and L. Guarente. 1997. Extrachromosomal rDNA circles--a cause of aging in yeast. *Cell*. 91:1033-42.

Soman, N.R., P. Correa, B.A. Ruiz, and G.N. Wogan. 1991. The TPR-MET oncogenic rearrangement is present and expressed in human gastric carcinoma and precursor lesions. *Proc. Natl. Acad. Sci. USA*. 88:4892-6.

Spang, A., I. Courtney, U. Fackler, M. Matzner, and E. Schiebel. 1993. The calcium-binding protein cell division cycle 31 of *Saccharomyces cerevisiae* is a component of the half bridge of the spindle pole body. *J Cell Biol*. 123:405-16.

Spann, T.P., A.E. Goldman, C. Wang, S. Huang, and R.D. Goldman. 2002. Alteration of nuclear lamin organization inhibits RNA polymerase II-dependent transcription. *J Cell Biol*. 156:603-8.

Spann, T.P., R.D. Moir, A.E. Goldman, R. Stick, and R.D. Goldman. 1997. Disruption of nuclear lamin organization alters the distribution of replication factors and inhibits DNA synthesis. *J. Cell Biol.* 136:1201-12.

Stirling, D.A., T.F. Rayner, A.R. Prescott, and M.J. Stark. 1996. Mutations which block the binding of calmodulin to Spc110p cause multiple mitotic defects. *J Cell Sci*. 109 (Pt 6):1297-310.

Stirling, D.A., and M.J. Stark. 2000. Mutations in SPC110, encoding the yeast spindle pole body calmodulin-binding protein, cause defects in cell integrity as well as spindle formation. *Biochim Biophys Acta*. 1499:85-100.

Strambio-de-Castillia, C. 1998. Identification and Characterization of Mlp1p and Mlp2p: Molecular Components of Filaments Located at the Interface Between the Nuclear Pore Complex and the Nuclear Interior. The Rockefeller University, New York, NY. 217.

Strambio-de-Castillia, C., G. Blobel, and M.P. Rout. 1999. Proteins connecting the nuclear pore complex with the nuclear interior. *J Cell Biol*. 144:839-55.

Strasser, K., S. Masuda, P. Mason, J. Pfannstiel, M. Oppizzi, S. Rodriguez-Navarro, A.G. Rondon, A. Aguilera, K. Struhl, R. Reed, and E. Hurt. 2002. TREX is a conserved complex coupling transcription with messenger RNA export. *Nature*. 417:304-8.

Sullivan, T., D. Escalante-Alcalde, H. Bhatt, M. Anver, N. Bhat, K. Nagashima, C.L. Stewart, and B. Burke. 1999. Loss of A-type lamin expression compromises nuclear envelope integrity leading to muscular dystrophy. *J Cell Biol*. 147:913-20.

Sundberg, H.A., and T.N. Davis. 1997. A mutational analysis identifies three functional regions of the spindle pole component Spc110p in *Saccharomyces cerevisiae*. *Mol Biol Cell*. 8:2575-90.

Sundberg, H.A., L. Goetsch, B. Byers, and T.N. Davis. 1996. Role of calmodulin and Spc110p interaction in the proper assembly of spindle pole body compenents. *J Cell Biol*. 133:111-24.

Suprapto, A. 2002. The Composition, Architecture, and Mechanism of the Yeast Nuclear Pore Complex: Painting Picture with Proteomics. The Rockefeller University. 169.

Terasaki, M., P. Campagnola, M.M. Rolls, P.A. Stein, J. Ellenberg, B. Hinkle, and B. Slepchenko. 2001. A new model for nuclear envelope breakdown. *Mol Biol Cell*. 12:503-10.

Thomas, B., and R. Rothstein. 1989. Elevated recombination rates in transcriptionally active DNA. *Cell*. 56:619-630.

Troyanskaya, O.G., K. Dolinski, A.B. Owen, R.B. Altman, and D. Botstein. 2003. A Bayesian framework for combining heterogeneous data sources for gene function prediction (in *Saccharomyces cerevisiae*). *Proc Natl Acad Sci U S A*. 100:8348-53.

Truant, R., R.A. Fridell, R.E. Benson, H. Bogerd, and B.R. Cullen. 1998. Identification and functional characterization of a novel nuclear localization signal present in the yeast Nab2 poly(A)+ RNA binding protein. *Mol Cell Biol*. 18:1449-58.

Vetter, I.R., A. Arndt, U. Kutay, D. Gorlich, and A. Wittinghofer. 1999. Structural view of the Ran-Importin beta interaction at 2.3 A resolution. *Cell*. 97:635-46.

Vinciguerra, P., N. Iglesias, J. Camblong, D. Zenklusen, and F. Stutz. 2005. Perinuclear Mlp proteins downregulate gene expression in response to a defect in mRNA export. *EMBO J*. 24:813-23.

Vinciguerra, P., and F. Stutz. 2004. mRNA export: an assembly line from genes to nuclear pores. *Curr Opin Cell Biol*. 16:285-92.

Visa, N., E. Izaurralde, J. Ferreira, B. Daneholt, and I.W. Mattaj. 1996. A nuclear cap-binding complex binds Balbiani ring pre-mRNA cotranscriptionally and accompanies the ribonucleoprotein particle during nuclear export. *J. Cell Biol.* 133:5-14.

Winey, M., and E.T. O'Toole. 2001. The spindle cycle in budding yeast. *Nat Cell Biol*. 3:E23-7.

Winey, M., D. Yarar, T.H. Giddings, Jr., and D.N. Mastronarde. 1997. Nuclear pore complex number and distribution throughout the *Saccharomyces cerevisiae* cell cycle by three-dimensional reconstruction from electron micrographs of nuclear envelopes. *Mol. Biol. Cell*. 8:2119-32.

Yang, C.H., E.J. Lambie, J. Hardin, J. Craft, and M. Snyder. 1989. Higher order structure is present in the yeast nucleus: autoantibody probes demonstrate that the nucleolus lies opposite the spindle pole body. *Chromosoma*. 98:123-8.

Yang, L., T. Guan, and L. Gerace. 1997. Integral membrane proteins of the nuclear envelope are dispersed throughout the endoplasmic reticulum during mitosis. *J Cell Biol*. 137:1199-210.

Yoder, T.J., C.G. Pearson, K. Bloom, and T.N. Davis. 2003. The *Saccharomyces cerevisiae* spindle pole body is a dynamic structure. *Mol Biol Cell*. 14:3494-505.

Zaal, K.J., C.L. Smith, R.S. Polishchuk, N. Altan, N.B. Cole, J. Ellenberg, K. Hirschberg, J.F. Presley, T.H. Roberts, E. Siggia, R.D. Phair, and J. Lippincott-Schwartz. 1999. Golgi membranes are absorbed into and reemerge from the ER during mitosis. *Cell*. 99:589-601.

Zenklusen, D., P. Vinciguerra, Y. Strahm, and F. Stutz. 2001. The yeast hnRNP-Like proteins Yra1p and Yra2p participate in mRNA export through interaction with Mex67p. *Mol Cell Biol*. 21:4219-32.

Zenklusen, D., P. Vinciguerra, J.C. Wyss, and F. Stutz. 2002. Stable mRNP formation and export require cotranscriptional recruitment of the mRNA export factors Yra1p and Sub2p by Hpr1p. *Mol Cell Biol*. 22:8241-53.

Zhao, X., and G. Blobel. 2005. A SUMO ligase is part of a nuclear multiprotein complex that affects DNA repair and chromosomal organization. *Proc Natl Acad Sci U S A*.

Zhao, X., C.Y. Wu, and G. Blobel. 2004. Mlp-dependent anchorage and stabilization of a desumoylating enzyme is required to prevent clonal lethality. *J Cell Biol*. 167:605-11.

Zimowska, G., J.P. Aris, and M.R. Paddy. 1997. A *Drosophila* Tpr protein homolog is localized both in the extrachromosomal channel network and to nuclear pore complexes. *J. Cell Sci.* 110:927-44.

Zimowska, G., and M.R. Paddy. 2002. Structures and dynamics of *Drosophila* Tpr inconsistent with a static, filamentous structure. *Exp Cell Res*. 276:223-32.

Strains. DO NOT PRINT AND DISTRIBUTE.

(Thomas and Rothstein, 1989)

(Adams and Kilmartin, 1999)

(Elliott et al., 1999)
(Davis, 1992)
(Sundberg and Davis, 1997)
(Geiser et al., 1991)